All-aromatic Hyperbranched Polyaryletherketone Networks

Vogel, Wouter

DOI
10.4233/uuid:c709d2ba-8e41-4f23-a35c-ab75b34ed2c8

Publication date
2019

Document Version
Final published version

Citation (APA)
Vogel, W. (2019). *All-aromatic Hyperbranched Polyaryletherketone Networks*. [Dissertation (TU Delft), Delft University of Technology]. https://doi.org/10.4233/uuid:c709d2ba-8e41-4f23-a35c-ab75b34ed2c8

All-aromatic Hyperbranched Polyaryletherketone Networks

Proefschrift

Ter verkrijging van de graad van doctor
aan de Technische Universiteit Delft,
Op gezag van Rector Magnificus prof.dr.ir. T.H.J.J. van der Hagen,
Voorzitter van het College van promoties,
In het openbaar te verdedigen op
11 februari 2019 om 10.00 uur
door

Wouter VOGEL

Master of Science in de scheikunde
Vrije Universiteit Amsterdam
Geboren te Naaldwijk

Dit proefschrift is goedgekeurd door de promotor:
Prof. Dr. T. J. Dingemans

Samenstelling promotiecommissie:

Rector Magnificus	voorzitter
Prof. Dr. T. J. Dingemans	Delft University of Technology, promotor

Onafhankelijke leden:

Prof. Dr. Ir. S. van der Zwaag	Delft University of Technology
Prof. Dr. S. J. Picken	Delft University of Technology
Prof. C. Dransfeld	Delft University of Technology
Prof. Dr. F. Kapteijn	Delft University of Technology
Dr. E. Mendes	Delft University of Technology

Andere leden:

Prof Dr. Ir. N. E. Benes	University of Twente

Het onderzoek in deze thesis is gesponsord door het Dutch Polymer Institute (DPI), postbus 902, 5600 AX Eindhoven, project #718.

DPI
The Polymer Research Platform

TU Delft Delft University of Technology

ISBN: 9789463234863

Cover design: Wouter Vogel (vogelwouter@gmail.com)

Published by: Gildeprint

Table of contents

Chapter 1

Introduction

1.1 High performance polymers

1.1.1 What are high-performance polymers?

In the search for stronger and lighter materials, the development of high performance polymers took off in the early 60s. Especially the aerospace industry was motivated to take part in this development as polymers used in aerospace industries need to meet demanding criteria. Currently, epoxy-based resins are frequently used but their flammability, moisture uptake and relatively low degradation temperature make them unsuitable for use at high temperatures.[1] The need for high-performance polymers with outstanding thermo-mechanical properties resulted in the exploration of polymers with high glass transition temperatures (T_g >150 °C), high decomposition temperatures (>450 °C) and excellent stability towards chemical environments. Polymers that fall in this category are, for example, polyphenylene sulphide (PPS), poly(aryletherketone)s (PAEKs), polyimides (PIs), polyesters and polyamides (Table 1.1). These polymers often contain a high number of aromatic units, which gives rise to the outstanding thermo-mechanical properties and fluid stability. Aromatic units are comprised of sp^2-hybridized carbons that are more stable than non-aromatic sp^3-hybridized carbons. Also, hetero atoms, like nitrogen and oxygen in poly(etherimide)s (entry 3, Table 1.1), can lead to improved properties such as fire resistance.[1] Polyimides and poly(etherimide)s can either be amorphous or semi-crystalline and can exhibit high glass transition temperatures (T_g) of around 300 ˚C, and are often used for their high heat, solvent and flame resistance.[2] The polymers shown in Table 1.1 can either be amorphous or semi-crystalline. The latter is a direct consequence of their rigid aromatic backbone, or hydrogen bonding interactions. The tendency for some of these polymers to crystallize plays a role in the processing step.

Table 1.1. Examples of high performance polymers and their properties.[3]

Entry	Polymer	Backbone structure	T_g (°C)	T_m (°C)	Morphology
1	Polyphenylene sulphide (PPS)	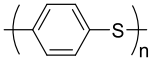	90	290	Semi-crystalline
2	Polyamide (PA)	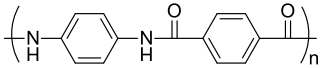	-	dec[a]	Nematic
3	Polyetherimide (PEI)	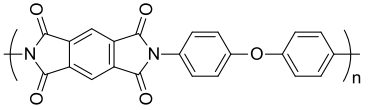	400	dec[a]	Amorphous
4	Polyester (PE) Vectra®	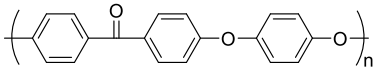	110	280	Semi-crystalline
5	Polyaryletherketone (PAEK)	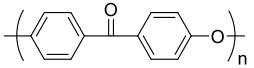	150	350	Semi-crystalline

[a] dec = decomposition

For example, poly(etherimide)s (PEIs) are often amorphous, whereas polyesters and poly(aryletherketone)s are semi-crystalline in nature. Of particular interest are polyetheretherketone (PEEK) and polyetherketone (PEK). The robust polymer backbone has phenyl rings connected with ketone- and ether-functionalities, which are very thermally and chemically stable. Typical degradation temperatures of these thermoplastics are over 500 ˚C, with a melting point around 350 ˚C. They are often semi-crystalline in nature and have a glass transition around 150 ˚C. The properties of PEK and PEEK are especially interesting for the aerospace industry, as next to the excellent properties, the thermoplastic nature opens up an opportunity for processing fibre-reinforced composites for aerospace and automotive applications. However, their limited solubility and high melting point (close to their decomposition temperature) makes it hard to process these materials, which in turn makes them more expensive.

1.1.2 What are the challenges?

High-performance polymers often have to be processed using high temperatures or harsh solvents, which is a disadvantage. Some of these polymers don't even melt and decompose before ever reaching a stable and processable fluid state. They suffer from low solubility, intractability, and low functionality. So far, several approaches have been reported to deal with these challenges. For example, using kinked monomers can reduced chain packing and crystallinity, making the polymers more soluble and lower melting, which in turn makes them easier to process (see Figure 1.1).[4,5] Also, adding alkyl substituents was found to improve the solubility and reduce crystallinity.[6–8] However, the synthesis of monomers comprised of multiple aromatic rings requires several synthetic steps

and are therefore costly, making them less interesting for industrial applications. Also, alkyl substituents tend to compromise the long-term thermo-mechanical performance of the final polymers.

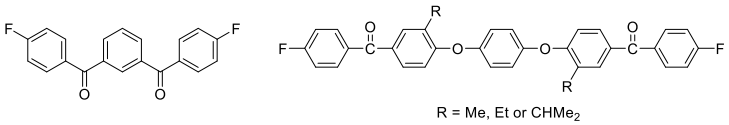

Figure 1.1. Kinked (*meta*-substitution of the central ring) monomer (left) or 5-ring monomers with alkyl substituents (right) can improve the solubility and reduce the crystallinity of the final polymer.

Reducing the chain length can also aid in processing. Low molecular weight polymers, or oligomers, often have a lower melting point (T_m) than high molecular weight polymers due to a reduction in chain entanglements. The oligomers have reduced viscosity if the molecular weight is below a certain threshold called the critical molecular weight of entanglement (CME).[9] A good example is PETI-5, or PhenylEthynyl Terminated Imide, a polyetherimide oligomer with an Mn of 5,000 g/mol, which was developed by researchers at the NASA Langley Research Center (Figure 1.2) in the late 90's.[10,11]

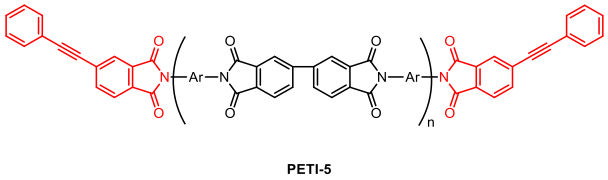

Figure 1.2. Simplified molecular structure of PETI-5, a 5,000 g/mol oligomeric polyetherimide end-capped with phenylethynyl phthalic anhydride (PEPA, red). Ar = combination of 3,3',4,4'-tetracarboxylic acid dianhydride (BPDA) and 85 mol% of 3,4'-oxydianiline (ODA) and 15 mol% 1,3-(3-aminophenoxy)benzene (APB).

The oligomers were end-capped with phenylethynyl end-groups to allow for thermal curing. The minimum melt viscosity before cure was 10^5 Pa s, while the T_g was increased from 210 ˚C to 270 ˚C after cure.[12,13] The strategy of employing thermally curable ethynyl or phenyethynyl containing moieties has also been used in other high-performance polymer formulations, for example, in poly(etherketone)s.[14–18]

Another approach to deal with processing difficulties of high-performance polymers would be the use of hyperbranched polymers, polymers with a completely different polymer backbone architecture. These amorphous polymers have little to no chain entanglements and could provide opportunities to meet the existing challenges. The lack of chain entanglements, and thus poor mechanical properties, are envisioned to be countered with introducing thermally reactive phenylethynyl end-groups, as will be described in this thesis.

1.2 Hyperbranched polymers

1.2.1 Introduction to hyperbranched polymers

Flory theorized about branched (later called hyperbranched) polymer structures around 1950,[19] but synthetic attempts to prepare the branched polymers were not undertaken until 1982 by Kricheldorf et al.[19,20] Kim and Webster proposed the name “hyperbranched polymers” (HBPs) a few years later in their work on hyperbranched polyphenylenes.[21] The hyperbranched polyphenylenes described by Kim and Webster were found to be soluble with molecular weights of over 50,000 g/mol. This is both an advantage in analysis and processing. These macromolecules were found to have a three-dimensional globular topology, which makes them significantly different from their linear analogs. Also, it

appeared that the T_g of these hyperbranched polymers heavily depends on the nature of the end-groups. A range in T_g's of 96–238 ˚C was obtained by varying the end-groups (Figure 1.3), although full substitution was difficult to achieve.[21]

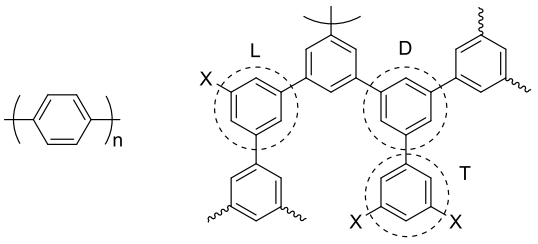

End-group (X)	T_g (˚C)
Br	238
H	127
CH_3	179
$(CH_3)_3Si$	152
Phenyl-α-vinyl	96

Figure 1.3. Linear *p*-polyphenylene (left) is only soluble for n<6, while hyperbranched polyphenylene (right) is soluble up to high molecular weights (>50 Kg/mol). L = linear unit, D = dendritic unit and T is terminal unit.

The degree of branching factor (DB) was introduced to describe the architecture of a polymer and can be measured by integrating the nuclear magnetic resonance (NMR) signals that correspond to certain units in the backbone (as shown in Figure 1.3). The DB ranges from 0 to 1, covering the range from linear polymers (DB=0) to perfectly branched polymers, called dendrimers (DB=1). Hyperbranched systems are basically imperfectly, and often randomly, branched structures. The DB can be controlled by using B_3 co-monomers as a core unit to increase the DB.[22] In contrast, AB co-monomers can be used to reduce the DB.[23] The polydispersity index (PDI) of hyperbranched polymers is often quite high. Methods to reduce the PDI are the afore mentioned use of B_3 core molecules or to use a slow monomer addition method.[24–28] The unique properties of hyperbranched polymers can be placed just in between that of linear and dendritic polymers (Table 1.2).

Table 1.2. General properties of linear, hyperbranched and dendrimeric polymers.[29]

Polymer	Linear	Hyperbranched	Dendrimer
Structure	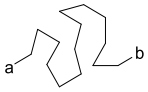	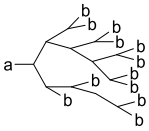	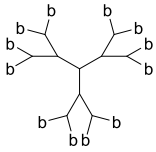
Topology	1D	3D, ellipsoidal	3D, globular
Synthesis	One-step, facile	One-step, facile	Multi-step, not facile
PD	Around 2	>2 to very broad	Close to unity
DB	0	0.4-0.6	1
Solubility	Low	High	Very high
Entanglements	Strong	Few or none	Very few or none
Functional groups	Termini only	At linear + terminal units	At terminal units
Viscosity	High	Low	Very low

Although the advantages of hyperbranched polymers over linear polymers are mainly related to viscosity and functional groups, the mechanical properties are poor due to a lack of chain entanglements. Nevertheless, hyperbranched systems are more easily prepared than dendrimers and do not suffer from

limited growth due to steric hindrance. There are several reasons to investigate hyperbranched systems in more detail. In terms of solution processing one might consider them if the linear analog is insoluble (e.g. *p*-polyphenylene). Also, the ability to reduce the melt-viscosity, improving the thermal stability, improving cure kinetics and their use in coatings and as drug delivery agents are appealing features.[30] The large number of functional groups in hyperbranched and dendrimeric systems raise the following question: what is more important for the final properties? The nature and number of the functional groups or the nature of the backbone of the polymer? The functional groups have a strong influence on the glass-transition temperature[31] and together with parameters, such as the degree of branching, there are many opportunities for tuning the final properties of these polymers. The concern that the availability of suitable monomers is limiting the applications has decreased with the number of papers being published over the last years. Today, many monomers are available from commercial sources that can be used to design and synthesize (hyper) branched polymers.

1.2.2 Current applications of hyperbranched polymers

Aliphatic HBPs currently find application as rheology modifiers[21] and toughening agents for epoxides,[32] but are also used in membranes,[33] coatings,[34] dyes, lubricants, wetting agents and more.[35] Synthetic aliphatic HBPs are commercially available, of which Starburst™ (Dendritech, Inc.), Superfect™ (Qiagen), Astramol™ (DSM), Hybrane™ (DSM) and Boltorn™ (Perstop) are examples (Hybrane™ and Boltorn™ are shown in Figure 1.4).[36]

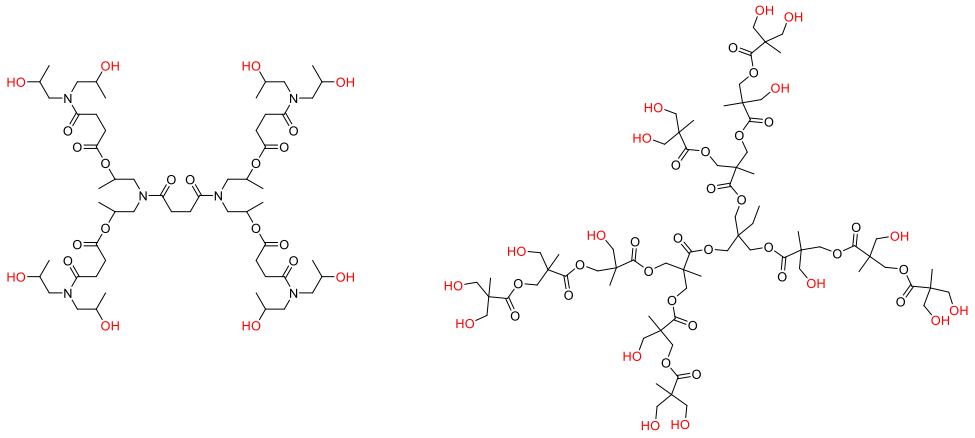

Figure 1.4. Commercially available polyesteramide Hybrane™ (left) and polyester Boltorn™ (right).

The main application for hyperbranched polymers is as rheology modifiers. This exploits the use of their remarkable flow behaviour. However, this thesis is focussed on *all-aromatic* hyperbranched polymers, as this type of polymer is more suitable for high-performance applications. Today, no commercial all-aromatic hyperbranched polymers are available.

1.2.3 Hyperbranched all-aromatic polymers

As mentioned before, Kim and Webster pioneered the synthesis of all-aromatic hyperbranched polymers and reported both the synthesis of hyperbranched polyphenylenes and polyamides.[21,37] HBPs already received much attention due to their unique properties like excellent solubility, low solution viscosity, large amount of (interchangeable) functional groups, easily tuneable glass transition, architecture, pore size and ease of synthesis.[29] These characteristics are in contrast with their linear analogs, who often suffer from low solubility, low

functionality and challenging processability due their high melting point and tendency to crystallize.

Several strategies have been presented in literature to synthesize all-aromatic hyperbranched polymers. One of the most common examples is the use of an A_2 (difunctional monomer) + B_3 (trifunctional monomer) system, where a network is formed immediately. This approach is often used to make membranes. A limitation in this approach is the risk of premature gel formation. Another approach is the use of AB_2 monomers (see also Table 1.4), which results in hyperbranched polymers that do theoretically not have the ability to form interchain connections and therefore are less prone to form gels during synthesis. The formation of aromatic HBPs exploiting AB_2 monomers will be described in this thesis. The monomers shown in Table 1.3 open routes towards additional functionalization of HBPs and can be regarded as macromonomers. All monomers shown can be polymerized under well-established solution-based polymerization conditions.

1.2.4 Hyperbranched polymer model systems

Several hyperbranched polymer chemistries were evaluated by us to serve as model systems to investigate our idea to combine processable hyperbranched polymers with reactive phenylacetylene end-groups to counter the poor mechanical properties due to reduced chain entanglements. Hyperbranched polyphenylene (entry 1, Table 1.3), generally presumed to be the most stable polymer, did not give the desired high molecular weight and sublimation of unreacted small molecules resulted in poor thermal stability during cure. Hyperbranched polyamides (entry 2, Table 1.3) were found to exhibit very high glass transition temperatures and flow points due to hydrogen bonding. The

absence of a mobile fluid phase prevented end-groups to react with one another and form crosslinks. Also, the amine groups appeared to be quite reactive and needed to be end-capped (i.e. protected) in the final polymer. This, together with solubility problems, were reasons to declare this material unsuitable as a model system. When considering hyperbranched polyesters (entry 3, Table 1.3) we found that the thermal stability was not sufficient and transesterification complicated analysis of the intermediate structures. When looking into hyperbranched poly(aryl ether ketone)s (HBPAEKs) (entry 4, Table 1.3), we found a thermally stable and robust system with no hydrogen bonding issues, which had functionalizable, yet stable fluorine end-groups, and showed flow behaviour to facilitate the intended curing studies.[38] Additional advantages were found in opportunities for analysis with fluorine NMR (^{19}F NMR) and the facile monomer synthesis.

Table 1.3. Examples of all-aromatic hyperbranched polymers prepared from AB_2 monomers.

Entry	Backbone	Monomer	End-group	T_g[a]	Ref
1	Polyphenylene	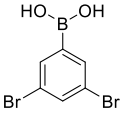	-Br	234	[21]
2	Polyamide	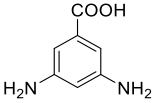	-NH_2	>400	[39]
3	Polyester	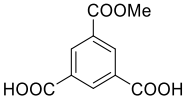	-COOH	250	[40,41]
4	Polyaryletherketone	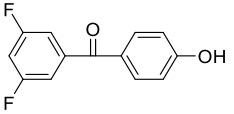	-F	162	[31, 42]

[a] Glass transition temperatures depend greatly on the end-groups

1.2.5 Hyperbranched poly(aryletherketone)s

Several methods to obtained HBPAEKs have been described in the literature and examples of monomers are summarized in Table 1.4. We used the AB_2 approach to obtain our desired hyperbranched polymers without the risk of gelation and therefore only the routes using this approach will be discussed. From all monomers, the approach reported by Hawker et al. (entry 2, Table 1.4) was deemed to be our preferred approach, as the monomers can be made via an easy and scalable two-step reaction and it was already shown in the literature that the corresponding polymers flow easily.[38] The other entries in Table 1.4 are more labour intensive to synthesize and thus less interesting.

Table 1.4. AB_2 monomers to synthesize poly(aryletherketone)s.

Entry	AB_2 monomer	End-groups	Ref
1	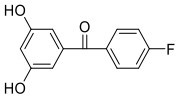	-OH	31
2	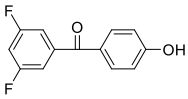	-F	31
3	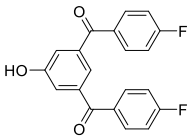	-F	43
4	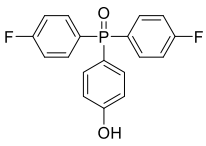	-F	44

1.3 Scope and outline

In this thesis we will describe an approach towards the design and synthesis of all-aromatic hyperbranched poly(aryletherketone)s with thermally polymerizable phenylethynyl end-groups. We will discuss how controlled crosslinking affects the (thermo)mechanical properties of the final thermoset films. The results will be contrasted with well-known linear aryletherketone-based polymers. We aim to establish the design rules with respect to monomer selection, end-groups concentration and processing considerations. We will demonstrate that these novel crosslinked all-aromatic hyperbranched poly(aryletherketone)s are excellent candidates for high temperature gas separation applications.

In **Chapter 2** we will explain the synthesis route towards HBPAEKs, describes the chemistry and shows how to use the existing end-groups. Their structures will be analysed by atomic force spectroscopy (AFM) and common analysis techniques like nuclear magnetic resonance (NMR), size exclusion chromatography (SEC). The HBPs will also be evaluated by rheology, where we can verify their non-entangled behaviour by looking at the stress relaxation. With rheology we can also observe curing events taking place with following the storage modulus and loss modulus over a temperature range.

In **Chapter 3** we will discuss the introduction of a thermally reactive end-group that can compensate the lack of chain entanglements to give mechanical properties to the polymers. We will show that this can be done in a controlled manner, supported by elemental analysis and NMR. The curing behaviour will be monitored with rheology and we will show how to obtain free standing materials from the initially brittle polymer networks. We will show the effect of adding reactive end-groups to the HBPAEKs and the (thermo)mechanical properties will

be tested with dynamic mechanical analysis (DMA). We will use tensile testing to observe the stress/strain behaviour and we expect to see brittle fracture and no necking, in contrast to linear PEEK. This will be the direct result of the great difference in polymer architecture.

In **Chapter 4** we will illustrate how gas separation membranes can be made from these hyperbranched polymer networks can be used as membranes, in collaboration with the University of Twente. With spectroscopic ellipsometry we will look into several features that govern the properties of membranes like excess free volume, swelling in CO_2 and water and the T_g. This will give access to fully aromatic HBPs with tuneable properties that can be spin-coated on a solid support. Crosslinking will provide the opportunity to tune the effective fractional free volume (EFFV) and the T_g.

The gas separation properties of the HBPAEK membranes will be described in **Chapter 5**. Also, the membranes will be exposed to elevated temperatures for a prolonged period of time and their performance will be compared with existing membranes.

1.4 References

1. Guo, Q. *Thermosets: Structure, Properties, and Applications - Google Books*. (Elsevier, 2018).
2. Johnson, R. O. & Burlhis, H. S. Polyetherimide: A new high-performance thermoplastic resin. *J. Polym. Sci. Polym. Symp.* **70,** 129–143 (2007).
3. Mark, J. E. *Polymer data handbook*. (Oxford University Press, 1999).
4. Singh, R. & Hay, A. S. Synthesis and physical properties of soluble, amorphous poly(ether ketone)s containing the o-dibenzoylbenzene moiety. *Macromolecules* **25,** 1017–1024 (1992).
5. Singh, R. & Hay, A. S. Synthesis of novel poly(ether ketone)s containing the o-dibenzoylbenzene moiety. *Macromolecules* **24,** 2637–2639 (1991).
6. Ueda, M., Toyoda, H., Nakayama, T. & Abe, T. Synthesis of photoreactive poly(ether ether ketone)s containing alkyl groups. *J. Polym. Sci. Part A Polym. Chem.* **34,** 109–115 (1996).
7. Ueda, M., Nakayama, T. & Mitsuhashi, T. Synthesis of photoreactive isopropyl-substituted poly(phenylene ether ether ketone). *J. Polym. Sci. Part A Polym. Chem.* **35,** 371–376 (1997).
8. Taguchi, Y., Uyama, H. & Kobayashi, S. Synthesis and properties of alkyl-substituted poly(aryl ether ketone)s showing high solubility toward organic solvents. *J. Polym. Sci. Part A Polym. Chem.* **34,** 561–565 (1996).
9. Wool, R. P. Polymer Entanglements. *Macromolecules* **26,** 1564–1569 (1993).
10. Wood, K. H., Orwoll, R. A., Jensen, B. J., Young Emory, P. R. & College

Harold McNair, H. M. CURE CHEMISTRY OF PHENYLETHYNYL TERMINATED OLIGOMERS. *42nd Int. SAMPE Symp.* **42,** 1271–1282 (1997).

11. Tang, Y., Xie, Y., Pan, W.-P. & Riga, A. Thermal properties of PETI-5/IM7. *Thermochim. Acta* **357,** 239–249 (2000).

12. Hou, T. H., Jensen, B. J. & Hergenrother, P. M. Processing and Properties of IM7/PETI Composites. *J. Compos. Mater.* **30,** 109–122 (1996).

13. Hergenrother, P. ., Connell, J. . & Smith, J. . Phenylethynyl containing imide oligomers. *Polymer* **41,** 5073–5081 (2000).

14. Núñez, F. M., de Abajo, J., Mercier, R. & Sillion, B. Acetylene-terminated ether-ketone oligomers. *Polymer* **33,** 3286–3291 (1992).

15. Delfort, B., Lucotte, G. & Cormier, L. Ethynyl-terminated polyethers from new end-capping agents: Synthesis and characterization. *J. Polym. Sci. Part A Polym. Chem.* **28,** 2451–2464 (1990).

16. Lucotte, G., Cormier, L. & Delfort, B. Ethynyl terminated ethers. Synthesis and thermal characterization of 2,2 bis (ethynyl-4-phenylcarbonyl-4-phenoxy-4-phenyl) propane and 2,2 bis (ethynyl-4-phenylsulfonyl-4-phenoxy-4-phenyl) propane. *Polym. Bull.* **24,** 577–582 (1990).

17. Taguchi, Y., Uyama, H. & Kobayashi, S. Synthesis of a novel cross-linkable poly(aryl ether ketone) bearing acetylene groups at chain ends. *Macromol. Rapid Commun.* **16,** 183–187 (1995).

18. Hedrick, J. L., Yang, a. C.-M., Scott, J. C., Economy, J. E. & McGrath, J. E. Elastomeric behaviour of crosslinked poly(aryl ether ketone)s at elevated temperatures. *Polymer* **33,** 5094–5097 (1992).

19. Flory, P. J. MOLECULAR SIZE DISTRIBUTION IN THREE DIMENSIONAL

POLYMERS .6. BRANCHED POLYMERS CONTAINING A-R-BF-1 TYPE UNITS. *J. Am. Chem. Soc.* **74,** 2718–2723 (1952).

20. Kricheldorf, H. R., Zang, Q. Z. & Schwarz, G. New polymer syntheses: 6. Linear and branched poly(3-hydroxy-benzoates). *Polymer* **23,** 1821–1829 (1982).

21. Kim, Y. H. & Webster, O. W. HYPERBRANCHED POLYPHENYLENES. *Macromolecules* **25,** 5561–5572 (1992).

22. Sennet, L., Fossum, E. & Tan, L.-S. Branched poly(arylene ether ketone)s with tailored thermal properties: Effects of AB/AB2 ratio, core (B3) percentage, and reaction temperature. *Polymer* **49,** 3731–3736 (2008).

23. Jikei, M., Fujii, K., Yang, G. & Kakimoto, M. Synthesis and properties of hyperbranched aromatic polyamide copolymers from AB and AB(2) monomers by direct polycondensation. *Macromolecules* **33,** 6228–6234 (2000).

24. Hanselmann, R., Hölter, D. & Frey, H. Hyperbranched Polymers Prepared via the Core-Dilution/Slow Addition Technique: Computer Simulation of Molecular Weight Distribution and Degree of Branching. *Macromolecules* **31,** 3790–3801 (1998).

25. Bharathi, P. & Moore, J. S. Controlled Synthesis of Hyperbranched Polymers by Slow Monomer Addition to a Core. *Macromolecules* **33,** 3212–3218 (2000).

26. Möck, A., Burgath, A., Hanselmann, R. & Frey, H. Synthesis of Hyperbranched Aromatic Homo- and Copolyesters via the Slow Monomer Addition Method. *Macromolecules* **34,** 7692–7698 (2001).

27. Cheng, K.-C. Kinetic model of hyperbranched polymers formed by self-condensing vinyl polymerization of AB∗ monomers in the presence of multifunctional core molecules with different reactivities. *Polymer* **44,** 877–882 (2003).

28. Cheng, K.-C., Chuang, T.-H., Chang, J.-S., Guo, W. & Su, W.-F. Effect of Feed Rate on Structure of Hyperbranched Polymers Formed by Self-Condensing Vinyl Polymerization in Semibatch Reactor. *Macromolecules* **38,** 8252–8257 (2005).

29. Yan, D., Gao, C. & Frey, H. *Hyperbranched Polymers: Synthesis, Properties, and Applications*. (Wiley, 2011).

30. Gao, C. & Yan, D. Hyperbranched polymers: from synthesis to applications. *Prog. Polym. Sci.* **29,** 183–275 (2004).

31. Hawker, C. J. & Chu, F. Hyperbranched Poly(ether ketones): Manipulation of Structure and Physical Properties. *Macromolecules* **29,** 4370–4380 (1996).

32. Jin, F.-L. & Park, S.-J. Thermal properties and toughness performance of hyperbranched-polyimide-modified epoxy resins. *J. Polym. Sci. Part B Polym. Phys.* **44,** 3348–3356 (2006).

33. Bhadra, S., Ranganathaiah, C., Kim, N. H., Kim, S.-I. & Lee, J. H. New hyperbranched polymers for membranes of high-temperature polymer electrolyte membrane fuel cells: Determination of the crystal structure and free-volume size. *J. Appl. Polym. Sci.* **121,** 923–929 (2011).

34. Johansson, M. *et al.* Design of coating resins by changing the macromolecular architecture: Solid and liquid coating systems. *Prog. Org.*

Coatings **48,** 194–200 (2003).

35. Seiler, M. Hyperbranched polymers: Phase behavior and new applications in the field of chemical engineering. *Fluid Phase Equilib.* **241,** 155–174 (2006).

36. Voit, B. I. Hyperbranched polymers: a chance and a challenge. *C. R. Chim.* **6,** 821–832 (2003).

37. Kim, Y. H. Highly branched polymers. *Adv. Mater.* **4,** 764–766 (1992).

38. Kwak, S.-Y. & Ahn, D. U. Processability of Hyperbranched Poly(ether ketone)s with Different Degrees of Branching from Viewpoints of Molecular Mobility and Comparison with Their Linear Analogue. *Macromolecules* **33,** 7557–7563 (2000).

39. Kim, Y. H. Lyotropic liquid crystalline hyperbranched aromatic polyamides. *J. Am. Chem. Soc.* **114,** 4947–4948 (1992).

40. Turner, S. R., Walter, F., Voit, B. I. & Mourey, T. H. HYPERBRANCHED AROMATIC POLYESTERS WITH CARBOXYLIC-ACID TERMINAL GROUPS. *Macromolecules* **27,** 1611–1616 (1994).

41. Brenner, A. R., Voit, B. I., Massa, D. J. & Turner, S. R. Hyperbranched polyesters: End group modification and properties. *Macromol. Symp.* **102,** 47–54 (1996).

42. Chu, F. & Hawker, C. J. A versatile synthesis of isomeric hyperbranched polyetherketones. *Polym. Bull.* **30,** 265–272 (1993).

43. Kricheldorf, H. R., Vakhtangishvili, L., Gert Schwarz, A. & Krüger, R.-P. Cyclic Hyperbranched Poly(ether ketone)s Derived from 3,5-Bis(4-fluorobenzoyl)phenol. *Macromolecules* **36,** 5551–5558 (2003).

44. Bernal, D. P., Bankey, N., Cockayne, R. C. & Fossum, E. Fluoride-terminated hyperbranched poly(arylene ether phosphine oxide)s via nucleophilic aromatic substitution. *J. Polym. Sci. Part A Polym. Chem.* **40,** 1456–1467 (2002).

Chapter 2

Cure Behaviour of Neat All-aromatic Hyperbranched Poly(aryletherketone)s

Abstract

We have prepared a series amorphous hyperbranched poly(aryletherketone)s (HBPAEKs) from an AB_2 monomer, (3,5-difluorophenyl)(4-hydroxyphenyl)methanone, with three different molecular weights, i.e. 22k, 69k and 123k. The globular structure of all HBPAEKs was confirmed using AFM and are in the range of 4, 6 and 7 nm, respectively. The as-prepared HBPAEKs undergo thermal post-condensation chemistry, which results in crosslinking. No additional reactive functionalities are needed, crosslinking takes place via unreacted –F and –OH functionalities present in the polymer structure. We observed typically non-entangled behaviour for the uncured HBPAEKs in the melt with a minimum storage modulus of 100-300 Pa at ~240 ˚C, after which the HBPAEKs start to cure. The T_g's of the uncured HBPAEKs range from 145 ^oC (22K) to 158 ^oC (123K). Upon crosslinking the Tg's show a small upward shift to 153 ^oC and 169 ^oC, respectively.

This chapter is based on the paper: "Cure Behaviour of Neat All-aromatic Hyperbranched Poly(aryletherketone)s" by Vogel et al., to be submitted.

2.1 Introduction

Typical processing temperatures for linear poly(aryletherketone)s (PAEKs) easily exceed 350 °C but HBPAEKs are able to show flow at temperatures as low as 190 °C, just 40 °C above their glass-transition temperature (T_g).[1] The general properties of hyperbranched polymers is in between that of dendrimers and linear polymers; the solubility and functionality are very high but they have little to no entanglements, which translates to poor mechanical properties.

Several attempts have been reported in literature to covalently crosslink hyperbranched polymers by using reactive end-groups and an overview of the chemistries used can be found in a review paper by Olofsson et al.[2]

For all-aromatic HBPs several crosslinking strategies have been briefly discussed in the previous chapter. The use of allyl, propargyl and epoxide end-groups provided thermally curable HBP networks.[3] Thermally curable phenylethynyl groups can be used to prepare HBP networks, which was demonstrated with hyperbranched polyimide precursors.[4] Also, Voit et al. demonstrated the possibility of curing alkyne functionalized hyperbranched polyphenylenes photochemically or with the use of organic azides.[5] Thermal analysis data (DSC), showing a curing exotherm is often the only information provided, while the (thermo)mechanical behaviour and stress-strain data are missing as samples are too brittle to handle. Crosslinking attempts for specifically HBPAEKs from A_2 + B_3 monomers have been described by Jiang et al. by both introducing phthalonitrile groups and a curing agent in the form of a diamine (*p*-BAPS).[6] With this two-step modification of the backbone they managed to prepare films and report some mechanical properties. A storage modulus (E') of ~1 GPa was measured with a dynamic mechanical analyser, but no stress-strain data was reported. Additionally, they described in a follow-up paper that they achieved

crosslinking by using phenylethynyl groups, again no information was provided with respect to mechanical properties.[7] They confirmed with DSC that the alkyne groups could indeed be thermally cured and a thermoset was obtained with a gel fraction of 93%.

In this chapter we will report on the ability of an all-aromatic HBPAEK model system to crosslink via a simple thermal treatment step in the melt phase, using existing unreacted functional groups (–F and –OH) that are present in the HBPAEK. To prove this, we prepared 3 HBPAEKs with different target molecular weights, i.e. 22k, 69k and 123k, as shown in Scheme 2.1, using (3,5-difluorophenyl)(4-hydroxyphenyl)methanone as the AB_2 monomer. The fact that neat HBPAEKs are able to crosslink without introducing additional functionalization has been largely overlooked.

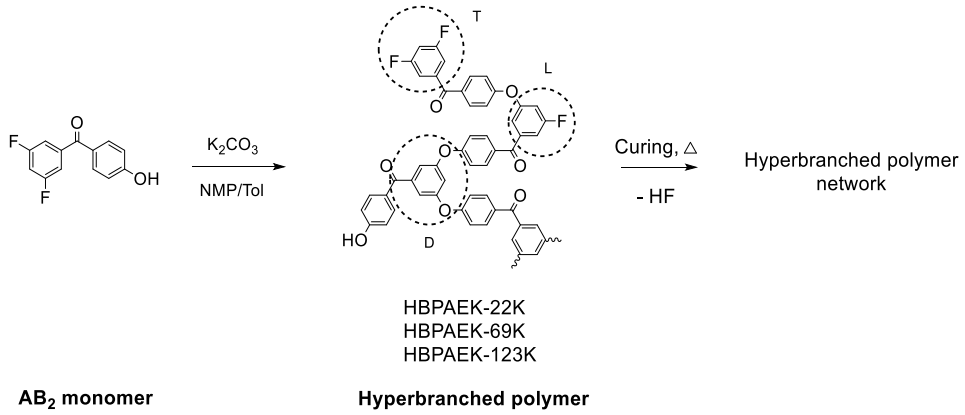

Scheme 2.1. Polymerization of the AB_2 monomer, 3,5-difluorophenyl(4-hydroxyphenyl)methanone, followed by thermal crosslinking. In the all-aromatic hyperbranched polymer: T = terminal unit, L = linear unit and D = dendritic unit. The molecular weights of the precursor polymers are 22k (HBPAEK-22K), 69k (HBPAEK-69K), and 123k (HBPAEK-123K), respectively. Thermal curing leads to a hyperbranched polymer network.

We will demonstrate that the crosslink density, and hence the final network properties, can be manipulated by controlling the molecular weight of the HBPAEK precursor and by controlling the crosslinking time and temperature.

2.2 Experimental section

2.2.1. Materials and equipment

3,5-difluorobenzoyl chloride was purchased from Alfa Aesar, Anisole, HBr and linear PEEK (Mn of ~10K, Mw of ~20K) from Sigma Aldrich and all were used as received. Dry NMP and dry toluene were obtained from Acros Organics and used as received.

Differential Scanning Calorimetry (DSC) curves were measured on a Perkin Elmer DSC8000 at 10 °C/min (heating and cooling) under nitrogen atmosphere in crimped aluminium sample pans. The thermal gravimetric analysis (TGA) measurements were done with a Perkin Elmer TGA4000 at 10 °C/min under nitrogen purge in aluminium pans. ^{1}H NMR (400 MHz) and ^{13}C NMR (100 Hz) spectra were recorded on a Varian AS-400 spectrometer and chemical shifts are given in ppm (σ) relative to tetramethylsilane (TMS) as an internal standard. The ^{1}H NMR splitting patterns are designated as follows: s (singlet), d (doublet), dd (double doublet), t (triplet), q (quartet), m (multiplet) and b (broad signal). The coupling constants if given are in Hertz. ^{19}F NMR (564 MHz) was recorded on a 600 MHz Bruker spectrometer in reference to $CFCl_3$. GPC measurements were performed using a Shimadzu GPU DHU-20A3 equipped with a refractive index detector; polystyrene standards were used for calibration of the instrument. All samples were dissolved at a 1 mg/mL concentration in NMP and filtered over a 0.45 µm PTFE filter prior to use. Samples for mass spectrometry were analysed on a Shimadzu GC/MS-QP2010S in electron-impact ionization (EI) mode with direct

injection. Data were acquired and processed using GCMS solution software. IR spectra were recorded from powdered samples on a Perkin Elmer Spectrum 100 FT-IR Spectrometer equipped with an ATR insert, measuring from 600-4000 cm^{-1}. Films were casted in a Petri dish and held under vacuum for 1h at 60, 1h at 100, 1h at 200, 1h at 300 °C, and 1h at 370 °C. Rheology experiments were performed with a TA Instruments ARES G2, 8 mm parallel plates (the relaxation experiments were performed on a Thermo Scientific Haake Mars III. Parallel plates of 8 mm were used at 1 Hz frequency with 2% strain.) Elemental analysis was performed by Mikroanalytisches Laboratorium KOLBE in Germany by using ICP with an accuracy of 0.01%, the measurements were performed in duplo and averaged out. Atomic force microscopy (AFM) has been utilized to visualize the resulting hyperbranched architecture prior to cross-linking. AFM micrographs of all samples were deposited by spin casting on a mica substrate from chloroform (30 ug/ml). The imaging was performed in PeakForce quantiative nanomechanical property maping (QNM) mode using a multimode AFM (Bruker) with a NanoScope V controller and silicon probes (resonance frequency of 70 Hz and spring constant of 0.4 N/m).

2.2.2. Syntheses

(3,5-difluorophenyl)(4-hydroxyphenyl)methanone, AB_2. A 1L round bottom flask was charged with 50 g (0.2 mol) (3,5-difluorophenyl)(4-methoxyphenyl) methanone, which was synthesized according to procedures described in literature.[8] To the flask was added 450 mL of acetic acid and the mixture was stirred and heated to 50 °C until a transparent solution was obtained. Then 300 mL HBr (48%) was added and a white precipitate was formed. The mixture was heated to 130 °C for a steady reflux (the mixture became transparent at 100 °C). The reaction was stirred overnight and TLC (DCM as eluent) confirmed the completion of the reaction (1 spot, Rf = 0.2). The reaction was cooled and the

mixture was evaporated to dryness. The white/pinkish solid was added to 1.5 L water and extracted with 3 x 300 mL of ether. The product was recrystallized from 100% EtOH and dried overnight in vacuum at 60 °C resulting in 43.1 g the target compound as a white solid, 91 %. MP: 150-151 °C. FT-IR (cm^{-1}): 3400-3000, 1640, 1582, 1438, 1329. MS (EI), m/z: 234 (M), 121. ^{1}H NMR (DMSO-d_6), δ = 10.58 (s,1H), 7.9 (d, J = 8.7, 2H), 7.51-7.47 (tt, J = 2.4 Hz, 1H), 7.31-7.29 (m, 2H), 6.90 (d, J = 8.7, 2H). 13C-NMR (DMSO-d_6), δ = 191.98, 163.67, 163.06, 161.20, 142.01, 133.12, 127.20, 115.89, 112.54, 107.34. Anal. Calcd for C13H8F2O2: C, 66.67; H, 3.44; F, 16.22. Found C, 66.58; H, 3.37; F, 16.06.

Fluorine-terminated HBPAEK. To a 250 mL round bottom flask equipped with Dean-Stark trap was added 15 g of AB_2 monomer, 100 mL dry NMP, 75 ml dry toluene and 15 g K_2CO_3. This was stirred for 3 h at 165 °C while de toluene/water azeotrope was collected. The temperature was subsequently raised over 30 minutes to 200 °C and the stirring was continued for 3-4 h (depending on the aimed Mw). The mixture was cooled to r.t. and precipitated in 3 L water. The collected solid was dissolved in THF, precipitated in MeOH and the collected solid was boiled in MeOH, filtered hot, boiled in EtOH and filtered hot and dried in vacuo at 60 °C and 150 °C overnight to obtain the target compound as an off-white and very fine powder, 11.2 g, 82%. FT-IR (cm^{-1}): 1663, 1581, 1501, 1435, 1321, 1233. ^{1}H NMR (400 MHz, $CDCl_3$), δ = 7.90-7.50 (m, 2H), 7.30-6.50 (m, 5H).

2.2.3. Synthesis of HBPAEK model systems

HBPAEKs were first synthesized by Hawker et al.[8] They can be synthesized via a nucleophilic aromatic substitution reaction using an AB_2-type monomer, where fluorine is displaced and an ether bond is formed. The advantage of this approach over the frequently used $A_2 + B_3$ synthesis route[9] is that there is very little risk of gelation of the reaction mixture, as the possibility of crosslinking between

polymers is theoretically not possible. Also, the type of end-groups is fixed at B, or fluorine (F), in this case.

The resulting HBPAEK polymers are different from conventional linear PAEKs. HBPAEK polymers form globular structures, where the large number of functional groups is mainly located at the periphery.[10,11] For the same Mw, hyperbranched polymers have a smaller radius of gyration (R_g) compared to their linear analogs.[12] The size of the globules might affect the properties of the final network and therefore 3 Mw's have been investigated. We have used the synthetic procedure, as outlined in Scheme 2.1, to successfully obtain three different molecular weight HBPAEKs by varying the reaction time from 3, 3.5 and 4 h, respectively.

2.3 Results and discussion

2.3.1. Size exclusion chromatography

The Mw after 3h stirring was in line with literature[8] and when we increased the reaction time, the Mw increased and the PDI, as expected, broadened (see Table 2.1).[1] We have removed low molecular weight impurities by extraction methods described in the experimental section. For the work reported in this chapter, we prepared polymers with a Mw of 22K (HBPAEK-22K), 69K (HBPAEK-69K) and 123K (HBPAEK-123K). Where HBPAEK-22K appears bimodal, the higher MWs are bi- and even tri-modal, as shown in Figure 2.1. This is most probably the result of the irregular structure and polycondensation mechanism of the HBPs.[13] When using SEC the real molecular weight of HBPs is underestimated, as we are measuring against linear polystyrene standards. The coil size for linear and hyperbranched polymers of the same Mw are not equal. SEC can only be used as an indication of

the true Mw. When the Mw increases the PDI also increased to values >10, most likely because polymer globules start to connect.

The conditions under which the Mw's for HBPAEKs are obtained is often not reported,[1,8] but this information is crucial when it comes to understanding the final polymer properties. Also, chromatograms are often not reported, which makes it impossible to evaluate the molecular weights and polydispersity.

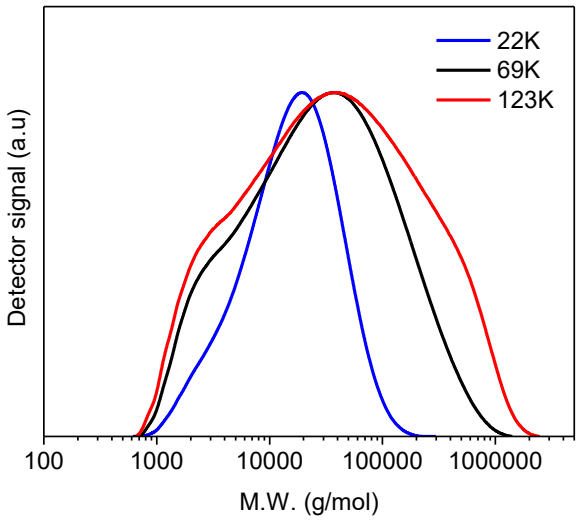

Figure 2.1. The SEC data of HBPAEK-22K, HBPAEK-69K and HBPAEK-123K in NMP. Both HBPAEK-22K and HBPAEK-69K are bimodal. HBPAEK-123K is trimodal. Broadening of the molecular weight is the result of linking several HBPAEK globular structures.

Table 2.1. Polymer SEC and AFM analysis results for HB PAEK-22K, HB PAEK-69 and HB PAEK-123K.

Entry	Reaction time (h)[a]	Mn (kg/mol)[b]	Mw (kg/mol)	PDI	DB[c]	Theoretical diameter (nm)[d]	Measured diameter (nm)[e]	Theoretical %F[f]	Measured %F[g]
1	3	9	22	1.9	0.47	6.11	4.33	8.95	6.82
2	3.5	9	69	7.3	0.50	8.11	5.90	8.89	6.91
3	4	10	123	12.9	0.51	9.38	7.38	8.73	7.78

[a] at 200 ˚C

[b] measured in NMP/LiBr at 1.0 mg/ml against linear polystyrene

[c] measured by ^{19}F NMR, using $DB = \frac{2T}{2T+L}$

[d] calculated from Rg=bN$^{1/4}$

[e] measured with atomic force microscopy (AFM)

[f] calculated using Chemdraw 15 software

[g] Ion chromatography (IC) elemental analysis, +/- 0.01%

2.3.2. Polymer elemental analysis

Elemental analysis can be used to determine the content of certain elements in a polymer. We can use this to determine the content of fluorine in our samples and learn about their composition over a range of molecular weights. For the HBPAEKs made from AB_2 monomers, the theoretical percentage of fluorine levels off at a value just below 9%, while the number of fluorine end-groups can be calculated by the degree of polymerization DP+1. Using elemental analysis, we observed a mismatch in the fluorine content, as reported in Table 2.1. The measured values are up to 24% lower when compared to the theoretical values. We propose that this lower content is the result of dehalogenation side-reactions during synthesis. Apparently, using a Dean Stark-trap is not enough to remove all the water that is formed during the formation of the reactive species and this water will presumably cause some hydrolysis (conversion of –F to –OH groups). The water content of the solvent might also play a role and is suggested to be the reason for the difference among the three Mw batches. Having more –OH groups will also explain why this polymerization reaction forms a gel when the reaction time is increased to 5h at 200 °C (4h is still soluble), as interchain connections (crosslinking) now become possible.

2.3.3. Degree of branching

An indicator for the HBPAEK architecture can be obtained by using a parameter called the degree of branching (DB). This value can be calculated by integration of the Fluorine (F) NMR signal corresponding to the different types of units that are found in a HBPAEK: linear (L) and terminal (T). Hawker and co-workers showed that for HBPAEK the DB can be determined by ^{19}F NMR.[8] The values obtained by the integration of the signals can be inserted into the following equation to obtain the degree of branching:

$$DB = \frac{2T}{2T+L} \qquad (1)$$

where T refers to the terminal units and L refers to the linear units, also shown in Scheme 2.1. All three HBPAEK batches have a DB of around 0.5, as listed in Table 2.1, which is the statistically expected value for these types of hyperbranched polymers.[14] In Figure 2.2 the ^{19}F NMR spectrum of 69K HBPAEK is shown as an example. The integration of terminal fluorine groups (T) on the left (-107.8 ppm) and linear fluorine groups (L) on the right (-108.2 ppm) give values of 1 and 0.99, respectively. As terminal units (T) contain two fluorine atoms, this value should be divided by two, before using equation 1.

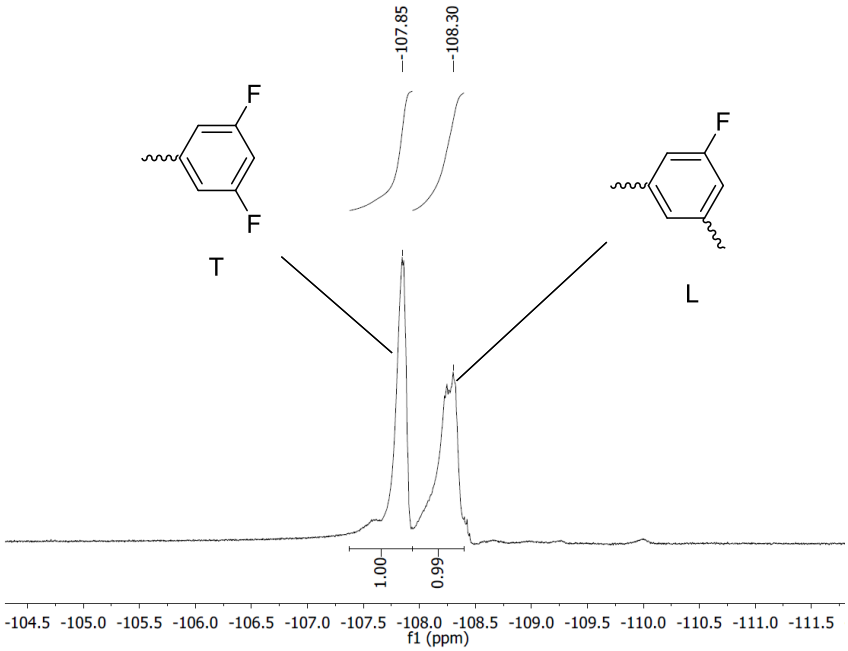

Figure 2.2. Representative ^{19}F NMR spectrum of HBPAEK-69K in $CDCl_3$ taken at 564 MHz, DB=0,50. The two distinct signals correspond to the terminal units T (-107.8 ppm) and linear units L (-108.2 ppm).

2.3.4. Atomic force microscopy

Hyperbranched polymers exhibit three-dimensional globular structures. From the Mw we can calculate a theoretical value for the average size of the globules. To calculate the theoretical radii of gyration, the following equation was used:

$$R_g = bN^{1/4} \qquad (2)$$

where b is the length of the monomer repeat unit (8.4 Å) and N is the number of monomers (derived from the Mw). The diameters calculated using this equation

are reported in Table 2.1. The dimension of branched polymer systems can be visualized with atomic force spectroscopy (AFM), as reported by Sheiko et al.[15,16] We have spin coated dilute HBPAEK solutions (30 µg/ml in $CHCl_3$) on mica substrates and analysed the globular shape of our 3 HBPAEK samples. The results are shown in Figure 2.3. The micrographs in Figure 2.3 show the presence of individual globular structures. Measurements of the HBPAEK globules are summarized in Table 2.1. The HBPAEK-22K shows agglomeration of the globules with a size of 50 nm, corresponding to about 25 globules. For the HBPAEK-69K and HBPAEK-123K this agglomeration is not observed.

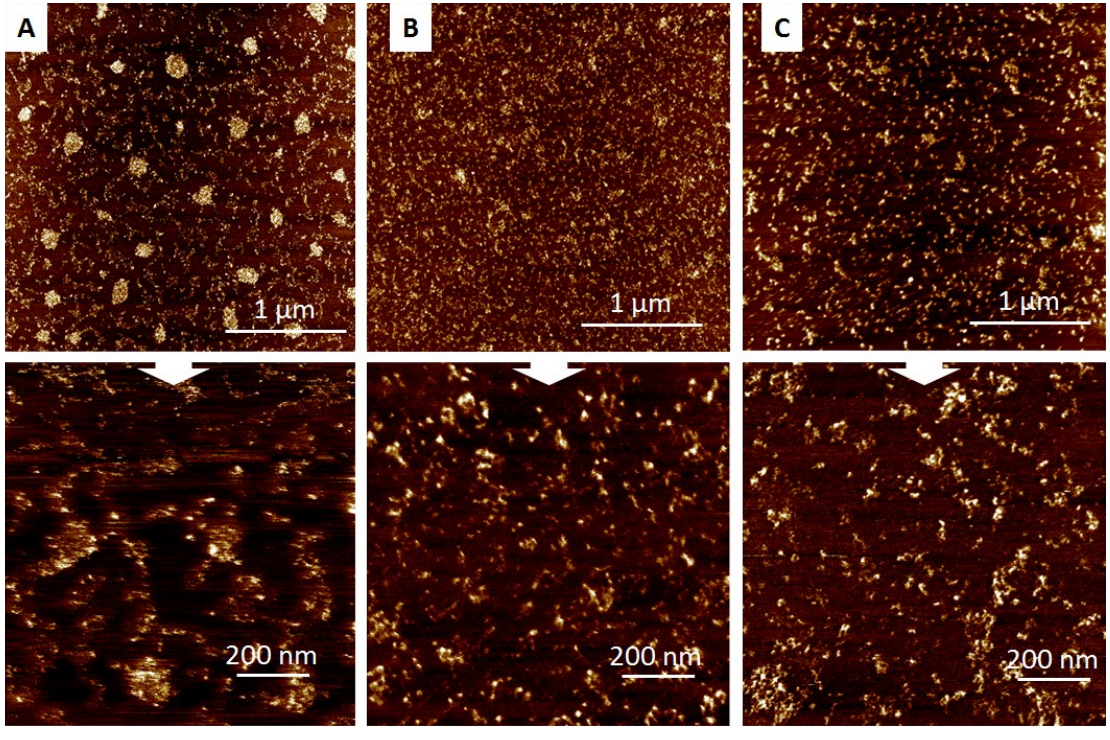

Figure 2.3. AFM pictures showing the individual polymer globules and clusters of the synthesized HBPAEKs (A=22K, B=69K, C=123K). Aggregation of the polymer globules is most apparent in A (HBPAEK-22K). These polymer globules can be considered hard spheres and show little to no overlap, which is consistent with literature.[17]

The dimensions of the individual HBPAEK globules and clusters could be measured using Nanoscope analysis software from Bruker. Using the section tool, height cross-sections of the "core" or densely hyper-branched areas were taken, and the distance from base-to-base were taken as the diameter of the globule. 29, 64 and 99 counts were taken and averaged for HBPAEK-22K, HBPAEK-69K and HBPAEK-123K, respectively. As expected, the measurements showed a clear trend that the globule size increases with Mw and the values are displayed in **Table 2.1**. The HBPAEK-22K polymer has the smallest diameter (4.33 nm) and the 123K the largest diameter (7.38 nm). The 2 nm difference in the theoretical and measured diameter could be related to the signal intensity of the polymer globules, as the increasing density towards the core of the globule will give a better response. Also, the determination of DP from the Mw, and the resulting factor N in equation 2, might be slightly inaccurate and this may explain the observed difference in diameter.

2.3.5. Thermal properties

Thermal stability

Poly(aryletherketone)s or PAEKs are amongst the most thermally stable polymers, mainly due to their fully aromatic backbone. Weight loss upon heating occurs only at very high temperatures (>500 °C), where phenols and benzofurans are found to be the major degradation products.[18] The degradation mechanism remains largely unknown. Transfer reactions and chain scission were proposed to be involved in the degradation mechanism and it is believed to not be chain-end-activated.[19] However, other proposed mechanisms do involve chain-ends and branching.[20] It is apparent that changes take place within the material (e.g. formation of double melting peak and crosslinking can be observed) when exposed to elevated temperatures.[21] If the chain-ends of the backbone are susceptible to heat and are

still reactive, the effect will be more significant for HBPAEKs, as they have a large amount of unreacted end-groups (–F and to a lesser extend –OH groups). The synthesized HBPAEKs show no weight loss up to 300 °C, independent of Mw as shown in Figure 2.4.

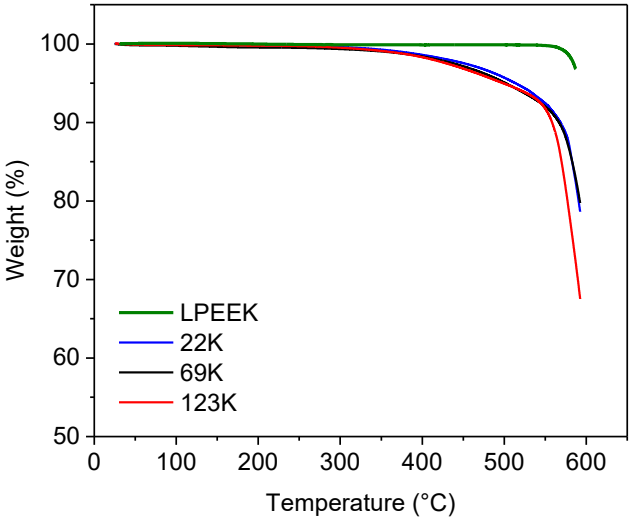

Figure 2.4. Thermal stability of the HBPAEK series with different Mw's, 10 °C/min, N_2. Linear high molecular PEEK (LPEEK) is included for reference purposes (Mw=20 kg/mol, PDI=2).

This might appear low, as a high-molecular weight linear reference polymer (LPEEK) shows superior thermally stability, but part of the weight loss is the result of post-condensation chemistry. Post-condensation takes place when the remaining –OH groups react with –F functionalities, which results in the evolution of HF gas. Using mass spectrometry, we could actually show that HF is indeed evolving from the sample, as can be seen in Figure 2.5. Unfortunately, we're not able to quantify the weight loss due to HF evolution but we believe the contribution of HF to the total weight loss to be small. The majority of the weight

loss is proposed to be the result of outgassing of low Mw fragments that were trapped between the branches, such as dimeric and trimeric species.

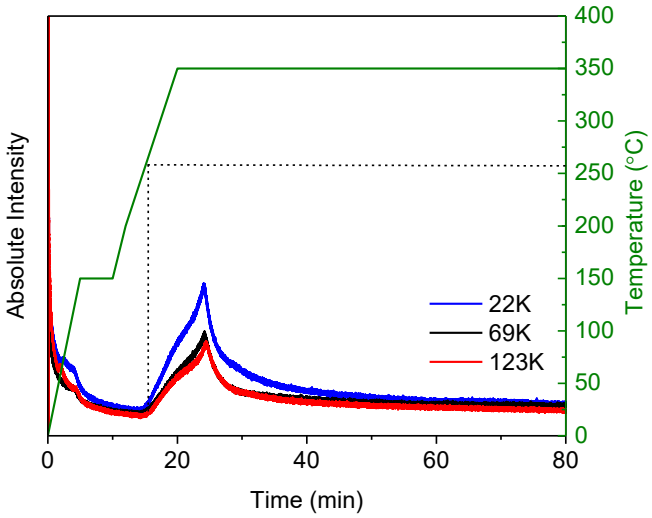

Figure 2.5. Evolution of HF is observed just above 250 °C and subsides after 20 minutes. The amount of HF formed could not be quantified.

Post-condensation was also confirmed when a small sample of HBPAEK-123K was thermally treated at 180, 200 and 240 °C for one hour. An increase of up to 3.4% in Mn and 19.8% in Mw was observed. At temperatures above 240 °C the solution could not be filtered anymore due to preliminary crosslinking and therefore no data was collected at higher temperatures.

Glass transition temperature

The T_g of hyperbranched polymers is highly dependent on the nature and number of the end-groups and this is, for example, also observed for hyperbranched polyphenylenes, polyesters and polyamides.[22,23,24] This feature gives access to polymers with a broad range in T_g's. The glass transition of HBPAEKs is similar to

linear PAEK, i.e. around 150 °C, but can vary from 97 to 290 °C with different end-groups.[8] We found that due to this extraordinary feature the T_g is also dependent on the number of end-groups per polymer and thus dependent on Mw. Figure 2.6 shows the T_g values for as-prepared HBPAEK-22K, HBPAEK-69K and HBPAEK-123K as obtained from DSC experiments (first heat).

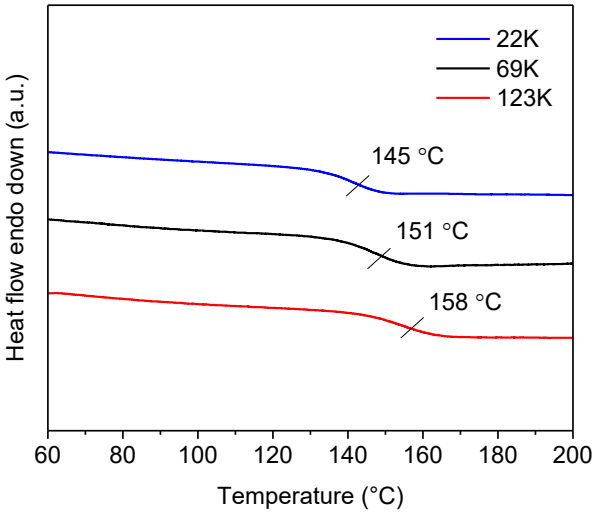

Figure 2.6. The T_g's of our HBPAEK series shows a slight Mw dependence. The highest Mw has the highest T_g. Heating rate of 10 °C/min and nitrogen atmosphere, first heat shown.

The T_g shows a slight dependence on the molecular weight of the polymer, i.e. the lowest molecular weight polymer (HBPAEK-22K) shows a T_g of 145 °C and upon increasing the molecular weight to 123 g/mol (HBPAEK-123K) the T_g increases to 158 °C. The DSC results are summarized in Table 2.2. The same DSC scans confirmed that all polymers are amorphous. No melting event or cure exotherm was observed up to 400 °C.

2.3.6. Rheological behaviour and crosslinking

Stress relaxation

The (non-)entangled state of hyperbranched polymers[25] has been thoroughly investigated and described in the literature and we expect that our systems will have little to no entanglements, as the short branches will inhibit this. As mentioned earlier, entanglements aid in the formation of a polymer network and we need to asses this if we want to investigate the network behaviour of our crosslinked HBPAEKs. We have performed a simple stress relaxation experiment using a rheometer with a parallel plate geometry to confirm that the melt behaviour is consistent with a non-entangled polymer melt. Above T_g, the network strength drops from 1 MPa to below a 100 Pa, which is very low and is considered as non-entangled behaviour. By applying a fixed strain of 2%, we can monitor the stress decay. We can get the stress relaxation modulus (G_r) of our HBPAEKs by using the following equation:

$$G_r(t) = \sigma(t) / \gamma_0 \qquad (3)$$

where σ is the stress and γ_0 is a constant strain. We can use this to monitor the behaviour of our HBPAEK polymer at different temperatures, below and above T_g. The results for our HBPAEK series are shown in Figure 2.7. For all three Mw's, where we observe that the minimum value for G increases with the Mw. Above T_g (≥160 °C), the value of G eventually drops 4 orders of magnitude to values <100 Pa, confirming non-entangled behaviour.

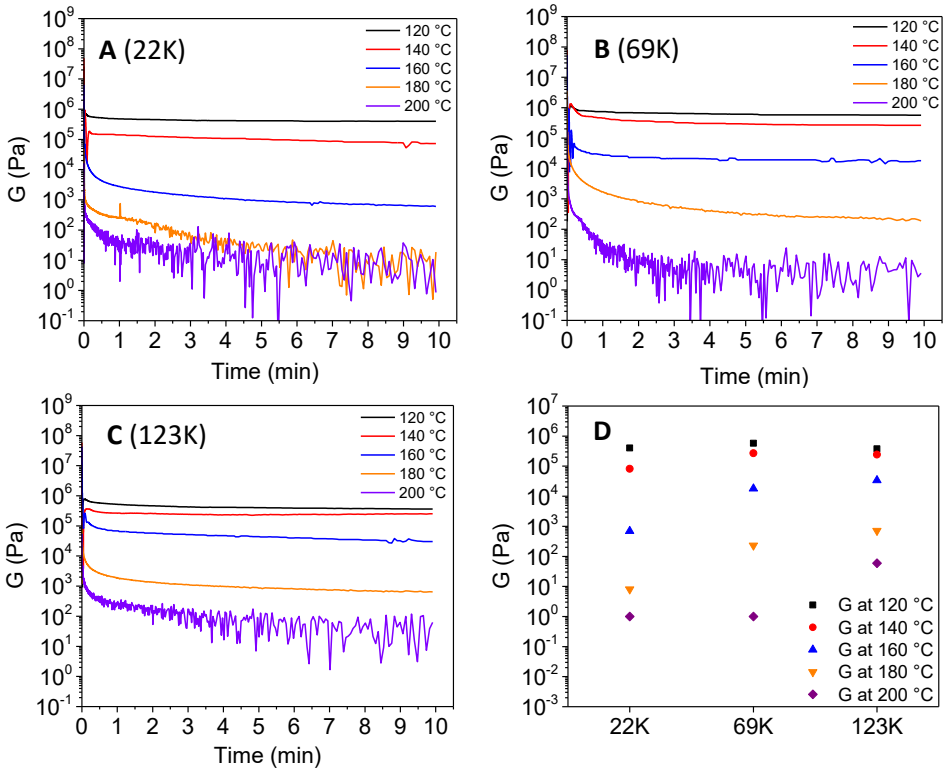

Figure 2.7. The stress relaxation (G) for all HBPAEKs as function of temperature and time. **A.** HBPAEK-22K; **B.** HBPAEK-69K; **C.** HBPAEK-123K; **D.** The stress relaxation data of all HBPAEKs after 8 min show that the minimum value for G increases with Mw.

In the experiments, summarized in Figure 2.7, we observed very low values for G, especially for HBPAEK-22K, which also indicates the ease of flow for these systems. This is an advantage for successive melt processing experiments.

Crosslinking

To understand the cure behaviour of our HBPAEKs and monitor network formation we studied the polymers in the rheometer using a cure program. Figure 2.8 shows the storage modulus (G') of the HBPAEK series as function of a temperature ramp to 350 °C, followed by an isothermal hold of one hour. All HBPAEKs show a melt-viscosity in the range of 100-300 Pa at 300 °C and when the hold temperature of 350 °C has been reached the storage modulus (G') levels off into a stable rubber plateau. The sample with the highest Mw, HBPAEK-123K, shows the highest initial values for G', as molecular mobility is more hindered. This dramatic drop in viscosity has already been reported for HBPAEKs[1] and is also observed for all-aromatic hyperbranched polyamides.[4] The difference in plateau values for the HBPAEKs are probably related to the amount of reactive end-groups present in each sample, where the HBPAEK-22K has the largest amount of focal points and thus the largest amount of reactive –OH groups. A large number of end-groups results in a rapid increase in G' and a higher plateau value, as shown in Figure 2.8. The water content during the synthesis of the HBPAEKs might also play a role, as more –OH groups may be formed. This could explain the fact that HBPAEK-123K exhibits a higher plateau value than HBPAEK-69K (the latter probably has less –OH groups when compared with HBPAEK-123K).

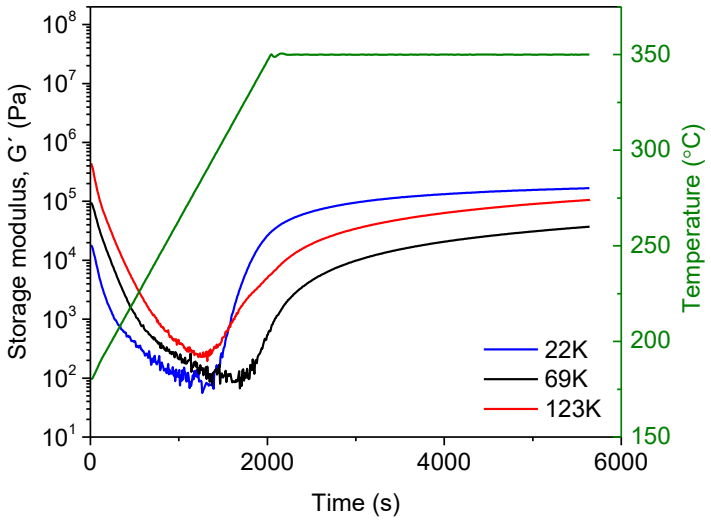

Figure 2.8. The storage modulus G' as function of time and temperature for all HBPAEKs. A temperature ramp of 5 ˚C/min was applied, followed by a 1 h cure at 350 ˚C. All HPAEKs show low melt-viscosities in the range of 100–300 Pa before they start curing, indicated by a rapid increase in G'. A stable G' plateau was obtained for all Mw's. The measurements were performed using 8 mm parallel plates under a nitrogen atmosphere.

The crossover values of the storage modulus (G') and the loss modulus (G"), which is considered the moment upon which a crosslinked network has been formed are listed in Table 2.2. The rheology results confirm that all HBPAEKs are able to cure via the remaining –F and –OH end-groups and reach a plateau, and the final plateau value is based on the Mw of the precursor. This has not been reported in earlier work on HBPAEKs[1,7] and shows the ability of these systems to form networks upon a simple thermal treatment without the need for additional crosslinking units.

Table 2.2. Cure and network characteristics of the HBPAEKs series as determined by parallel plate rheology.

Mw (kg/mol)	Crossover G'/G" (°C)[a]	Initial T_g (°C)[b]	T_g after curing at 350 °C (°C)[b]
22	240	145	158
69	300	151	156
123	302	158	169

[a] 8 mm parallel plates under nitrogen with a heating rate of 5 ˚C per min

[b] measured by DSC, 20 °C per min under nitrogen

From Table 2.2 we can learn that the crossover temperature of the 22K HBPAEK is much lower (~60 °C) than that of the 69K and 123K HBPAEKs. This can be explained by the larger surface area of the HBPAEK-22K globules and the larger concentration of –OH functionalities. These globules are smaller and have more surface area to react. The rapid increase in viscosity, i.e. faster cure kinetics, for HBPAEK-22K is in line with this observation. From the rheology data we can determine the processing window for the HBPAEKs. These materials can be processed to a temperature just below the crossover temperature without any chemical changes to the material. After this, crosslinking and network formation should be anticipated with reduced solubility.

To investigate the dependence of network formation on the cure temperature we investigated different cure temperatures for HBPAEK-123K, as this polymer has the highest T_g. As shown in Figure 2.9, the polymer starts to cure just above 300 °C so we have set 325 °C as lowest curing temperature and 375 °C as highest with a one-hour hold.

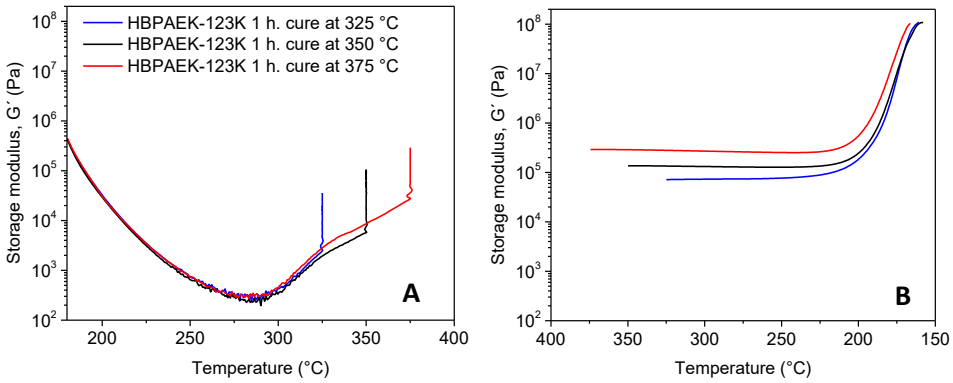

Figure 2.9 A. Storage modulus G' of HBPAEK-123K as function of temperature. HBPAEK-123K starts to cure just before 300 ˚C. The temperature ramp was set for 5 °C/min under nitrogen to the pre-set cure temperature of an 1 hour at 325, 350 or 375 °C. A 15-25 fold increase in G' could be achieved for the selected cure temperatures. **B.** Cooling scans after the isothermal hold experiments. The rubber plateaus are stable up to 230 °C, after which the polymers cool down into a glassy state and G' increases rapidly.

HBPAEK-123K starts forming a network around 300 °C and the G' increases upon a thermal hold of 1h. A higher crosslinking temperature results in a higher value for G'. The crosslink density, and thus the final properties of the polymer network, can be controlled by adjusting the cure temperature, as displayed in Figure 2.9A. The cooling runs after these isothermal runs are shown in Figure 2.9B.

From the cooling curves we see that a stable plateau has formed from which we can calculate the molecular weight of entanglement or M_e. This M_e is different from linear polymers as the M_e in the case of HBPAEKs relates to the globular polymers that are linked together at the periphery, where the largest number of unreacted functionalities are located. This is schematically represented in Figure

2.10A. At the periphery of the globule the HBPAEKs react and become part of a covalently linked network and the branches in between do not (cannot!) participate, localizing the covalent crosslinks at the periphery. When we contrast this with a classic network forming polymer such as an epoxy system, shown in Figure 2.10B, the difference is that the branched structure that is obtained early in the reaction remains reactive and a homogeneous and densely crosslinked network is obtained.

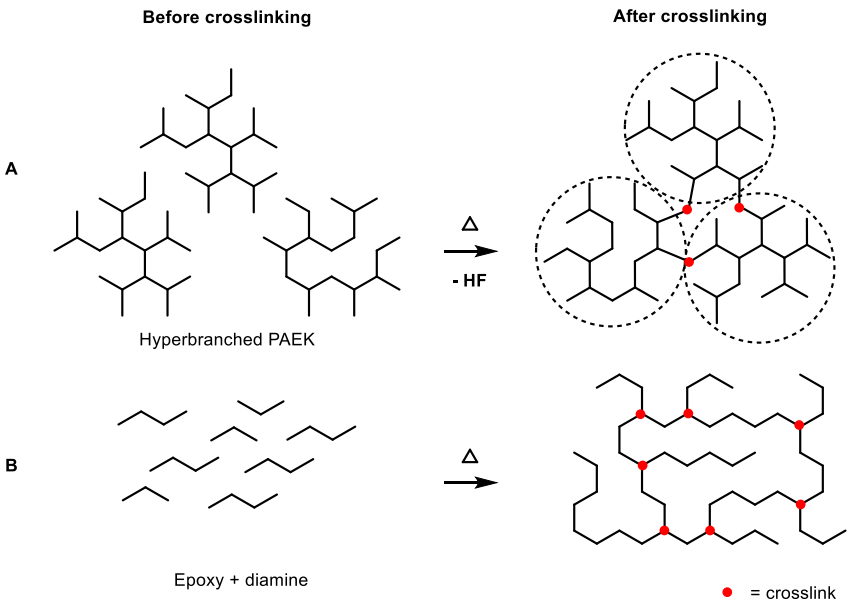

Figure 2.10. Topology of different crosslinking patterns. **A.** Crosslinking via hyperbranched PAEK precursors. Crosslinking takes place at the periphery of the globular structures. **B.** Crosslinking of a classic epoxy–diamine mixture. The diamine has a functionality (f) of 4, which results in a heavily branched and densely crosslinked structure, with crosslinks homogeneously distributed.

The crosslinks formed provide the strength of the final network polymer. In the case of hyperbranched polymers the only contribution to the network strength comes from the crosslinks at the periphery. Higher plateau values result in a lower M_e and thus a higher crosslink density. The following equation was used to calculate the plateau values:[26]

$$G'=\rho RT/M_e \qquad (4)$$

where G' is the storage modulus (in Pa), ρ is the density (taken from linear PEEK: 1300 kg/m^3),[27] R is the gas constant (8.3 m^{3}Pa/Kmol), T is the cure temperature used (Kelvin) and M_e is the molecular weight of entanglement (kg/mol). The resulting M_e values calculated for HBPAEK-123K are based on the plateau values as shown in Figure 2.9B. The values are listed in Table 2.3 and are 90, 49 and 24 kg/mol for curing at 325, 350 and 375 °C, respectively. This shows the trend that a higher curing temperature will result in a lower M_e and thus a higher crosslink density.

Table 2.3. Glass transition (T_g), plateau modulus and gel fraction for 123K HBPAEK, cured at different temperatures. The T_g before cure is 158 °C.

Curing T	**T_g (°C)[a]**	**G' plateau (KPa)[b]**	**M_e (kg/mol)**	**Gel fraction (%)[c]**
325 °C (598 K)	162	72	90	75
350 °C (623 K)	169	137	49	76
375 °C (648 K)	165	291	24	98

[a] measured as mid-point value with DSC, 20 °C per min under nitrogen

[b] measured with a rheometer, using 8 mm parallel plates under nitrogen with a heating rate of 5 ˚C per min (Figure 2.9B)

[c] measured after soaking in $CHCl_3$ at r.t. overnight followed by drying the sample

The cured HBPAEK-123K show an increase in thermal stability in comparison with their uncured precursors, as shown in Figure 2.11. Still, the thermal stability of the crosslinked HBPAEKs is lower than that of linear PEEK. Evaporation of small molecules and phenolic fragments are proposed to be the reason for this. Nonetheless, the weight loss for all cured HBPAEK samples is less than 2 wt.% at 500 °C.

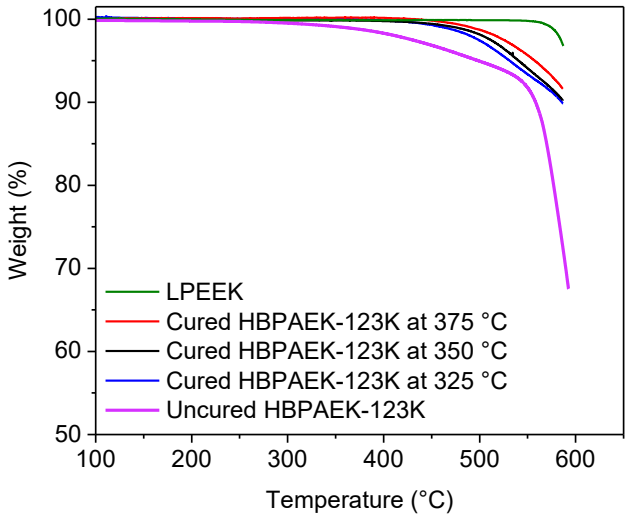

Figure 2.11. Dynamic thermogravimetric analysis results of HBPAEK-123K films cured at 325 °C, 350 °C and 375 °C for 1 h, respectively. Included are uncured HBPAEK-123K and LPEEK for reference purposes; nitrogen atmosphere and a heating rate of 10 °C/min. All cured HBPAEKs show < 2 wt% loss at 500 °C.

Sol/gel fraction

The sol/gel fraction is a measure of how well connected a polymer network is. For HBPAEK-123K, this was determined on films that were obtained after the polymer was solution cast from a 10 w/w% concentration in NMP in a Petri dish and thermally cured. The solvent was evaporated in discrete steps (under vacuum, 1h at 45 °C, 1h at 60 °C, 1h at 100 °C, 1h at 200 °C, 1h at 300 °C) after which the temperature was further increased to the target cure temperature. At temperatures below 300 °C, e.g. 250 and 275 °C, the polymer film is still largely soluble in chloroform. However, when the films are cured at 325, 350 and 375 °C crosslinking takes place and this process can be monitored by determining the sol-gel fraction. The gel fraction, i.e. the network insoluble part, as function of crosslinking temperature is listed in Table 2.3. The results confirm that crosslinking is most efficient at 375 °C for 1 hour as the gel fraction reaches 98%. The accuracy of these sol/gel fraction measurements are limited by the inhibited mobility of the sol fraction due to a large amount of branching. For HBPAEK-123K, the T_g, gel fraction and modulus plateau increase with an increased cure temperature. The increase in T_g is minimal, as this is limited by the number of crosslinks at the periphery. The T_g is mostly determined by the unperturbed polymer of the HBPAEK.

Solution casting of HBPAEKs to prepare free-standing films in glass Petri dishes or on Kapton did not provide films that could be mechanical tested, as the films were too brittle. The brittleness and poor handleability of crosslinked HBPAEKs will be addressed in Chapter 3.

2.4 Conclusions

We have demonstrated that amorphous hyperbranched poly(aryletherketone)s (HBPAEKs) can undergo thermal post-condensation via their unreacted –OH and –F end-groups that are positioned at the periphery of their globular structure. As a result, crosslinked HBPAEKs can be obtained without the use of additional crosslinking functionalities. The HBAPEKs adopt a globular structure as confirmed by AFM and the globular size is a function of their initial (pre-cure) molecular weight, i.e. 4, 6 and 7 nm for 22K (HBPAEK-22k), 69K (HBPAEK-69k) and 123K (HBPAEK-123k), respectively. With rheology, we confirmed the non-entangled melt behaviour for these polymer globules and found a minimum storage modulus in the range of 100-300 Pa at 240 °C depending on the precursor Mw. Above this temperature the polymers start to cure, which is confirmed by a rapid increase in viscosity and a moderate increase in T_g from 158 °C to 169 °C (HBPAEK-123k). Upon cure, a stable rubbery plateau was obtained and this plateau could be tuned by changing the crosslinking temperature. From this plateau an M_e value of 90, 49 and 25 kg/mol for HBPAEK-123k could be calculated when cured at 325, 350 or 375 °C, respectively. The M_e values and high gel fraction of 98% confirms that the HBPAEK globules are connected. Despite network formation, cured free-standing films are too brittle to handle and could not be used for mechanical testing.

2.5 References

1. Kwak, S.-Y. & Ahn, D. U. Processability of Hyperbranched Poly(ether ketone)s with Different Degrees of Branching from Viewpoints of Molecular Mobility and Comparison with Their Linear Analogue. *Macromolecules* **33,** 7557–7563 (2000).

2. Olofsson, K., Andrén, O. C. J. & Malkoch, M. Recent advances on crosslinked dendritic networks. *J. Appl. Polym. Sci.* **131,** 39876–39889 (2014).

3. Baek, J. B., Qin, H., Mather, P. T. & Tan, L. S. A new hyperbranched poly(arylene-ether-ketone-imide): Synthesis, chain-end functionalization, and blending with a bis(maleimide). *Macromolecules* **35,** 4951–4959 (2002).

4. You, K. *et al.* Phenylethynyl- and naphthylethynyl-terminated hyperbranched polyimides with low melt viscosity. *High Perform. Polym.* **27,** 970–978 (2015).

5. Pötzsch, R. & Voit, B. Thermal and Photochemical Crosslinking of Hyperbranched Polyphenylene With Organic Azides. *Macromol. Rapid Commun.* **33,** 635–639 (2012).

6. Liu, T. *et al.* Preparation and properties of film materials of poly(aryl ether ketone)-based phthalonitrile resins. *Polym. Eng. Sci.* **55,** 2313–2321 (2015).

7. Mu, J., Zhang, C., Wu, W., Chen, J. & Jiang, Z. Synthesis, Characterization, and Functionalization of Hyperbranched Poly(ether ether ketone)s with Phenoxypheyl Side Group. *J. Macromol. Sci. Part A* **45,** 748–753 (2008).

8. Hawker, C. J. & Chu, F. Hyperbranched Poly(ether ketones): Manipulation

of Structure and Physical Properties. *Macromolecules* **29,** 4370–4380 (1996).

9. Ghosh, A., Banerjee, S. & Voit, B. Aromatic Hyperbranched Polymers: Synthesis and Application. *Adv. Polym. Sci.* **266,** 27–124 (2014).

10. Tomalia, D. a. *Dendrimers and Other Dendritic Polymers*. *Polymer Recycling* **1,** (John Wiley & Sons, Ltd, 2001).

11. Kim, Y. H. & Webster, O. W. Water-Soluble Hyperbranched Polyphenylene; "A Unimolecular Micelle"? *J. Am. Chem. Soc.* **112,** 4592–4593 (1990).

12. Rubinstein, M. & Colby, R. H. *Polymer Physics*. (Oxford University Press, 2003).

13. Uhrich, K. E. & Hawker, C. J. One-Pot Synthesis of Hyperbranched Polyethers. *Macromolecules* **25,** 4583–4587 (1992).

14. Hölter, D. & Frey, H. Degree of branching in hyperbranched polymers. 2. Enhancement of the DB: scope and limitations. *Acta Polym.* **48,** 298–309 (1997).

15. Song, E. H., Shang, J. & Ratner, D. M. *Polysaccharides*. *Polymer Science: A Comprehensive Reference, 10 Volume Set* **9,** (Elseiver, 2012).

16. Sheiko, S. S. & Möller, M. Visualization of macromolecules - A first step to manipulation and controlled response. *Chem. Rev.* **101,** 4099–4123 (2001).

17. Lederer, A. & Burchard, W. *Hyperbranched Polymers*. (The Royal Society of Chemistry, 2015). doi:10.1039/9781782622468

18. Day, M., Cooney, J. D. & Wiles, D. M. The thermal degradation of poly(aryl—ether—ether—ketone) (PEEK) as monitored by pyrolysis—GC/MS and TG/MS. *J. Anal. Appl. Pyrolysis* **18,** 163–173 (1990).

19. Hay, J. N. & Kemmish, D. J. Thermal decomposition of poly(aryl ether ketones). *Polymer (Guildf).* **28,** 2047–2051 (1987).

20. Patel, P. *et al.* Mechanism of thermal decomposition of poly(ether ether ketone) (PEEK) from a review of decomposition studies. *Polym. Degrad. Stab.* **95,** 709–718 (2010).

21. Zhang, Z. & Zeng, H. Effects of thermal treatment on poly(ether ether ketone). *Polymer (Guildf).* **34,** 3648–3652 (1993).

22. Jikei, M. & Kakimoto, M.-A. Hyperbranched aromatic polyamides prepared by direct polycondensation. *High Perform. Polym.* **13,** S33–S43 (2001).

23. Jikei, M. *et al.* Synthesis of hyperbranched aromatic polyamide from aromatic diamines and trimesic acid. *Macromolecules* **32,** 2061–2064 (1999).

24. Jikei, M., Fujii, K. & Kakimoto, M. Synthesis and characterization of hyperbranched aromatic polyamide copolymers prepared from AB(2) and AB monomers. *Macromol. Symp.* **199,** 223–232 (2003).

25. Hult, A., Johansson, M. & Malmström, E. in *Advances in Polymer Science* **143,** 1–34 (Springer Berlin Heidelberg, 1999).

26. Lobo, H. & Bonilla, J. W. *Handbook of plastics analysis*. *Plastics engineering* **68,** (2003).

27. Lee, Y. & Porter, R. S. Crystallization of Poly(ether ether ketone) Oriented by Solid-state Extrusion. *Macromolecules* **24,** 3537–3542 (1991).

Chapter 3

Thermomechanical Properties of Cured Phenylethynyl End-capped HBPAEK Reactive Precursors

Abstract

We have investigated the rheology and thermo(mechanical) properties of hyperbranched poly(aryletherketone)s (HBPAEKs), in which we replaced 10, 20 or 40% of the remaining fluorine (–F) functionalities with reactive 4-(phenylethynyl)phenol (PEP) end-groups. All PEP-terminated HBPAEKs show a rapid increase in melt viscosity between 250–350 °C, confirming that the PEP end-groups are effective crosslinking functionalities. PEP concentration, temperature and time allows us to control the degree of crosslinking and hence the final thermo(mechanical) properties. Free standing, flexible films, could be prepared by curing the reactive PEP-precursors. Films have T_g's in the 150 to 250 °C range and storage moduli of 3-4 GPa. For the first time, the stress–strain behaviour of crosslinked HBPAEKs could be studied. Crosslinked films exhibit a maximum tensile strength of ~40 MPa at 2% elongation, which corresponds to a toughness of ~0.3 kJ/m^3. We have successfully demonstrated that reactive hyperbranched all-aromatic poly(aryletherketone)s can be solution processed and crosslinked into flexible, high T_g, transparent films.

3.1 Introduction

In Chapter 2 we reported on the synthesis, rheology and thermo(mechanical) behaviour of neat HBPAEK systems before and after cure. Crosslinking appears to be possible using a thermally activated post condensation reaction using remaining –OH and –F functionalities. Rheology unambiguously confirmed crosslinking. However, a minimal increase in after cure T_g and poor mechanical properties of cast films suggest that crosslinking is minimal. Crosslinking hyperbranched polymers using reactive functionalities is one route towards compensating for the lack of chain entanglements and several approaches have been reported in the literature,[1–5] but in this chapter we will focus specifically on a strategy towards crosslinking hyperbranched poly(aryletherketone)s (HBPAEKs). Researchers such as Jiang et al. used an A_2 + B_3 monomer approach in order to obtain –OH terminated HBPAEKs. After introducing phthalonitrile groups, they crosslinked the HBPAEKs with *p*-bis[4-(4-aminophenoxy)-phenyl]sulfone (*p*-BAPS) to obtain free standing films that could be characterized by dynamic mechanical analysis (DMA). The T_g dramatically increased from 165 to 325 °C and films exhibited a storage modulus of 1.4 GPa.[6] No stress-strain experiments were reported in this paper and no data was reported on the handleability of the films. This method requires the need for a crosslinking additive (*p*-BAPS) and the use of an A_2 + B_3 system, which may result in gelation. Having to avoiding gelation is less attractive as it will limit processing to dilute precursor solutions only. In a follow-up paper, Jiang et al. described how phenylethynyl groups like 4-(phenylethynyl)phenol (PEP) can crosslink hyperbranched poly(etheretherketone)s (HBPEEKs), as shown in Scheme 3.1.[7,8]

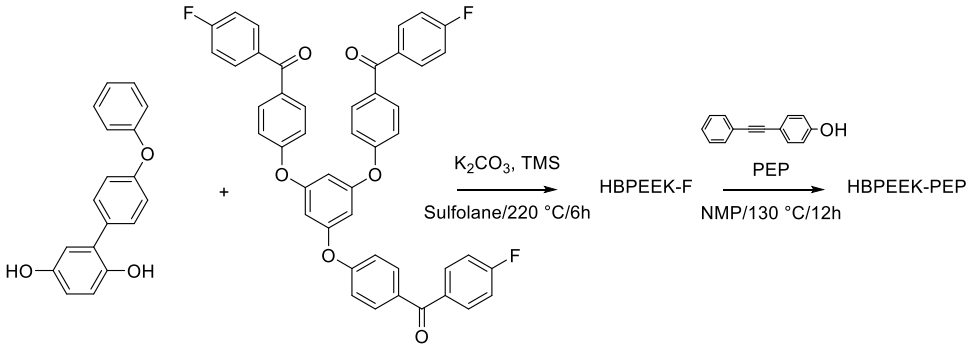

Scheme 3.1. Polymerization of A_2 and B_3 monomers towards hyperbranched poly(etheretherketone)s. The authors reported that all fluorine end-groups were replaced by 4-(phenylethynyl)phenol (PEP).[7,8]

The authors pointed out that gelation was difficult to avoid. The presented approach also involves the use of expensive monomers and only limited FTIR and NMR analysis of the resulting polymer was presented. The introduction of the PEP reactive functionality was confirmed by an additional IR peak at 2215 cm^{-1} and the disappearance of the C-F peak at 1112 cm^{-1} and an additional peak at 7.52-7.59 ppm in ^1H NMR. Without any quantification the authors concluded that full end-group conversion was achieved. Again, no stress-strain curves of the cured free-standing films were reported. The only evidence for crosslinking was supported by DSC experiments where the authors observed a reaction exotherm, associated with the PEP group, and an increase in T_g from 105 to 236 °C. In summary, researchers have reported A_2 + B_3 systems with different reactive end-group functionalities. Only in a few cases authors presented DMA experiments on cured films and no data whatsoever has been reported on stress–strain behaviour. It is not clear if the crosslinking functionalities are effective in connecting adjacent globules, and at what concentration, but what is clear is that in all reports a

thorough time–temperature cure profile is lacking. There is no sol–gel data reported and no melt rheology data.

Based on the limited literature available, we believe that phenylethynyl, or phenylacetylene, remains the best reactive functionality for crosslinking HBPAEKs. The phenyl-triple bond functionality is part of a list of thermally curable end-groups.[9] The triple bond can thermally rearrange and form free radicals at T >300 °C, and the free radicals in turn can recombine, i.e. chain extend or crosslink without generating volatiles.[10] Proposed after cure structures include, amongst others, alkenes (f=2) and cyclotrimerized (f=3 and f=4) products. This end-group is also known for providing ductile high T_g thermoset resins, i.e. PETI-5, which was briefly discussed in Chapter 1.[11] As mentioned before, the phenylethynyl groups at the periphery of the globules will be responsible for connecting adjacent globules. A complete substitution of all fluorine groups for PEP groups, as reported by Jiang et al., is envisioned to be unnecessary and probably results in an over-crosslinked (brittle) network.

In this Chapter we will present a HBPAEK series where we varied the phenylethynyl end-group concentration. We used HBPAEK-69 (Chapter 2) and replaced 10, 20 or 40% of the fluorine (–F) functionalities with PEP and the samples were labelled HBPAEK-69K-10PEP, HBPAEK-69K-20PEP and HBPAEK-69K-40PEP, respectively. From Chapter 2 we have learned that neat HBPAEK-69K can only modestly crosslink so if we can increase the degree of crosslinking for this molecular weight with PEP, other molecular weights are envisioned to follow a similar trend. The reactive PEP end-group (shown in red in Scheme 3.2) was synthesized via a Sonogashira coupling using 4-iodophenol and phenylethynyl.[12] This specific end-group has an alcohol functionality that allows us to attach the phenylethynyl functionality to the polymer backbone in the same fashion as the polymerization of the AB_2 monomers, namely via a nucleophilic aromatic

substitution, as shown in Scheme 3.2. The triple bond will remain dormant until its thermal cure temperature is reached.

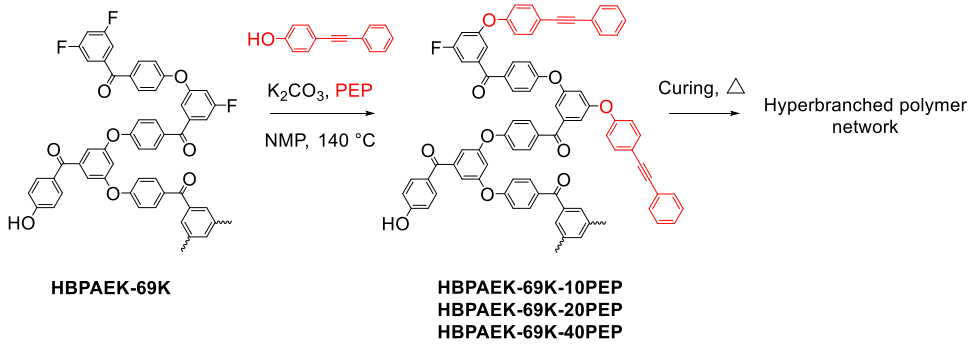

Scheme 3.2. Synthesis of PEP end-capped HBPAEK-69K, followed by thermal crosslinking. Three HBPAEK-69K reactive analogs were prepared with 10% (HBPAEK-69K-10PEP), 20% (HBPAEK-69K-20PEP) and 40% PEP (HBPAEK-69K-40PEP). Thermal curing leads to a hyperbranched polymer network.

In addition to the synthetic details, we will report extensively on the crosslinking behavior of this series as function of time and temperature and how crosslinking can be followed using FTIR, Raman and parallel-plate rheology. We will discuss the (thermo)mechanical behavior of cured films in detail. Both DMTA and stress–strain results will be presented and how PEP concentration, time and temperature at cure will affect the final after cure mechanical performance.

3.2 Experimental section

3.2.1. Materials and equipment

HBPAEK-69K was prepared according to the procedure described in Chapter 2. 4-Iodophenol was purchased from TCI and used as received. $Pd(PPh_3)_2Cl_2$ and PPh_3

were purchased from Sigma Aldrich and used as received. Phenylethynyl was also purchased from Sigma Aldrich and vacuum distilled before use. Triethyl amine was purchased from Alfa Aesar. Dry NMP and dry toluene were obtained from Acros Organics and used as received. A reference PEKK film sample was obtained from Solvay (Ajedium film CYPEK FC).

Differential Scanning Calorimetry (DSC) curves were measured on a TA instruments 2500 series at 10 °C/min (heating and cooling) under nitrogen atmosphere in crimped aluminium sample pans. Thermal gravimetric analysis (TGA) measurements were performed with a TA instruments 5500 TGA at 10 °C/min under nitrogen purge in aluminium pans. ^{1}H NMR (400 MHz) and ^{13}C-NMR (100 Hz) spectra were recorded on a Varian AS-400 spectrometer and chemical shifts are given in ppm (δ) relative to tetramethylsilane (TMS) as an internal standard. The ^{1}H NMR splitting patterns are designated as follows: s (singlet), d (doublet), dd (double doublet), t (triplet), q (quartet), m (multiplet) and b (broad signal). The coupling constants, if given, are reported in Hertz. GPC measurements were performed using a Shimadzu GPU DHU-20A3 equipped with two Shodex LF-804 column and refractive index detector; polystyrene standards were used for calibration of the instrument. All samples were dissolved at a 1 mg/mL concentration in NMP and filtered over a 0.45 µm PTFE filter prior to use. Samples for mass spectrometry were analysed on a Shimadzu GC/MS-QP2010S in electron-impact ionization (EI) mode, equipped with an Optic-3 injector and SGE capillary column (PBX5, 30m, 0.25mm). Data were acquired and processed using GCMS solution software. IR spectra were recorded from powdered samples on a Perkin Elmer Spectrum 100 FT-IR Spectrometer, measuring from 600-4000 cm^{-1}.

Films were casted in a Petri dish and held under vacuum for 1h at r.t., 1h at 30 °C, 1h at 45 °C, 1h at 60 °C, 1h at 100 °C, 1h at 200 °C, 1h at 300 °C, and 1h at 350 °C. Rheology experiments were performed with a Perkin Elmer HAAKE

instrument in a parallel plate geometry (8 mm plates) and frequency of 1 Hz with 2% strain. Dynamic mechanical thermal analysis (DTMA) was performed on the HBPAEKs films (approximately 20x3x0.05 mm) at a frequency of 0.1, 1 and 10 Hz at a heating rate of 2 °C/min under nitrogen with a Perkin Elmer Diamond DMTA. Only the storage modulus (E') and loss modulus (E'') data collected at 1 Hz is reported. The thermal gravimetric analysis (TGA) measurements were done with a Perkin Elmer TGA 4000 at 10 °C/min under nitrogen purge in aluminium pans. Tensile testing was performed on an Instron 3365 at a rate of 0.1 mm/min with thin film samples. Coefficients of thermal expansion (CTE) were measured with a PerkinElmer Diamond Thermal Mechanical Analyser (TMA) between -50 and 50 °C at a heating rate of 5°C/min.

3.2.2. Syntheses

4-(phenylethynyl)phenol (PEP). We adopted a synthetic method reported by Tang et al.[12] with a slightly modified work-up procedure. To a 1 L 1-neck round-bottom flask was added $Pd(PPh_3)Cl_2$ (0.8 g, 1 mmol), CuI (0.43 g, 2 mmol) and PPh_3 (0.30 g, 1 mmol). The flask was placed under vacuum and subsequently back-filled with Argon. 4-Iodophenol (25 g, 0.11 mmol) in 650 ml Et_3N and phenylacetylene (16.35 ml, 0.15 mol) in 150 ml Et_3N were added. This was stirred for 24 h before the yellow suspension was filter, washed with Et_3N and concentrated. The resulting dark oil was purified via column chromatography over silica in DCM (Rf = 0.2) to give the desired product, 4-(phenylethynyl)phenol (PEP) as a slightly orange product (19 g, 87%). MS (EI), m/z: 194 (M). FT-IR (cm^{-1}): 3400-3000, 2225, 1608, 1590, 1509, 1440, 1371. MP: 125 °C. ^1H NMR ($CDCl_3$): δ = 7.53-7.51 (d, 2H), 7.44-7.42 (d, 2H), 7.34-7.33 (d, 3H), 6.82-6.80 (d, 2H), 5.2-4.6 (b, 1H). ^{13}C NMR

($CDCl_3$): 155.57, 133.27, 131.44, 128.31, 127.99, 123.48, 115.67, 115.50, 89.20 (acetylene), 88.09 (acetylene).

HBPAEK-69K-20PEP. To a 100 ml flask was added 2 g of neat HBPAEK-69K (8.54 mmol) and this was dissolved in 30 ml NMP. K_2CO_3 (0.47 g, 3.4 mmol) and PEP (0.33 g, 1.7 mmol) were added and the solution was stirred at 140 °C for 4 h. The traces of water formed during the reaction are expected to not influence the reaction at this temperature and therefore no Dean-Stark trap was used. The dark solution was precipitated in ice-cold water and neutralized with 1 M HCl. The precipitate was collected, dried in vacuo at 60 °C overnight, dissolved in THF and precipitated in methanol. The pale yellow/white solid was dried in vacuo at 60 °C for 24 h. The yield was quantitative. ^{1}H NMR (400 MHz, $CDCl_3$), δ = 7.90-7.50 (m, 2H), 7.30-6.50 (m, 5H). ^{13}C NMR ($CDCl_3$): 192.88, 162.89, 160.30, 140.72, 132.61, 118.88, 116.48, 112.78, 107.70, 94.47 (acetylene), 89.03 (acetylene). HBPAEK-69K-10PEP and HBPAEK-69K-40PEP were prepared in a similar fashion.

3.3 Results and discussion

3.3.1. Size exclusion chromatography

The HBPAEK-69K precursor end-capped with 10, 20 and 40% end-cap are labelled HBPAEK-69K-10PEP, HBPAEK-69K-20PEP and HBPAEK-69K-40PEP and the obtained GPC curves are summarized in Figure 3.1 and contrasted with neat HBPAEK-69K start material.

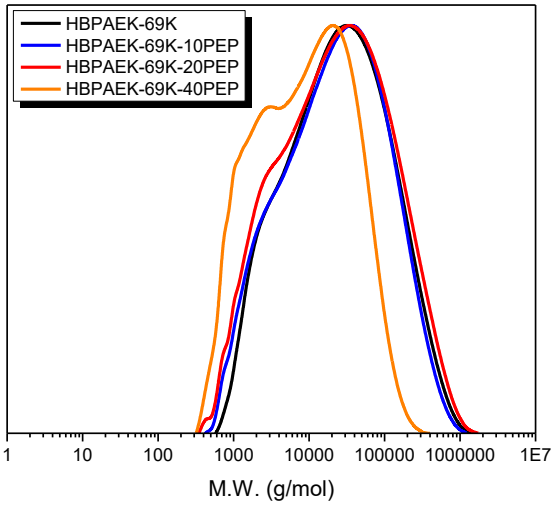

Figure 3.1. SEC data of HBPAEK-69K with and without PEP end-cap in NMP at a concentration of 1 mg/ml. With 10% and 20% PEP the MW distribution remains virtually the same. For HBPAEK-69K-40PEP (orange) the MW distribution broadens and shifts towards lower molecular weights.

Increasing the end-group concentration did not change the MW for the 10 and 20% derivatives, however, when the PEP concentration is increased to 40%, the molecular weight shifts from an Mw of 69K to 20K, as shown in Table 3.1.

Table 3.1. SEC data on neat HBPAEK-69K, HBPAEK-69K-10PEP, HBPAEK-69K-20PEP and HBPAEK-69K-40PEP at a concentration of 1 mg/ml in NMP.

HBPAEK-69K with % PEP	**Mn (kg/mol)**	**Mw (kg/mol)**	**PDI**
0	9	69	7,29
10	7	60	8,71
20	6	71	11,4
40	3	20	6,07

Replacing a large fraction of the electronegative fluorine atoms with non-polar phenyl acetylene functionalities most likely impacts the polymer solubility, i.e. affect the polymer–solvent interaction, which in turn may account for the observed shift in molecular weight and MW broadening.

3.3.2. Raman spectroscopy

Several spectroscopic methods allow for the identification of PEP in our HBPAEK series, albeit with very little sensitivity. ^{13}C NMR has limitations as the acetylene carbon atoms are quaternary and therefore difficult to detect. Visualisation with infrared (IR) spectroscopy is also difficult due to the symmetry of the acetylene triple bond in the PEP end-group. The carbon–carbon symmetric stretch vibration typically results in a very weak signal around 2100 cm^{-1}. In contrast, Raman spectroscopy is capable of detecting functional groups that have such a symmetric stretch. The Raman spectra of the HBPAEK-69K PEP series are summarized in Figure 3.2.

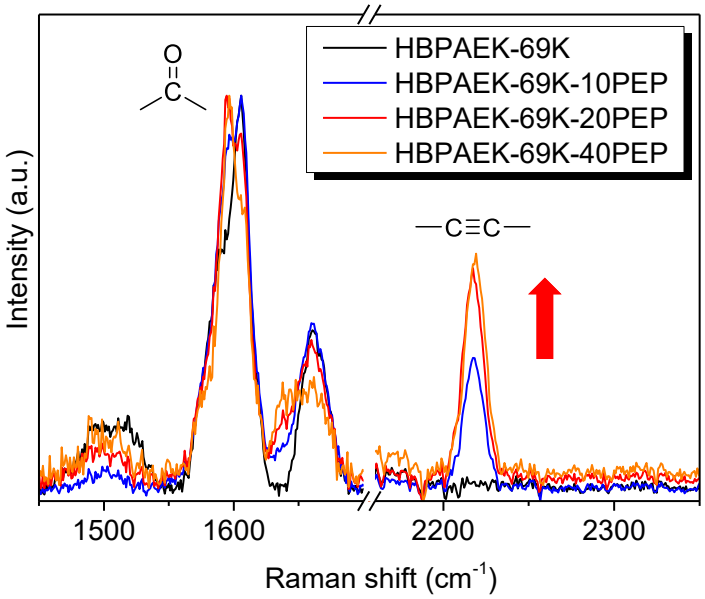

Figure 3.2. Raman spectra of neat HBPAEK-69K and the PEP end-capped HBPAEK-69K series. The signal that corresponds with the carbon-carbon triple bond is visible at 2240 cm^{-1} and increases with an increasing concentration of PEP.

The intensity of the alkyne signal at 2240 cm^{-1} increases with an increased concentration of PEP end-cap, while the ketone signal at 1660 cm^{-1} remains constant. The resolution is quite poor, which is mainly the result of the background fluorescence caused by the high aromatic content of the polymer. The resolution was unfortunately too poor to allow quantification of the PEP end-groups in the polymer, so we used elemental analysis to further quantify to which extent the fluorine groups on HBPAEK-69K were replaced by PEP.

3.3.3. Nuclear Magnetic Resonance

The degree of branching (DB) of a hyperbranched polymer can be determined by nuclear magnetic resonance (NMR) and gives information on the architecture of

the polymer. In our case all HBPAEK polymers have a degree of branching of 0.5, which is typical for a randomly branched polymer. We can also use NMR to monitor the number of fluorine end-groups replaced by PEP. ^{19}F-NMR shows the two different fluorine end-groups in the polymer, belonging to the fluorine atoms on the linear units and terminal units. As they become replaced with our reactive PEP end-group, the intensity of both signals decreases. This is shown in Figure 3.3, where the decrease in NMR signal intensity confirms a decrease in fluorine as the concentration of PEP increases, effectively displacing fluorine in the polymer.

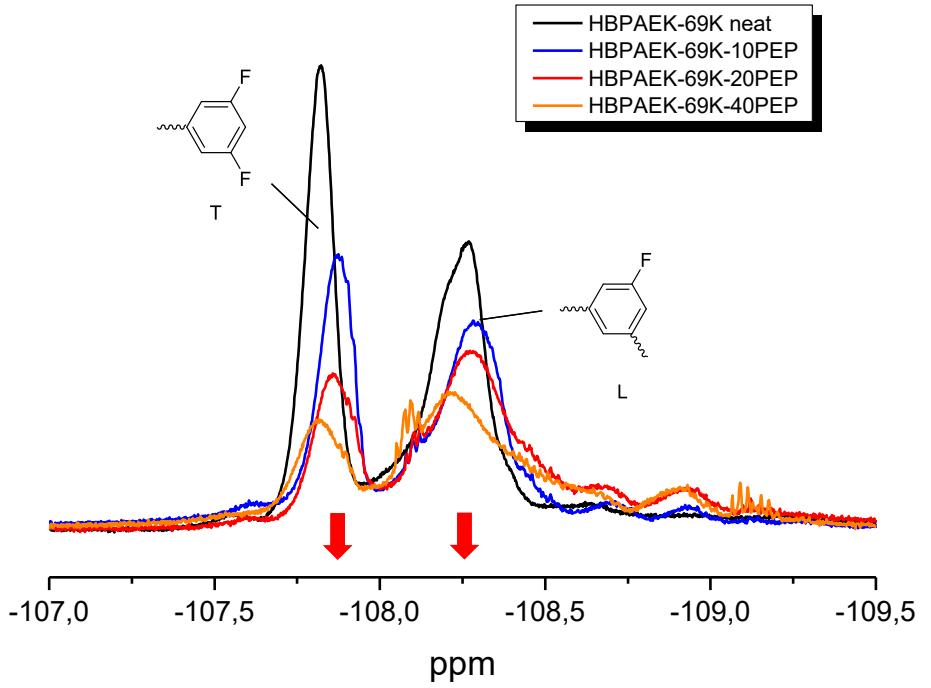

Figure 3.3. ^{19}F NMR spectrum of the neat and PEP end-capped HBPAEK-69K series, measured at a concentration of 40 mg/0.6 ml in $CDCl_3$. The concentration of fluorine end-groups decreases with increasing amount of PEP end-cap. T = terminal fluorine units, L = linear fluorine units.

The area under the NMR curve can be calculated by integration and was taken as an absolute area with a straight-line mode baseline with Origin Pro 2016 software. The calculated values for both the linear and terminal units are shown below in Table 3.2.

Table 3.2. Integration results for neat and PEP end-capped HBPAEK-69K. The area of the terminal (T) units and linear (L) units of the HBPAEK-69K is set as 100%, combined they are set as 100% for the total decrease in area in the 4th column. The decrease is compared with the reduction of fluorine from elemental analysis (EA).

%PEP	Area T (%)	Area L (%)	Total decrease (%)	EA decrease (%F)
0	100	100	0	0
10	63,1	83,6	26,7	19,8
20	38,0	73,2	44,4	34,9
40	25,6	58,8	57,8	43,9

From Table 3.2 we see that the total decrease in area for all PEP end-capped HBPAEK does not correspond with the target amount of PEP we wanted to replace. A possible explanation for this could be that -F groups are replaced with –OH groups during the addition of the PEP end-group, as water is formed during the conversion of the PEP end-group to its corresponding potassium salt.
The data from the area under the NMR curves can be compared with the results from elemental analysis, this will be addressed in the next paragraph.

3.3.4. Elemental analysis

With NMR measurements we could clearly observe a trend in decreasing fluorine content and this could also be confirmed with elemental analysis, where the fluorine content is directly measured by combustion ion chromatography and the results are listed in Table 3.3. The measured content of fluorine for the neat polymer is lower than calculated by Chemdraw 15 software, as discussed in Chapter 2, where the most probable explanation was found to be hydrolysis of some of the fluorine groups. For the PEP end-capped HBPAEKs we see a clear trend in reduction of the fluorine content of the PEP functionalized polymer. This is additional proof that we can replace the fluorine groups for the reactive PEP end-groups in a controlled fashion. The percentage decrease in fluorine content is shown in Table 3.3 and compared to the reduced area under the curve from the NMR spectra. Both methods show that more fluorine is replaced than intended and this is probably related to additional dehalogenation during synthesis. Elemental analysis is very sensitive, requires a less sensitive sample preparation and errors in the integration of the NMR curves are avoided. That makes EA less prone to error and thus more reliable.

Table 3.3. Elemental analysis, DSC, sol/gel and rheology data on neat and PEP end-capped HBPAEK-69K.

HBPAEK-69K with PEP (%)	Theoretical amount of F (%)[a]	Measured amount of F (%)[b]	T_g (°C)[c]	T_g after cure at 350 °C (°C)[d]	Storage modulus (GPa)[e]	M_e (kg/mol)[f]
0	8.89	6.91 (+/-0.01)	151	169[g]	-	$11,0*10^2$
10	8.00	5.54 (+/-0.01)	152	177	2.5	16,4
20	7.11	4.50 (+/-0.01)	154	187	2.8	22,5
40	5.33	3.88 (+/-0.01)	132	185	2.7	11,9

[a] Calculated using Chemdraw 15 software
[b] Measured by elemental analysis
[c] Uncured, from DSC, 20 °C/min under nitrogen
[d] Determined by DTMA, as max in G"
[e] From initial slope tensile test, at r.t.
[f] $M_e=\rho RT/G'$, with $\rho=1.3$ kg/m^3 at 623K.

3.3.5. Glass transition temperature

The glass transition temperatures (T_g) of the PEP-functionalized HBPAEK series were measured with differential scanning calorimetry (DSC). The DSC scans of the first heat are shown in Figure 3.4 and the results are summarized in Table 3.3.

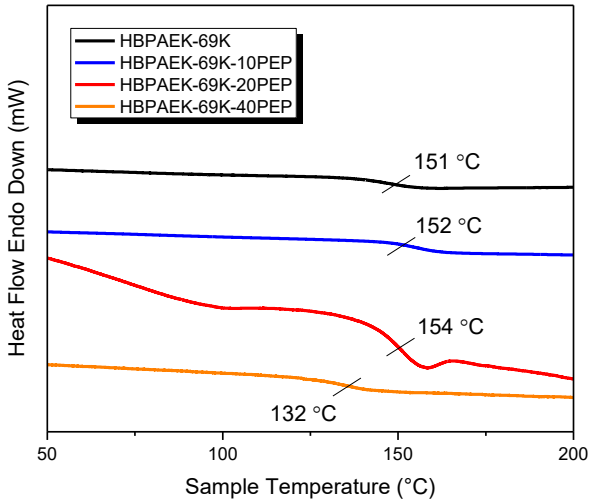

Figure 3.4. First heat of the DSC scans of HBPAEK-69 and the PEP end-capped HBPAEK-69K series, measured using a heating rate of 20 °C/min under nitrogen.

All polymers remain amorphous, there is no indication that (high concentrations of) PEP induces crystallization. Introducing PEP does not seem to have a major effect on the T_g. The T_g of HBPAEK-69K is 151 °C and introducing 10% PEP or 20% PEP increases the T_g to 152 and 154 °C, respectively. The notable exception is HBPAEK-69-40PEP where the T_g drops by ~20 °C to 132 °C. This is the result of a dramatic change in polarity going from a HBPAEK with a high content of electronegative fluorine atoms at the periphery to a HBPAEK with a high content of non-polar phenylacetylene functionalities. This is in line with earlier reported T_g changes for HBPAEKs. Hawker et al. showed that replacing the polar –F end-

group for the less polar benzophenone end-group results in a T_g drop from 162 °C to 117 °C.[13]

3.3.6. Rheological behaviour and crosslinking

The viscoelastic behaviour of neat HBPAEK-69K and the PEP end-capped HBPAEKs were evaluated using parallel-plate rheology and the results are summarized in Figure 3.5. Whereas HBPAEK-69K shows a gradual decrease in storage modulus (G') over the whole temperature range up to 350 °C, the PEP terminated analogs show a minimum in G' around 250 °C. More specifically, HBPAEK-69-10PEP and HBPAEK-69-20PEP show a minimal G' value of 500 Pa and HBPAEK-69-40PEP shows a G' as low as 10 Pa. The crosslinking event for the PEP end-capped HBPAEK-69K series starts around 250 °C, which is evident by a rapid increase in G'. This is much earlier than the crosslink temperature of the phenylethynyl functionality as reported in literature, which is around 300 °C.[10] Neat HBPAEK-69K lacks PEP reactive end-groups and shows a slow increase of G' during the 350 °C 1h. hold, which is the result of thermal induced post condensation chemistry, as discussed in Chapter 2. Crosslinking of the PEP terminated HBPAEKs is almost complete when the hold temperature of 350 °C is reached. The moderate increase in G' during the 1h. hold can be attributed to additional crosslinking of the PEP functionalities and/or crosslinking via any remaining free –OH and –F functionalities. For all PEP terminated HBPAEKs a similar rubber plateau level of 500 KPa is obtained after a 1h. hold at 350 °C. The reference polymer, HBPAEK-69K, does not reach a plateau and in fact G' is still increasing after the 1 h. hold.

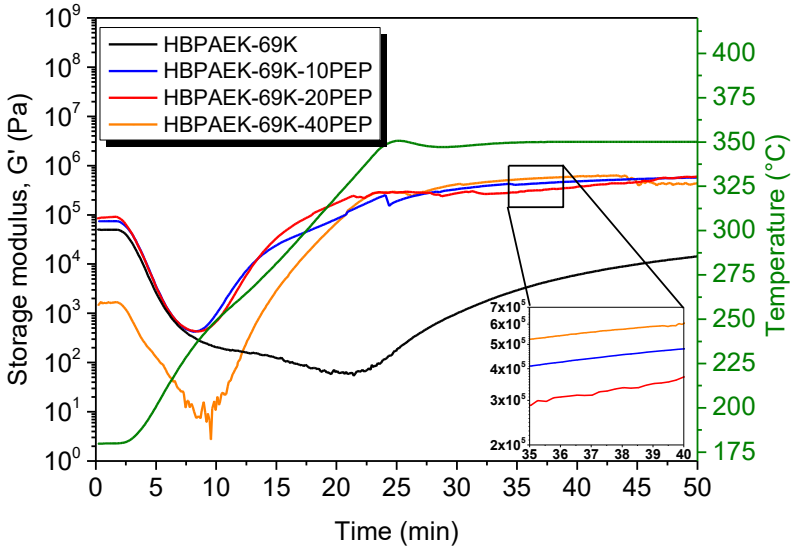

Figure 3.5. Rheology curves of HBPAEK-69K and HBPAEK-69K with 10, 20 and 40% PEP; 8 mm pellets under nitrogen, 5 °C/min ramp to 350 °C followed by an isothermal hold of 1h. at 350 °C.

The molecular weight of entanglement (M_e) can be calculated from the G' plateau value at 350 °C after a 25 min hold and is calculated to be in the range of 11–18K for HBPAEKS with PEP and 373K for the neat HBPAEK-69K without PEP, as shown in Table 3.3. This means the crosslinking density is much higher for the HBPAEKs with PEP. The crosslinking density (υ) can be calculated by using the following equation:[14]

$$\upsilon = G'/RT \qquad (1)$$

where G' is the shear storage modulus at 350 °C (623 K) and R is the universal gas constant (8.3 m^3 Pa/Kmol). The calculated values are summarized in Table 3.4.

Table 3.4. Crosslinking densities and molecular weight of entanglement of neat HBPAEK-69K and 10, 20 and 40% PEP end-capped HBPAEK-69K.

Entry	% PEP	G' after 40 min at 350 °C (kPa)	Crosslink density (mol/m^3)[a]	M_e (kg/mol)[b]
1	0	6,11	1,18	11,0*10^2
2	10	411	79,4	16,4
3	20	299	57,9	22,5
4	40	564	109	11,9

[a] Crosslinking density (υ) was calculated using Eq. (1).

[b] M_e=ρRT/G', with ρ=1.3 kg/m^3 at 623K.

The crosslink density from the neat HBPAEK-69k (Table 3.4, entry 1) is the result of the coupling of –F and –OH and is at least a factor 50 lower than the PEP end-capped HBPAEK-69Ks. From the rheology experiments we conclude that the HBPAEK-69K can cure via existing end-groups (Chapter 2) but the process is slow and the crosslink density is much lower. Adding reactive PEP end-groups speeds up the crosslinking reaction and additionally gives a higher crosslinking density.

3.3.7. Thermal gravimetric analysis

The thermal gravimetric analysis of the cured HBPAEKs showed a <2% weight loss at 450 °C with a char yield of >90% at 550 °C. The TGA plots are shown in Figure 3.6.

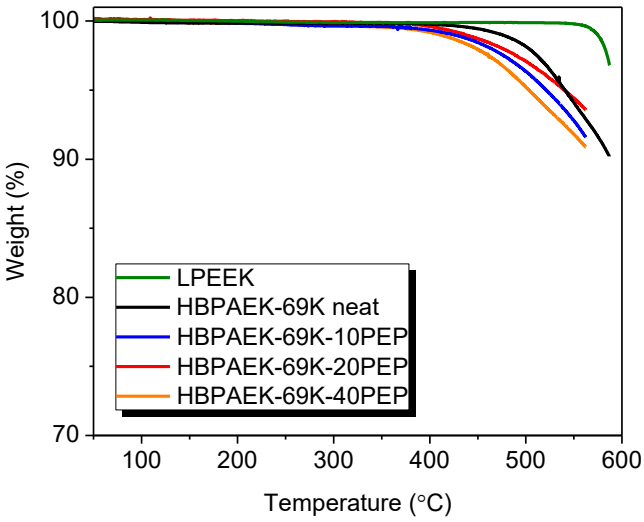

Figure 3.6. Thermogravimetric analysis results for HBPAEK-69K and HBPAEK-69K with 10, 20 and 40% PEP cured at 350 °C for 1 h. Included is LPEEK for reference purposes; nitrogen atmosphere and a heating rate of 10 °C/min.

The cured neat and PEP end-capped HBPAEK-69K show a higher weight loss than the linear PEEK reference and the HBPAEK-69 start material, probably the result of outgassing of smaller weight fractions that were trapped within the polymer branches. All the weight loss values are listed in Table 3.5.

Table 3.5. Thermogravimetric analysis of neat and 10, 20 and 40% end-capped HBPAEK-69K against LPEEK as a reference.

Entry	$T_{d2\%}$ (°C)[a]	$T_{d5\%}$ (°C)[b]	Char yield at 550 °C (%)
LPEEK	>550	>550	98.8
Neat HBPAEK-69K	503	541	94.1
HBPAEK-69K-10-PEP	464	521	92.7
HBPAEK-69K-20-PEP	476	540	94.4
HBPAEK-69K-40-PEP	448	503	91.8

[a] $T_{d2\%}$ is reported at the 2% weight loss under N_2 using a heating rate of 10 °C/min

[b] $T_{d5\%}$ is reported at the 5% weight loss under N_2 using a heating rate of 10 °C/min

3.3.8. Film casting

The HBPAEKs films were cast from a 10 wt./wt.% solution in NMP onto glass petri dishes with a diameter of 6 cm. We obtained light brown coloured transparent films by applying a stepwise temperature program under vacuum, as described in the experimental section. We found that the HBPAEK films adhere strongly to the glass substrate, which often resulted in cracked films upon cooling due to the large difference in coefficient of thermal expansion (CTE) between the polymer film and the glass substrate. The CTE of the cured HBPAEK with PEP films is about $20*10^{-6}$ $°C^{-1}$, which is about 5 times higher than the CTE of the Petri Dish (Pyrex glass). The CTE of the crosslinked HBPAEK with PEP is slightly lower than that of linear PEKK (Solvay) reference sample, which is reported as $25.5*10^{-6}$ $°C^{-1}$. Applying mould release agent significantly reduced the adhesion of the HBPAEKs to the glass substrate and the films with PEP reactive end-groups could easily be removed after the temperature treatment. The HBPAEK-69K without PEP end-groups

remained too brittle for mechanical testing. The HBPAEKs are more effectively crosslinked with PEP, compared to the post-condensation process described in Chapter 2. As cast HBPAEK-based films, with and without PEP end-groups, are shown Figure 3.7.

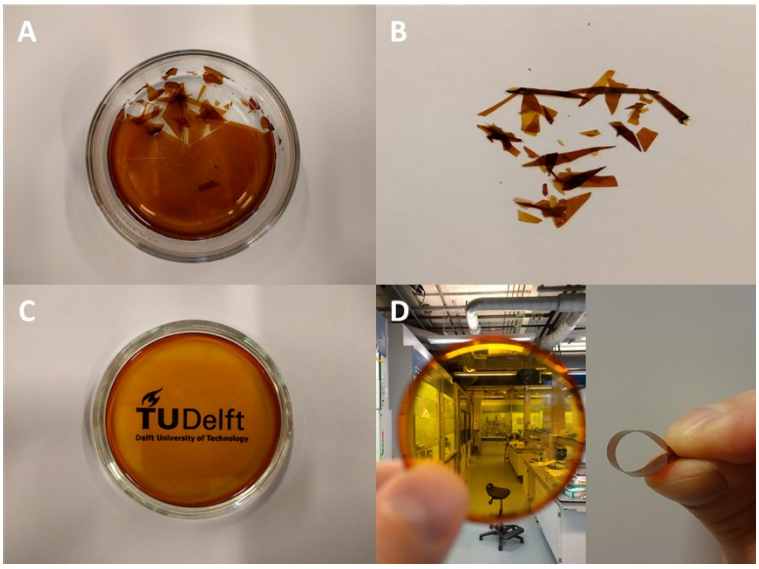

Figure 3.7. Pictures of cast HBPAEK-69K films after curing at 350 °C. **A.** HBPAEK-69K, cast on a glass Petri dish (6 cm diameter), already cracks upon cooling in the oven after thermal curing. **B.** Free standing films cannot be obtained from the HBPAEK-69K film as the material is too brittle. **C.** HBPAEK-69K with 40% PEP gave a homogeneous transparent film without cracks. **D.** A free standing flexible film could be removed from the glass and exhibits excellent handleability/flexibility. The films are 50 +/- 1 µm thick.

As expected, cured HBPAEK-69K films are too brittle and do not result in free standing films. The lack of chain entanglements and low crosslink density result in films that cannot carry any mechanical load. The contrast with PEP end-capped

HBPAEK-69K is significant, as the increased crosslink density results in films that can even be bend 180° without breaking.

3.3.9. Sol/gel fraction

The sol/gel fraction of the neat and end-capped-HBPAEK-69K polymers films, after being cured at 350 °C, was determined by soaking pieces of film (1x1 cm) for 24 h. at room temperature in chloroform, which is a good solvent for the polymer. Neat HBPAEK-69K gives a significant lower gel fraction than the PEP end-capped HBPAEKs, which show gel fractions of up to 98%, as shown in Table 3.6.

Table 3.6. Sol/gel fraction of neat and PEP end-capped HBPAEK-69K. Chloroform was used as solvent to soak a piece of film (1x1 cm) for 24 h, after which the film was collected, dried in a vacuum oven for 3 days at 60 ˚C and weighed.

HBPAEK-69K with % PEP	Sol fraction (%)	Gel fraction (%)
0	22	78
10	2	98
20	2	98
40	6	94

This supports the hypothesis that the neat HBPAEK-69K polymer globules are not well-connected and slightly crosslinked only. This explains why soluble fractions could be removed from this polymer. In other words, introducing PEP in this series HBPAEKs is an effective method towards improving the crosslink density and hence the film mechanical properties.

3.3.10. Mechanical testing

Dynamic mechanical thermal analysis

The flexible and transparent cured HBPAEK films were tested using a DMTA, which allowed us to monitor the glass transition and thermal behaviour over a temperature range, and the results are shown in Figure 3.8. The initial storage modulus is in the 3-4 GPa range, which is in line with reported values for all-aromatic high-performance polymers and is also in the same range as the reference sample (linear PEKK, Solvay). The glass transition is marked by a sudden drop in E', typically observed for amorphous polymers. The films are robust and do not break over the whole temperature range with an increase in E' from 325 °C due to post-curing of unreacted phenylethynyl groups and/or cure via remaining -F/-OH groups. The rubbery plateau of the PEP end-capped HBPAEKs is increased with the amount of crosslinker.

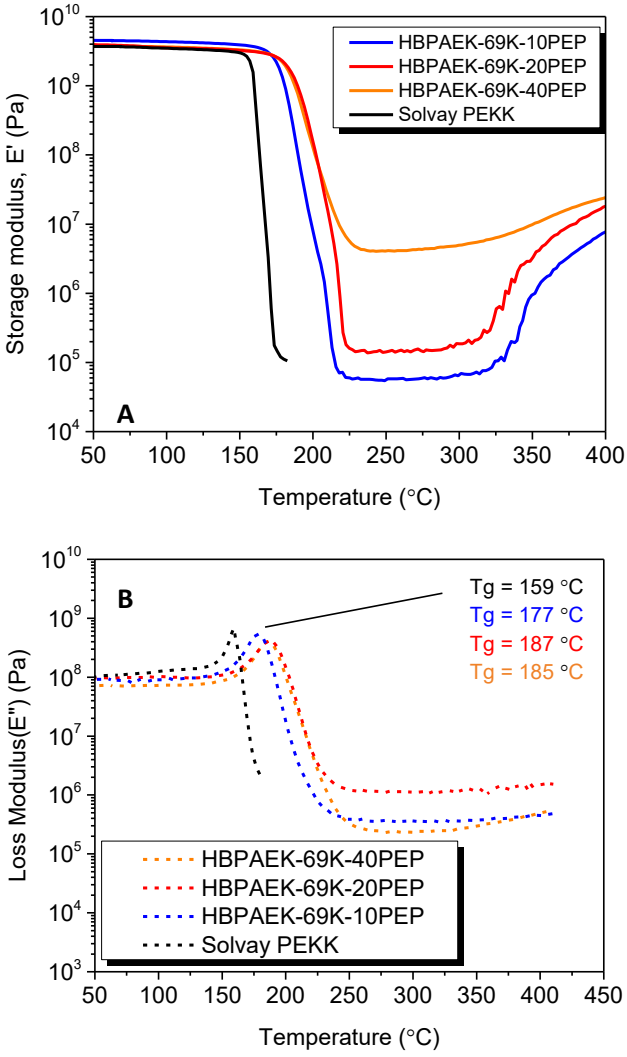

Figure 3.8. A. DMTA curves of partially PEP end-capped HBPAEKs, under nitrogen, 2 °C per min, 1 Hz. The PEKK reference measurements terminates at 175 °C (above T_g), as the film softens and elongates too much. An increase in G' after 300 °C is observed for all HBPAEK-PEP samples, which is probably due to additional crosslinking. **B.** G" from DMTA for PEP end-capped HBPAEKs, the T_g is reported at the maximum of G".

The T_g's of the PEP-terminated HBPAEKs are much higher than that of linear PEKK. PEKK became too soft and stretched too much so the measurement terminated at 180 °C. The T_g's of the HBPAEKs are visible around 200 °C and all films remain intact over the whole temperature range as a result of network formation.
The crosslinking density (υ) can be calculated by using the following equation:

$$\upsilon = E'/3RT \qquad (2)$$

where E' is the storage modulus of the cured film at 350 °C (623 K) and R is the universal gas constant (8.3 m^3 Pa/Kmol).[15] The calculated values are displayed in Table 3.7.

Table 3.7. Calculated crosslinking densities for the HBPAEK-69K films with 10, 20 and 40% PEP end-groups, crosslinked at 350 °C.

Entry	HBPAEK -69K with X % PEP	E' at 350 °C (MPa)[a]	Crosslinking density (kmol/m^3)[b]	M_e at 350 °C (kg/mol)[c]
1	0	-	$1,2*10^{-3}$ [d]	$11*10^2$ [d]
2	10	0,94	0,060	22
3	20 first run	3,3	0,22	41
5	second run	22	1,4	0,90
6	third run	38	2,5	0,53
7	40	9,8	0,63	2,1

[a] From DMTA, N_2 atmosphere, 2 °C per min, 1 Hz.

[b] Crosslinking density (υ) was calculated using Eq. (2).

[c] From DMTA, $M_e=\rho RT/(E'/3)$, with $\rho=1.3$ kg/m^3.

[d] From rheology, as the films are too brittle for mechanical testing.

The storage modulus at 350 °C increases with the percentage of PEP added to the HBPAEK-69K and this also results in an increased crosslinking density. The crosslink densities that are calculated from the DMTA results are higher than from the rheology results displayed in Table 3.4. This is probably the effect of the cure program used, as the HBPAEK films for DMTA were solution-casted and cured stepwise in a vacuum oven and were exposed to a higher temperature for a longer period of time in between the temperature stages.

The HBPAEKs curves in Figure 3.8 show an increase in G' after the rubbery plateau, between 225–325 °C, indicating a post-curing event. To further explore this, a HBPAEK-69K-20PEP film was measured three times in a row and the results are displayed in Figure 3.9. The T_g for HBPAEK-69K-20PEP in Figure 3.9 shifts from 187 to 252 °C and the rubbery plateau increases an order of magnitude from 3 MPa to 22 MPa to even 40 MPa (at 350 °C). This indicates that the post-curing results in a network with a higher crosslink density, as also calculated and shown in entries 2, 3 and 4 in Table 3.7. An increase in crosslink density directly relates to a lower M_e value, which is confirmed and also shown in Table 3.7. The samples showed increased brittleness after being exposed repeatedly to the thermal cure program, indicating that the crosslink density matters and can in fact be used as a tool to control the final mechanical properties.

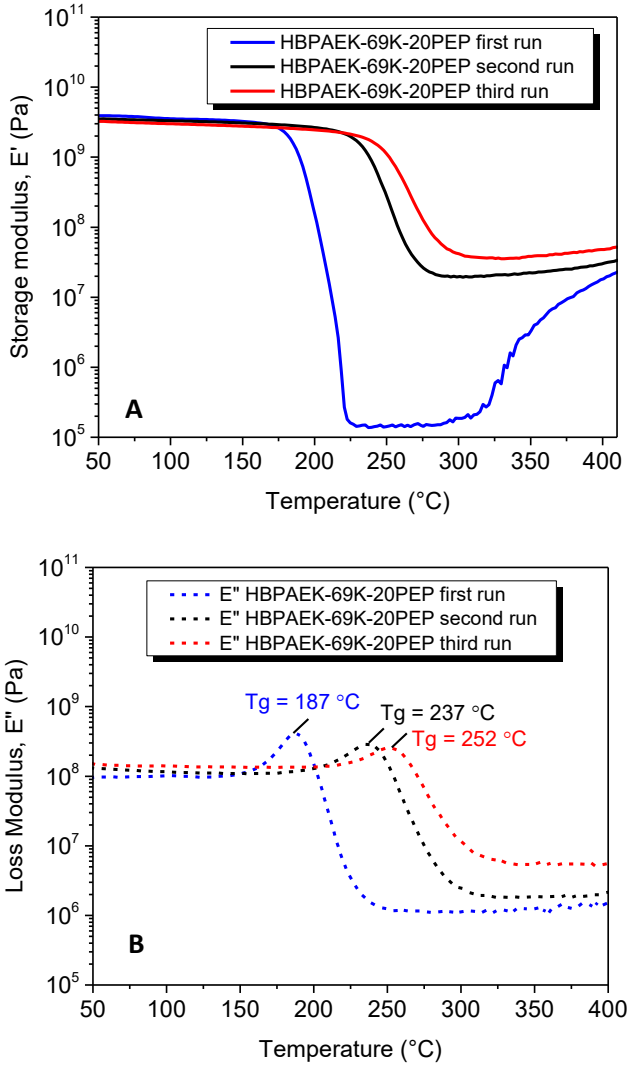

Figure 3.9. A. Storage modulus (E') against temperature of three consecutive runs on 1 sample film of HBPAEK-69K-20PEP; N_2 atmosphere, 2 °C per min, 1 Hz. **B.** Loss modulus (E").

Tensile testing

In order for HBPs to form networks that carry mechanical loads, the individual polymer globules need to be connected, hereby also taking the packing efficiency

in account and the chance of end-groups finding each other to connect. Figure 3.10 summarizes the stress-strain results of the PEP end-capped HBPAEK-69K series, including a commercial PEKK reference sample. The elastic modulus can be calculated from the initial slope and adopts a value of ~2-4 GPa, as also displayed in Table 3.8.

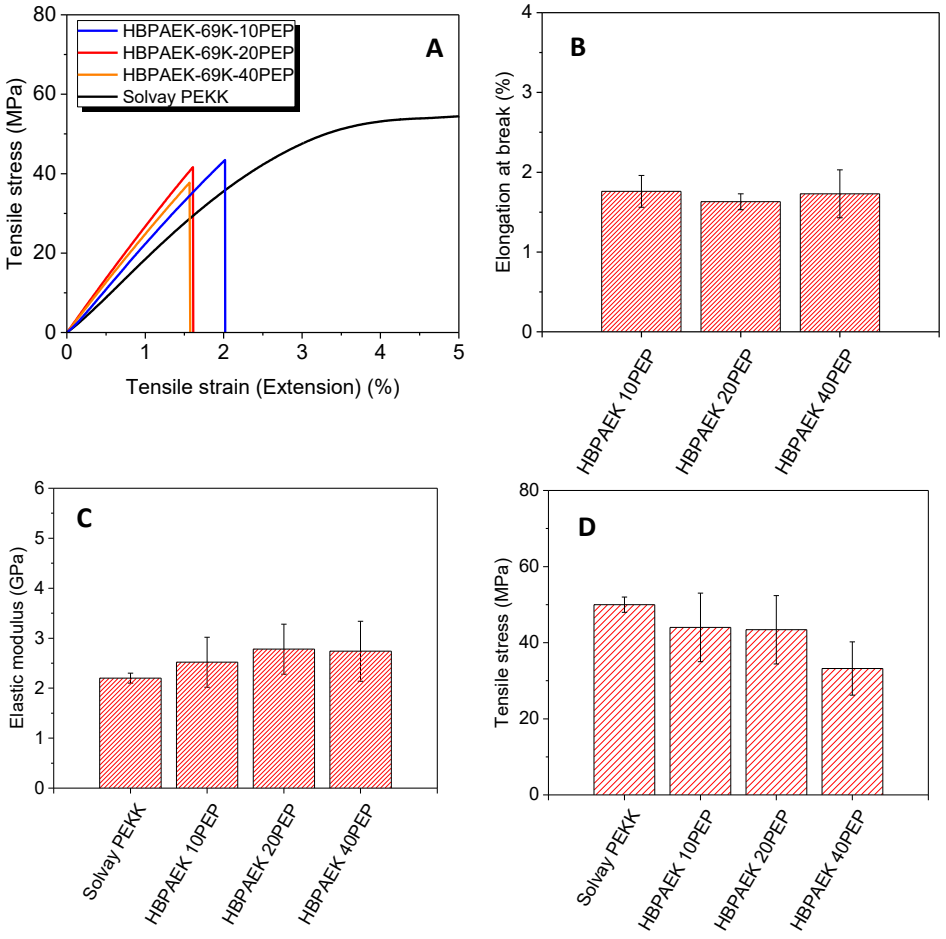

Figure 3.10. Tensile data of PEP end-capped HBPAEK-69K films and linear PEKK (Solvay) reference film, measured at a strain rate of 0.1 mm/min. **A.** Stress-strain behaviour of the PEP end-capped HBPAEK-69Ks and the PEKK reference. All

HBPAEK films were cured at 350 °C for 1 h. **B.** Elongation at break **C.** Elastic modulus **D.** Maximum tensile stress. The error bars shown represent the upper and lower values obtained from 3 film samples.

The HBPAEK have a higher initial storage modulus, compared to the linear PEKK reference. The maximum tensile stress, maximum tensile strain and toughness are lower, due to the large difference in polymer backbone architecture.

Table 3.8. Tensile data of cured HBPAEK-69K films. A Solvay PEKK film is included for reference purposes. Applied strain rate is 0.1 mm/min.

HBPAEK with PEP (%)	**Storage modulus E' (GPa)[a]**	**Max tensile stress (MPa)**	**Max tensile strain (%)[b]**	**Toughness (kJ/m^3)[b]**
10	2.52 ± 0.5	44.0 ± 9	1.76 ± 0.2	0.39 ± 0.1
20	2.78 ± 0.5	43.40 ± 9	1.63 ± 0.1	0.34 ± 0.1
40	2.74 ± 0.6	33.24 ± 7	1.73 ± 0.3	0.21 ± 0.1
Solvay PEKK	2.2 ± 0.1	52 ± 2 [b]	-[c]	1.77 ± 0.05

[a] obtained from initial slope

[b] measured up to 5% elongation

[c] sample did not break as a maximum elongation of 5% was used

The toughness of these HBPAEKs can be calculated from the stress-strain curve in Figure 3.10A by integrating the area under the curve and a value of ~0.3 kJ/m^3 was obtained, which is in the range of typical epoxide thermosets.[16] Thus in terms of stress-strain behaviour, the HBPAEKs behave like typical epoxide thermosets that also have a relatively low elongation at break (<5%).[17] The concentration of PEP does not result in a significant change in mechanical properties. A concentration

of 10% PEP is already enough to effectively crosslink the HBPAEK-69K and any additional connections that are made via the crosslinks do not contribute to the overall strength.

The crosslinked HBPAEK films show brittle fracture, which is different than what is observed for the linear PEKK reference sample. In the linear PEKK sample, plastic deformation is observed after 2% elongation, while no plastic deformation is visible with PEP crosslinked HBPAEKs. The fact that HBPAEKs only show elastic deformation probably comes directly from the difference in polymer architecture, as the HBPAEK do not have chain entanglements and have a lot of branches. This is schematically represented in Figure 3.11.

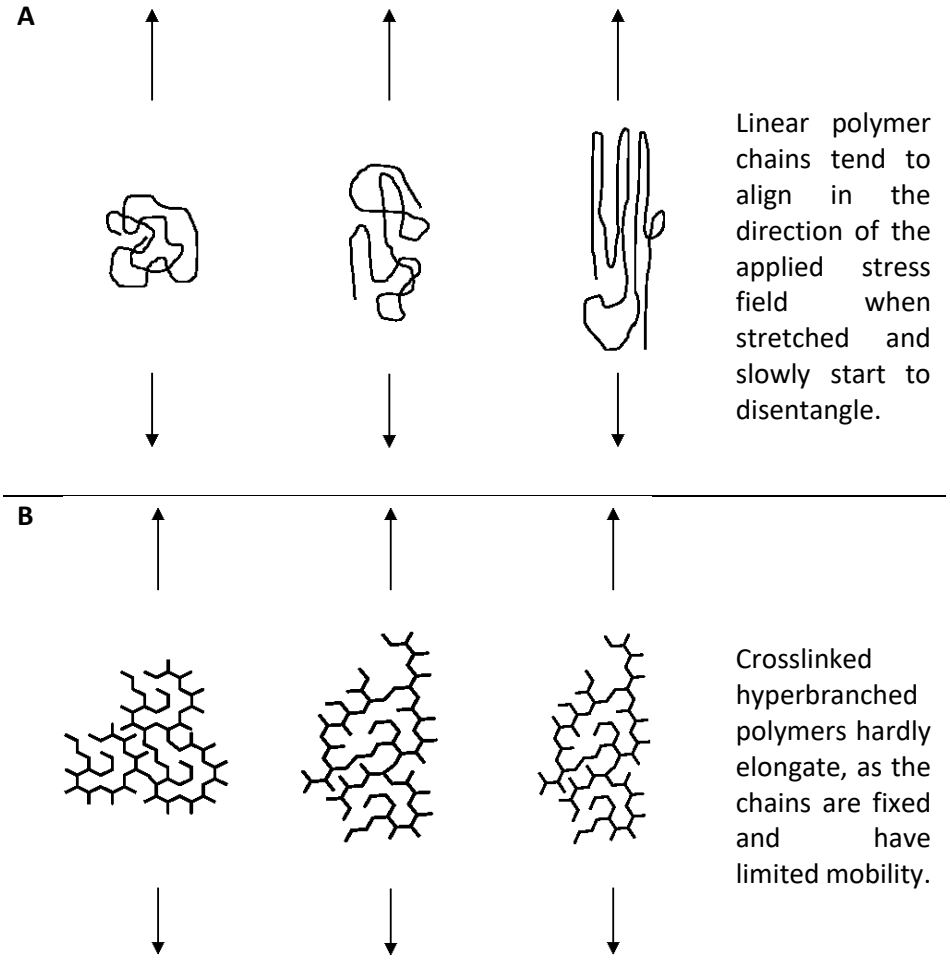

Figure 3.11. Schematic representation of the response of different polymer architectures on an applied stress field. **A.** Elongation of a linear polymer. **B.** elongation of a crosslinked hyperbranched polymer.

Typically, linear amorphous polymers go through several stages when being stretched.[18] Firstly, there is elastic deformation where the polymer is able to recover its shape after the stress is released. Secondly, the polymer reaches its yield point after which it enters a plastic deformation region and no recovery back

to its original shape is possible. This yield point often involves a slight drop in stress due to the formation of a so-called neck. Thirdly, upon further stretching the polymer chains start to disentangle, followed by a drawing region where the tensile strength increases dramatically due to alignment of the chains. Finally, the polymer fractures.

Crystallinity, crosslinking or branching can influence the tensile behaviour, as the polymer network will limit chain mobility. When a semi-crystalline polymer is stretched, the drawing region is limited and no dramatic gain in tensile stress is observed. Semi-crystalline polymers such as polyethylene typically display necking behaviour and a yield point in tensile stress-strain curves. Yield points are associated with a deformation mechanism, which absorbs energy. For semi-crystalline polymers the mechanism involves orientation and destruction of micron to colloidal scale semi-crystalline morphologies.

When a polymer is crosslinked, the polymer chains cannot stretch as easily as they are fixed, resulting in a very different stress-strain behaviour, where brittle fracture occurs even before the yield point. An un-crosslinked hyperbranched polymer does not have chain entanglements and thus cannot elongate, which often makes them too brittle to even confirm this behaviour on a tensile tester.

As discussed in the previous chapter, a crosslinked hyperbranched polymer shows structural similarities with a crosslinked epoxide polymer network and therefore similar tensile behaviour is expected. This is also what we observed from the obtained stress-strain curves.

3.4 Conclusion

We have demonstrated that introducing reactive 4-(phenylethynyl)phenol (PEP) end-groups (10, 20 and 40%) at the hyperbranched polyaryletherketone (HBPAEK-69K) chain ends is a route towards flexible and transparent films with useful mechanical properties. The T_g increased from 151 to 187 °C after cure, and even to 252 °C when applying a post cure procedure. Rheology experiments revealed a rapid increase in storage modulus between 250–350 °C, confirming that the PEP end-groups are effective crosslinking functionalities. The M_e was calculated for the neat HBPAEK-69K and PEP end-capped HBPAEK-69K, with values of 11-18 kg/mol for the PEP crosslinked HBPAEK, compared to 1100 kg/mol for the neat HBPAEK-69K. An increase in PEP concentration resulted in an increase in crosslink density and a corresponding decrease in M_e. All PEP end-capped HBPAEK-69Ks could be crosslinked into flexible free standing films with a storage modulus of 3-4 GPa. Crosslinked films exhibit a maximum tensile strength of ~40 MPa at 2% elongation, which corresponds to a toughness of ~0.3 kJ/m^3. In conclusion, our results show that a carefully designed reactive HBPAEK formulation with a proper cure protocol can give crosslinked films that exhibit mechanical properties comparable to that of an epoxy-based thermoset.

3.5 References

1. Núñez, F. M., de Abajo, J., Mercier, R. & Sillion, B. Acetylene-terminated ether-ketone oligomers. *Polymer* **33,** 3286–3291 (1992).

2. Delfort, B., Lucotte, G. & Cormier, L. Ethynyl-terminated polyethers from new end-capping agents: Synthesis and characterization. *J. Polym. Sci. Part A Polym. Chem.* **28,** 2451–2464 (1990).

3. Lucotte, G., Cormier, L. & Delfort, B. Ethynyl terminated ethers. Synthesis and thermal characterization of 2,2 bis (ethynyl-4-phenylcarbonyl-4-phenoxy-4-phenyl) propane and 2,2 bis (ethynyl-4-phenylsulfonyl-4-phenoxy-4-phenyl) propane. *Polym. Bull.* **24,** 577–582 (1990).

4. Taguchi, Y., Uyama, H. & Kobayashi, S. Synthesis of a novel cross-linkable poly(aryl ether ketone) bearing acetylene groups at chain ends. *Macromol. Rapid Commun.* **16,** 183–187 (1995).

5. Hedrick, J. L., Yang, a. C.-M., Scott, J. C., Economy, J. E. & McGrath, J. E. Elastomeric behaviour of crosslinked poly(aryl ether ketone)s at elevated temperatures. *Polymer* **33,** 5094–5097 (1992).

6. Liu, T. *et al.* Preparation and properties of film materials of poly(aryl ether ketone)-based phthalonitrile resins. *Polym. Eng. Sci.* **55,** 2313–2321 (2015).

7. Li, X. *et al.* Facile synthesis and characterization of hyperbranched poly(aryl ether ketone)s obtained via an A2 + BB'2 approach. *Polym. Int.* **59,** 1360–1366 (2010).

8. Mu, J., Zhang, C., Wu, W., Chen, J. & Jiang, Z. Synthesis, Characterization, and Functionalization of Hyperbranched Poly(ether ether ketone)s with Phenoxypheyl Side Group. *J. Macromol. Sci. Part A* **45,** 748–753 (2008).

9. Iqbal, M. All-aromatic liquid crystal thermosets and composites thereof. *PhD Thesis* (TU Delft, 2010).

10. Roberts, C. C., Apple, T. M. & Wnek, G. E. Curing chemistry of phenylethynyl-terminated imide oligomers: Synthesis of13C-labeled oligomers and solid-state NMR studies. *J. Polym. Sci. Part A Polym. Chem.* **38,** 3486–3497 (2000).

11. Hergenrother, P. ., Connell, J. . & Smith, J. . Phenylethynyl containing imide oligomers. *Polymer* **41,** 5073–5081 (2000).

12. Yuan, W. Z. *et al.* Disubstituted Polyacetylenes Containing Photopolymerizable Vinyl Groups and Polar Ester Functionality: Polymer Synthesis, Aggregation-Enhanced Emission, and Fluorescent Pattern Formation. *Macromolecules* **40,** 3159–3166 (2007).

13. Hawker, C. J. & Chu, F. Hyperbranched Poly(ether ketones): Manipulation of Structure and Physical Properties. *Macromolecules* **29,** 4370–4380 (1996).

14. Jiang, H., Su, W., Mather, P. T. & Bunning, T. J. Rheology of highly swollen chitosan/polyacrylate hydrogels. *Polymer* **40,** 4593–4602 (1999).

15. Li, M., Bijleveld, J. & Dingemans, T. J. Synthesis and properties of semi-crystalline poly(decamethylene terephthalamide) thermosets from reactive side-group copolyamides. *Eur. Polym. J.* **98,** 273–284 (2018).

16. Cambridge University Engineering Department. *Materials data sources*. *Materials & Design* (Elsevier, 2003).

17. Goodman, S. H. *Handbook of thermoset plastics*. (Elsevier Science, 1998).

18. Ward, I. M. & Sweeney, J. *Mechanical properties of solid polymers*. *John*

Wiley & Sons (1983).

Chapter 4

Crosslinked HBPAEK Membranes for Gas Separation Applications

Abstract

We have explored crosslinked HBPAEK thin films (~ 150 nm) as membranes for high-pressure gas separation applications. By end-capping the all-aromatic HBPAEKs with 10 or 20 mol% phenylacetylene, processable precursors were obtained that could be cured into membranes with Tg's as high as 250 °C and an excess fractional free volume (EFFV) of 9.5%. Upon exposure to CO_2, the membranes showed minimal swelling (~3%) at 50 bar and no signs of plasticization. When exposed to air with a relative humidity of 50%, the membranes showed 0.15% swelling, which is considered to be low. Crosslinking the HBPAEK using phenylacetylene is critical in terms of achieving a high Tg and high EFFV. Our results show that replacing only 10 mol% of the fluorine end-groups on the HBPAEKs with phenlyacetylene will suffice.

This chapter is based on the paper: "All-aromatic Crosslinked Hyperbranched Poly(aryletherketone)s for gas separation at elevated temperatures" by Vogel et al., to be submitted.

4.1 Introduction

In contrast to linear PAEKs, which are often highly crystalline and intractable, HBPAEKs are readily soluble in common organic solvents at room temperature, and this enables film-casting and spin-coating of all-aromatic PAEK-based membranes. By spin-coating the soluble HBPAEK precursor onto a solid support, mechanical properties are less of a concern. In this way the excellent properties and tunability of HBPAEKs can be further explored as membranes. In this Chapter we will report on the preparation and characterisation of crosslinked HBPAEKs films as high-pressure gas separation membranes.

Polymeric membranes provide an energy efficient technique to separate valuable gases. Of particular interest is the separation of CO_2 from high-pressure gas mixtures containing e.g. methane to make natural gas and biogas suitable for use as fuels.[1,2] To enhance the membrane performance, people often increase the excess free fractional volume (EFFV) in the polymer, or improve the affinity of the polymer towards the permeating component.[3,4] Well-known polymers for the separation of CO_2 from other gasses are the thermally and chemically stable 4,4'-(hexafluoroisopropylidene)diphthalic anhydride (6FDA)-based polyimides. The CF_3 groups are believed to restrict torsional motion of the phenyl rings leading to less ordered chain packing and increased excess free volume.[5] Polyimides functionalized with CF_3 groups are known to exhibit both higher permeability and permselectivity compared to conventional polyimides due to this additional bulkiness,[6,7] while debate continues on the role of the fluorine atoms and their affinity for certain gases.[8,9] In addition, all-aromatic poly(aryletherketone)s (PAEKs) are interesting candidates for their use as high-performance polymer membranes due to their chemical stability and ability to operate at high temperatures.[10,11] However, processing these polymers is hard and requires high

temperatures or harsh solvents. They are also semi-crystalline, which is a disadvantage for gas separation membranes as the crystal domains hinder gas transport. For these reasons PAEKs have not received much attention as membranes for gas separation.

While polymers like linear polyetherketone (PEK) or polyetheretherketone (PEEK) are practically insoluble in common solvents, HBPAEKs are soluble at room temperature in solvents such as THF, $CHCl_3$ and NMP,[12] which offer significant advantages in terms of solution-based thin film processing, as shown in Figure 4.1. These thin films can be used as membranes for the gas separation of, for example, H_2 and CO_2. A benefit of HBPAEKs is their amorphous nature due to their high degree of branching (DB=0.5). Additionally, branching increases the excess free volume (EFFV) of the polymer network, which is an important design parameter for a gas separation membrane.[13] To improve the mechanical properties of the HBPAEK and to increase the EFFV and T_g of the final membranes, we explored the possibility of (1) crosslinking the polymers via self-condensation (Chapter 2), and (2) by adding reactive end-groups in the form of phenylacetylene (Chapter 3).[14] The resulting rigid polymer network is also envisioned to be stable towards CO_2 induced plasticization, a frequently occurring phenomenon for membranes where the gas separation capabilities are significantly reduced or even lost due to increased mobility of the polymer chains.

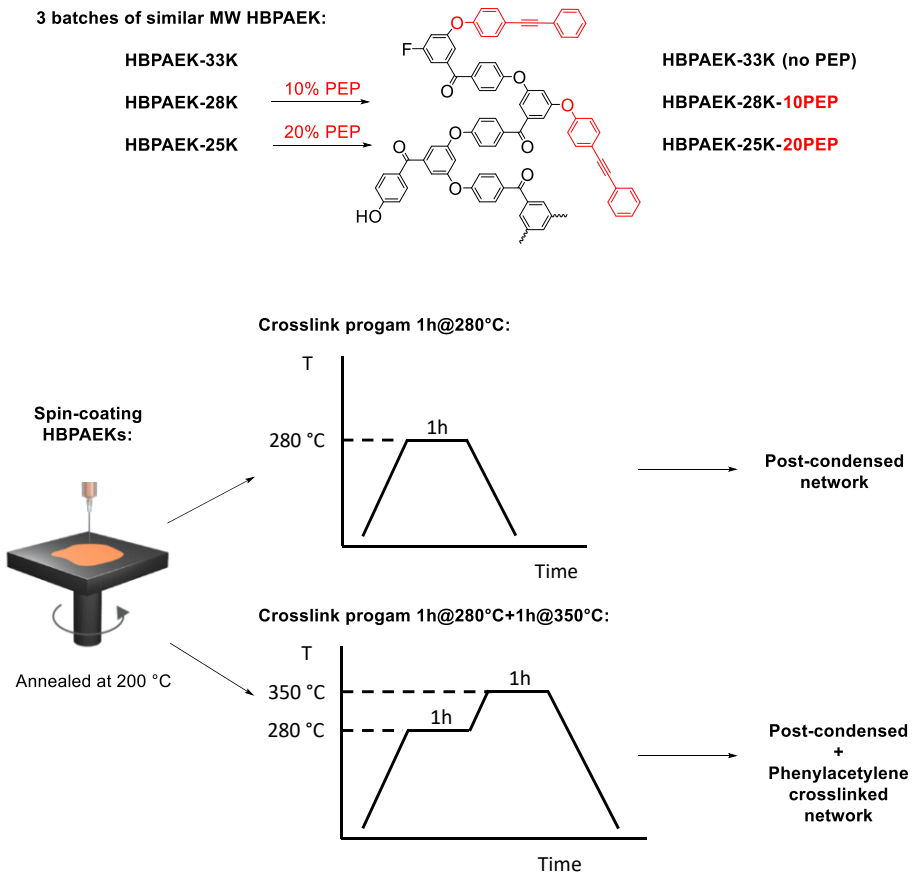

Figure 4.1. Three batches of HBPAEKs with a similar MW were used for this study: HBPAEK-33K, HBPAEK-28K and HBPAEK-25K. Fluorine-terminated HBPAEK-33K was used as a reference for the phenylacetylene end-capped HBPAEK-28K-10PEP and HBPAEK-25K-20PEP. All three compounds were spin-coated on an alumina substrate and exposed to two different curing profiles, i.e. 1h@280°C or 1h@280+1h@350°C, to induce crosslinking via post-condensation only (Chapter 2) or to induce crosslinking via both post-condensation and phenylacetylene end-group cure chemistry (Chapter 3).

In this chapter we will report on the thin film properties and membrane performance of neat HBPAEK-33K and two phenylethynyl crosslinked HBPAEKs, i.e. HBPAEK-28K-10PEP and HBPAEK-25-20PEP. We prepared thin films via spin-coating and we will discuss how different cure profiles affect the glass transition temperature (T_g) and excess fractional free volume (EFFV). Spectroscopic ellipsometry will be used to monitor CO_2 induced plasticization. Additionally, we will discuss the CO_2 sorption of the membranes, as well as the hydrophobicity and water sorption to evaluate their potential as gas separation membranes.

4.2 Experimental section

4.2.1. Materials and equipment.

Dry NMP was obtained from Acros Organics and used as received. Phenyl acetylene was purchased from Sigma Aldrich and vacuum distilled before use. Glass transition temperatures of the HBPAEKs before cure were measured at mid-point with differential scanning calorimetry (DSC) using a TA instruments 2500 series with a rate of 10 °C/min under nitrogen atmosphere. The thermal gravimetric analysis (TGA) measurements were done with a TA instruments 5500 TGA at 10 °C/min under nitrogen purge in aluminium pans.

^{1}H NMR (400 MHz) and ^{13}C NMR (100 Hz) spectra were recorded on a Varian AS-400 spectrometer and chemical shifts are given in ppm (δ) relative to tetramethylsilane (TMS) as an internal standard. The ^{1}H NMR splitting patterns are designated as follows: s (singlet), d (doublet), dd (double doublet), t (triplet), q (quartet), m (multiplet) and b (broad signal). The coupling constants, if given, are in Hertz.

Size exclusion chromatography (SEC) spectra were obtained using a Waters 2695 separations module liquid chromatograph, Waters 2414 refractive index detector at room temperature, and Waters 2996 photodiode array detector with styragel HR columns. Tetrahydrofuran was used as the mobile phase and the flow rate was set to 1 mL/min. The instrument was calibrated using polystyrene standards in the range of 580 to 892,800 Da. All samples were dissolved at a 1 mg/mL concentration in THF and filtered over a 0.45 µm PTFE filter prior to use.

The density of HBPAEKs was measured using an AccuPyc II 1340 gas displacement density analyser (Micrometrics, USA), using helium as gas source. For each sample, 150 individual density measurements were performed, where only the last 50 measurements were used to obtain the average density.

4.2.2. Syntheses

Three batches of similar MW fluorine-terminated HBPAEKs were synthesized according to the same experimental procedure that was described in Chapter 2: HBPAEK-33K, HBPAEK-28K and HBPAEK-25K. The differences in MW come from slight deviations in reaction time and are not expected to affect this study. From these 3 batches, HBPAEK-28K was end-capped with 10% PEP and HBPAEK-25K was end-capped with 20% PEP. The PEP end-capped HBPAEKs for this Chapter were synthesized via the method described in this section.

HBPAEK-28K-10PEP. To a 100 ml flask was added 2 g of 28K HBPAEK and this was dissolved in 30 ml NMP. K_2CO_3 (0.24 g, 1.7 mmol) and PEP (0.17 g, 0.85 mmol) were added and the solution stirred at 160 °C overnight. The dark solution was precipitated in ice-cold water and the solid was collected, washed in a Soxhlet apparatus for 24 h with MeOH and dried in vacuo at 60 °C. The yield was quantitative. ^{1}H NMR (400 MHz, $CDCl_3$), δ = 7.88-7.51 (m, 2H), 7.31-6.50 (m, 5H).

^{13}C NMR ($CDCl_3$): 192.80, 162.90, 160.32, 140.69, 132.61, 118.91, 116.51, 112.78, 107.70, 94.49 (phenylacetylene), 89.05 (phenylacetylene).

HBPAEK-25K-20PEP. To a 100 ml flask was added 2 g of 25K HBPAEK and this was dissolved in 30 ml NMP. K_2CO_3 (0.47 g, 3.4 mmol)) and PEP (0.33 g, 1.7 mmol) were added and the solution stirred at 160 °C overnight. The dark solution was precipitated in ice-cold water and the solid was collected, washed in a Soxhlet apparatus for 24 h with MeOH and dried in vacuo at 60 °C. The yield was quantitative. ^{1}H NMR (400 MHz, $CDCl_3$), δ = 7.90-7.50 (m, 2H), 7.30-6.50 (m, 5H). ^{13}C NMR ($CDCl_3$): 192.88, 162.89, 160.30, 140.72, 132.61, 118.88, 116.48, 112.78, 107.70, 94.47 (phenylacetylene), 89.03 (phenylacetylene).

4.2.3. Ellipsometry

Film preparation

Thin HBPAEKs films with a thickness of ~150 nm were spin-coated (Laurell WS-400B-6NPP-Lite) on a silicon wafer (100, front side polished, CZ test grade, Silchem). Depending on the wafer size, 40-120 µL of HBPAEK (1.5 wt% in $CHCl_3$ or 3 wt% in cyclopentanone) was deposited with a spin-coating speed of 4000 rpm for 30 seconds. Films were annealed for 30 minutes at 200 °C under nitrogen atmosphere.

T_g measurements by in-situ spectroscopic ellipsometry

The thickness and refractive index of HBPAEKs films on silicon wafers were measured as function of time and temperature by *in-situ* spectroscopic ellipsometry (SE). Measurements were performed on a M2000-XI ellipsometer (J.A. Woolam Co., USA) equipped with a heating stage (THMSEL600, Linkam, UK), calibrated as described elsewhere.[15] Measurements were conducted at a fixed

angle of 70°, in the full wavelength range of 210-1000 nm under a 100 mL/min dry nitrogen flow. The initial T_g before thermal treatment was measured by heating the samples to 200 °C with 5 °C /min, where the samples were held for 15 min and sequentially cooled down again with 5 °C /min. The T_g was determined according to a literature reported procedure.[16]

Thermal cure programs

The two different temperature programs that were used to crosslink the HBPAEKs are shown in Figure 4.2. Program "1h@280 °C" has a heating and cooling rate of 5 °C /min, and a 1h dwell temperature of 280 °C to induce crosslinking via post-condensation only. Program "1h@280°C+1h@350°C" has a heating and cooling rate of 5 °C /min and a dwell of 1h at 280 and 1h 350 °C to induce crosslinking via both post-condensation and reactive phenylacetylene end-groups. At least two different samples were measured for each temperature program.

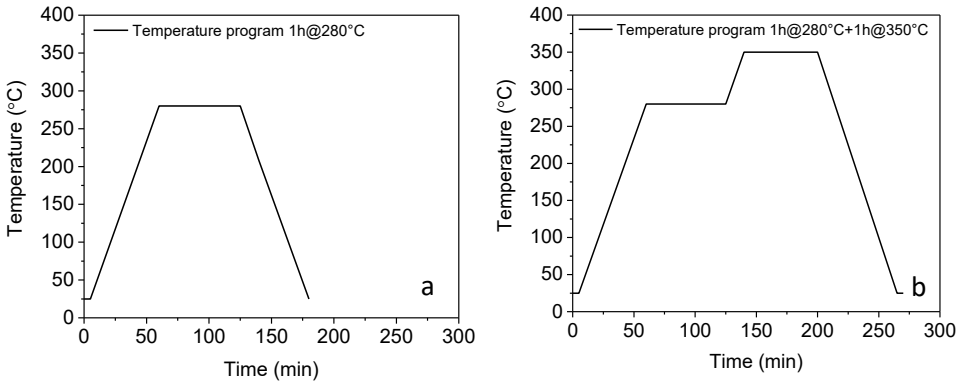

Figure 4.2. The thermal crosslink profile used for this study as a function of temperature versus time. (a) Temperature profile with an isothermal hold at 280 °C for 1h. (b) Temperature profile with a isothermal hold at 280 °C for 1h and 350 °C for 1h.

The obtained spectra were analysed using CompleteEASE (v4.86, J.A. Woollam Co., USA). The HBPAEK film was modelled as an isotropic Cauchy layer fitted in the wavelength range from 500-1000 nm (fit parameters: thickness, A, B, and k, the Urbach absorption tail), on top of a Silicon wafer with a 2 nm native oxide layer. The temperature dependent optical parameters of the silicon wafer are taken from the literature.[17]

CO_2 sorption by in-situ spectroscopic ellipsometry

CO_2 sorption experiments were conducted at elevated gas pressures with an Alpha-SE ellipsometer® (J.A. Woollam Co. Inc.). All measurements were performed at a fixed angle of 70° and a wavelength range of 370-900 nm. A home-built cell stainless steel cell (Pmax=200 bar, Tmax=200 °C) equipped with a temperature and pressure control system was used. The pressure was controlled and stabilized using a syringe pump (Teledyne ISCO, 500D), and the temperature of the pump was kept constant using a water bath at 35 °C. A correction for pressure-induced birefringence of the cell windows was performed using a high-pressure CO_2 calibration measurement on a 500 nm SiO_2/Si wafer.

The obtained spectra were modelled using CompleteEASE (v4.86, J.A. Woollam Co., USA). The HBPAEK film was modelled as an isotropic Cauchy layer fitted in the wavelength range from 500-900 nm (fit parameters: thickness, A, B, and k, the Urbach absorption tail). The ambient was fitted as a Cauchy dispersion with the pressure dependent refractive index of CO_2.[18] From the film thickness and the refractive index the concentration of sorbed CO_2 can be calculated using the Clausius-Mosotti equation.[19,20]

4.2.4. Membrane preparation and characterization

HBPAEK membranes for gas separation experiments were prepared by dynamically spin-coating the polymer on an α-alumina porous support with a 3 μm thick γ-alumina top-layer (Pervatech, the Netherlands). HBPAEKs were dissolved in cyclopentanone (3 wt%) overnight. 0.15 mL of polymer solution was spun for 10 seconds at 500 rpm, followed by 5 minutes at 1000 rpm. The membranes were annealed directly after their synthesis to remove anisotropy induced by spin-coating. All membranes were heated to 200 °C with a heating rate of 10 °C/min for 30 minutes in a chamber furnace under a nitrogen atmosphere (Carbolite HTMA 5/28 500 °C). The membranes were cured by using the cross-link programs described in the previous section. The membrane thickness, used to calculate permeability, was assumed to be constant for all membranes, due to the identical spin-coating conditions.

4.2.5. Contact angle measurements

Static contact angle measurements on spin-coated HBPAEK films on silicon wafers were performed by the sessile drop method (2 μL, Mili-Q water) with an OCA 15 (Dataphysics, Germany). The contact angle was determined 3s after applying the water droplet to the surface with Python (v3.5) software using the scipy.ndimage package (v0.18.1) .

4.2.6. H_2O sorption by in-situ spectroscopic ellipsometry

SE measurements with varying humidity were performed using a M2000-X (J.A. Woollam Co., USA) ellipsometer equipped with a heated liquid cell (J.A. Woollam Co., USA) at a fixed angle of 75°. The temperature of the liquid cell was set to 35 °C. Nitrogen gas was bubbled through two bubblers in series filled with water, and mixed with dry nitrogen. The sum of the two flows was kept constant at 300

mL/min. A humidity sensor (Sensirion digital humidity sensor, SHTW2) was placed at the outlet of the cell, and the humidity in the cell was calculated from the humidity and temperature measured at the outlet of the cell by using the Buck equation.[21] The maximum humidity for this set-up was 50%.

4.3 Results and discussion

4.3.1. Size exclusion chromatography

The molecular weight of the investigated HBPAEKs are all in the same range to exclude possible effects of molecular weight on the polymer membrane properties. The SEC curves are shown in Figure 4.3.

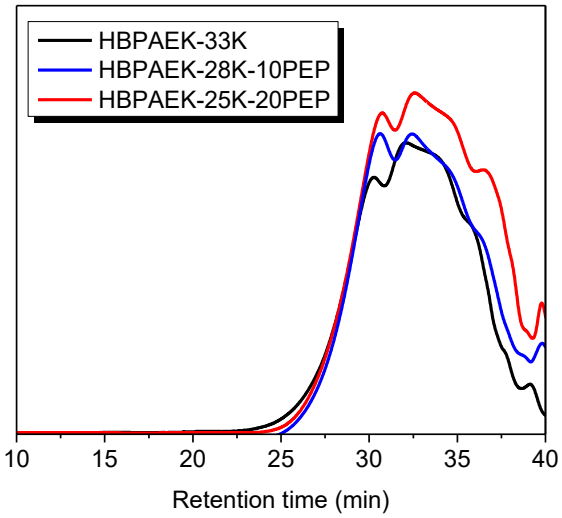

Figure 4.3. SEC data of HBPAEK-33K, HBPAEK-28K-10-PEP and HBPAEK-25K-20PEP in THF at a concentration of 1 mg/ml. All samples show a broad distribution and low MW fractions are visible towards the tail of the curves at a retention time close to 40 min.

The obtained M_n, M_w and polydispersity (PDI) from the SEC curves are listed in Table 4.1. There is no effect of adding the 10 and 20% PEP on the molecular weight, as was also observed in Chapter 3. The PDI values of all polymers are relatively high, characteristic for hyperbranched polymers. The degree of branching for all HBPAEKs was around the theoretical value of 0.5, as determined by the literature procedure using ^{19}F NMR and discussed in Chapter 2.

Table 4.1. SEC, T_g, TGA, density and contact angle data for HBPAEK-33K, HBPAEK-10PEP and HBPAEK-20PEP.

HBPAEK	Mn (kg/mol)[a]	Mw (kg/mol)[a]	PDI[a]	T_g [b] (°C)	$T_{d2\%}$[c] (°C)	Density[d] (g/cm^3)	Contact angle[e] (°)
HBPAEK-33K	5	33	7	155	452	1.50 ± 0.04	96 ± 5
HBPAEK-28K-10PEP	6	28	5	201	406	1.45 ± 0.01	103 ± 9
HBPAEK-25K-20%PEP	4	25	6	189	393	1.44 ± 0.02	100 ± 4

[a] Obtained with size exclusion chromatography in THF (1 mg/ml)
[b] Obtained with DSC as mid-point value, 20 °C/min under nitrogen
[c] 2% weight loss, 10 °C/min under nitrogen
[d] Obtained by helium pycnometry for uncross-linked HBPAEKs, error represents the standard deviation
[e] Error represents the 95% confidence interval

4.3.2. Thermal properties

HBPAEKs are, like their linear analogue, thermally very stable. In Figure 4.4 the weight loss as function of temperature of the uncross-linked and crosslinked HBPAEKs is shown. All HBPAEKs show an initial weight loss starting around 270 °C, that corresponds to the post-condensation process (Chapter 2), where fluorine and hydroxyl groups react and release HF. Outgassing of small MW fractions start at temperatures above 400 °C, shown by the decrease in mass. The degradation of small MW fractions, e.g. dimer, trimer etc. is proposed to cause the difference amongst the three compounds, where the HBPAEK having the highest amount of PEP groups also shows the highest abundance of lower molecular weight molecules, which is supported by the SEC curves of Figure 4.3.

In Figure 4.4 an increase in thermal stability is observed for the HBPAEK-28K-10PEP and HBPAEK-25K-20PEP when these materials are cured at 280-350 °C, whereas the neat HBPAEK did not show an improvement in thermal stability upon curing. This is most probably caused by crosslinking of the lower molecular weight fractions which are, after curing, part of the network structure.

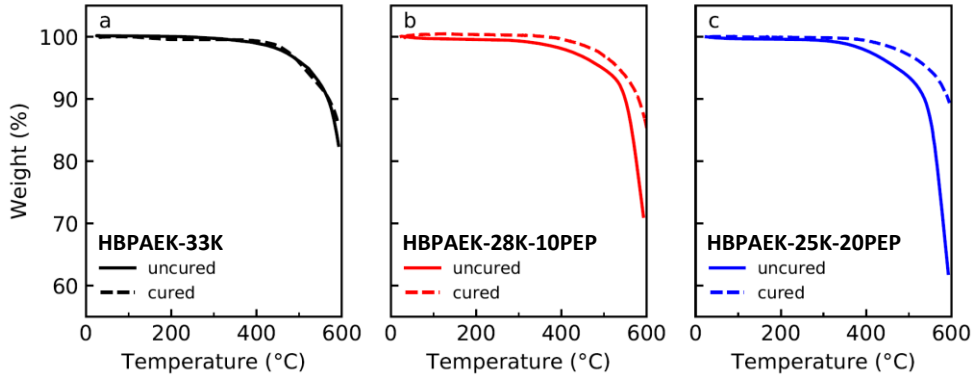

Figure 4.4. Weight loss as function of temperature for (a) HBPAEK-33K, (b) HBPAEK-28K-10PEP, and (c) HBPAEK-25K-20PEP. The solid lines represent the uncured polymers, and the dashed lines the cured polymers (cured using program 1h@280°C+1h@350°C).

Glass transition temperature

The glass transition temperature (T_g) of the uncross-linked HBPAEKs was measured by DSC and the curves are shown in Figure 4.5. The T_g for the neat HBPAEK is 155 °C. Introducing PEP end-groups results in a significant increase (up to 46 °C) in T_g. A change in T_g when the end-groups are replaced is recurrently observed for HBPs in literature. For example, Hawker reported a T_g range of 97-290 °C with hyperbranched poly(etherketone)s[22] and Webster a range of 96-238 °C for hyperbranched polyphenylenes.[23,24]

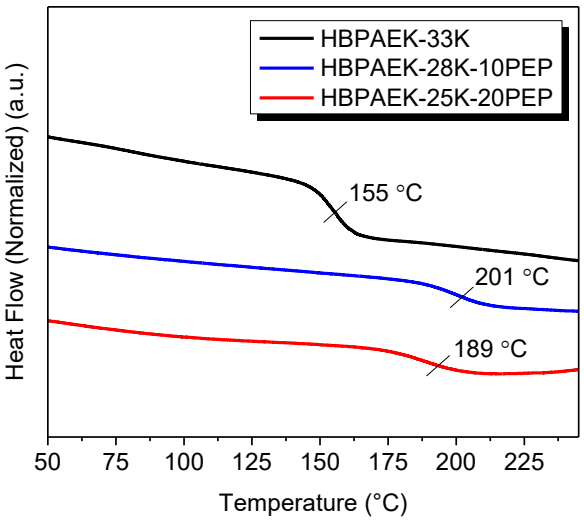

Figure 4.5. The DSC curves (endo down) showing the glass transition temperatures of uncross-linked HBPAEK-33K, HBPAEK-28K-10PEP and HBPAEK-25K-20PEP, as first heat, 20 °C/min under N_2 atmosphere.

This increase is in sharp contrast with the T_g of the end-capped HBPAEK reported in the previous chapter, however, the synthesis route is different and because we've used a longer reaction time and higher reaction temperature it may be possible that HBPAEK globules have started to inter connect and form larger agglomerates.

4.3.3. Relative film thickness and refractive index as function of thermal treatment

Figure 4.6a shows the relative thickness and Figure 4.6b the refractive index as a function of time for HBPAEK-28K-10PEP cross-linked at 280-350 °C. The thickness of the polymer film increases during heating to 280 °C due to thermal expansion. The temperature at which the change in the slope occurs, represents the T_g. While the temperature is constant at 280 °C, the polymer shows a little overshoot in

thickness due to the thermal expansion directly followed by a decrease in thickness because of densification during crosslinking. The same effect is visible while heating to 350 °C, but more pronounced due to the higher temperature. Upon cooling, the material shrinks, and shows a T_g at a much higher temperature due to crosslinking of the material. The final film thickness has decreased by 3% after crosslinking due to compaction.

The refractive index of the HBPAEK film decreases upon heating due to thermal expansion. While the refractive index is more or less constant during the first isothermal hold at 280 °C, it increases by 0.5% at the 350 °C isothermal hold due to crosslinking of the phenylethynyl functionalities. The final refractive index is unchanged compared to the index of the uncross-linked polymer. The changes in the thickness are relatively small, and the refractive index data is less accurate than the thickness, therefore small structural changes are not shown in the refractive index data. The data for HBPAEK-33K and HBPAEK-25K-20PEP were collected using a similar procedure and the graphs are shown in Appendix A.

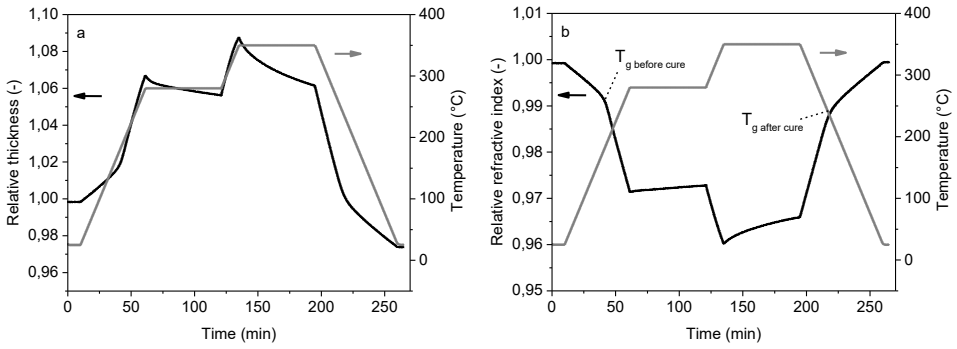

Figure 4.6. Thermal behaviour of a HBPAEK-28K-10PEP thin film using the 280-350 °C cure program. (a) Relative thickness as function of time, and (b) relative refractive index as function of time.

The linear coefficient of thermal expansion (CTE) can be calculated using:

$$\alpha = \frac{1}{d} \cdot \frac{\mathrm{d}d}{\mathrm{d}T} \qquad (1)$$

Where α is the linear coefficient of thermal expansion (°C^{-1}), d the initial thickness (m), dd the change in thickness (m), and dT the change in temperature (°C). The CTE can be extracted from the slope of the thickness versus time when above the T_g. The values of the thickness and temperature were obtained for both the heating and cooling phase. The initial temperature was defined as T_{max}-80, and the final temperature as T_{max}-5. The initial and final thicknesses were obtained at these temperatures. Figure 4.7 shows an example of how data points were selected. All red points represent the data for the CTE at heating, and the blue points at cooling. The squares correspond to the thickness data, and the circles to the temperature data.

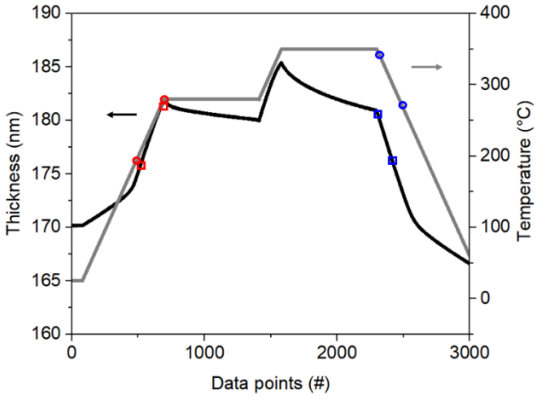

Figure 4.7. Data points selection that were used to calculate the linear coefficient of thermal expansion (red = heating and blue =cooling). The initial temperature was defined 80 degrees below the maximum temperature, and the final temperature 5 degrees below the maximum temperature.

Although there is a relatively large spread in the CTE between the three HBPAEKs studied, the CTE is always significantly larger upon cooling compared to heating (Table 4.2). This indicates that during the heating phase, there is already compaction of the material because of crosslinking, and thus that crosslinking is already occurring during heating of the polymer.

Table 4.2. Linear coefficient of thermal expansion of HBPAEK-33K, HBPAEK-28K-10PEP and HBPAEK-25K-20PEP as measured by SE. The average of two samples is taken.

Cure Profile	**HBPAEK-33K (10^{-6} °C^{-1})**		**HBPAEK-28K-10PEP (10^{-6} °C^{-1})**		**HBPAEK-25K-20PEP (10^{-6} °C^{-1})**	
	Heat	Cool	Heat	Cool	Heat	Cool
1h@280°C	461	540	486	537	475	528
1h@280-350°C	456	504	476	551	478	521

4.3.4. Spectroscopic ellipsometry

To study the effect of post-condensation and crosslinking of PEP on the T_g and EFFV, the change in film thickness and refractive index of HBPAEK films were measured by *in-situ* spectroscopic ellipsometry (SE) equipped with a heating stage. The polymers were heated using two different temperature programs, which enabled us to investigate how the crosslinking temperature affects the thermal and optical properties. The films were either heated to 280 °C, with a 1-hour dwell or heated to subsequently 280 °C and 350 °C with a 1-hour dwell at both isothermal stages. The temperature profiles are plotted as a function of time in the experimental section in Figure 4.2. Additionally, the coefficients of thermal expansion were derived with SE, using the thickness versus temperature slope.

The glass transition temperature (T_g) and excess free fractional volume (EFFV) of the polymers can be obtained from these SE data.[16]

Figure 4.8 graphically illustrates the dependence of the T_g for all HBPAEKs upon crosslinking. The values shown are the average taken of at least two individual measurements, where the absolute difference in T_g between the measurements was always smaller than 3 °C.

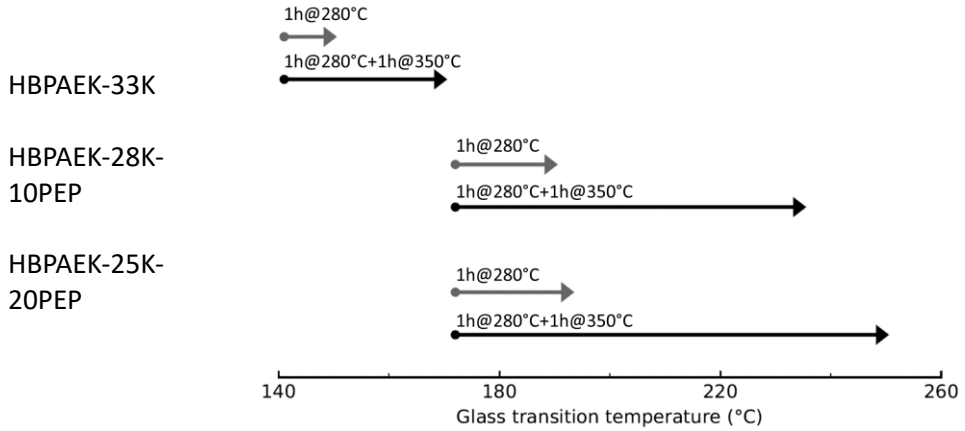

Figure 4.8. The change in T_g as a function of the cross-link temperature for the different HBPAEKs measured by in-situ SE. The arrows indicate the change in T_g before and after crosslinking. The temperature program is mentioned above the corresponding arrow and refers to an isothermal hold at that temperature.

The T_g of all polymers increases with crosslinking due to the reduced chain mobility and is clearly related to the amount of PEP cross-linker. Introducing phenylacetylene end-groups increases the T_g to 172 °C and can reach values of up to 250 °C after curing. The initial values of the T_g for the uncross-linked HBPAEKs obtained by ellipsometry are lower compared to those obtained by DSC (Figure 4.5), although the trend is similar. This difference originates from the difference in measurement technique.

When the polymers are heated to 280 °C, a post-condensation process starts, resulting in a relatively small increase in T_g for all polymers. This curing starts around 270 °C, based on rheology data presented in Chapter 3, and will continue with increasing the temperature. At temperatures above 300 °C, the phenylacetylene groups of the PEP end-groups start to cross-link. The temperature program towards 350 °C results in a more pronounced effect on the T_g, as the T_g increases at least 35% compared to the uncross-linked polymer. The effect on the HBPAEKs without the phenylacetylene groups is limited, as the T_g will only increase marginally due to the post-condensation, as no phenylacetylene groups are present. When comparing polymers with and without PEP, we conclude that phenylacetylene crosslinking has the largest contribution to the increase in T_g.

Similar to the T_g, the EFFV of the polymers could be calculated from the SE temperature dependent data by using the following equation:

$$EFFV = \frac{h_{DG} - h^*_{DL}}{h_{DG}} \qquad (2)$$

Where h_{DG} is the glassy thickness and h^*_{DL} (D for dilation) the extrapolated liquid thickness.[16] Figure 4.9 shows the EFFV for all polymers before and after thermal treatment. The same trend is observed for the EFFV as for the T_g and that is crosslinking the HBPAEK results in an increase in EFFV.

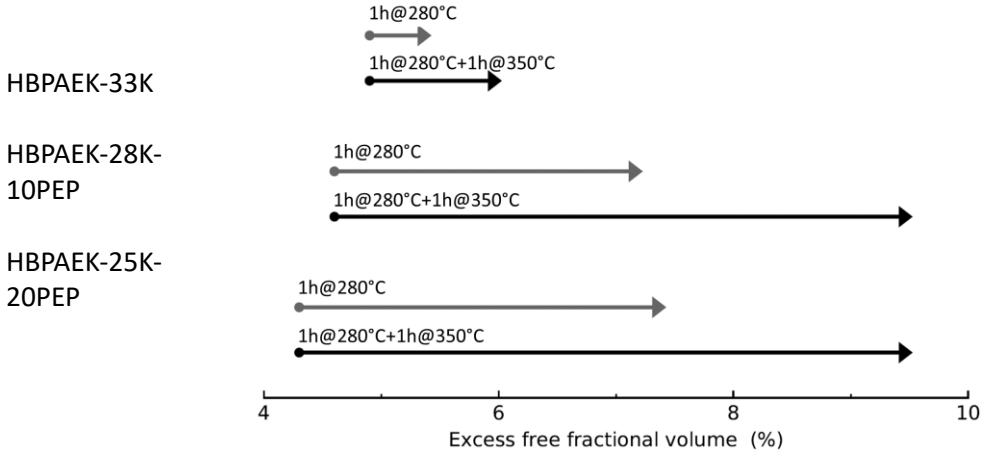

Figure 4.9. The change in EFFV as function of the cross-link temperature for the different HBPAEKs measured by in-situ SE. The arrows indicate the change in EFFV before and after crosslinking. The temperature program is indicated above the corresponding arrow and refers to an isothermal hold at that temperature.

A more significant increase in EFFV is observed when HBPAEKs with phenylacetylene end-groups are cross-linked. When the T_g is increased due to crosslinking, the polymer will be in the glassy state at a higher temperature, thus at an earlier point in time when cooling down. Therefore, the EFFV will be higher when cooled down to room temperature, as schematically shown in Figure 4.10. PEP containing HBPAEKs that are cured at 280 °C are found to have a higher EFFV as compared to cured neat HBPAEKs, which stresses the effect of introducing different end-groups on the EFFV of a hyperbranched polymer.

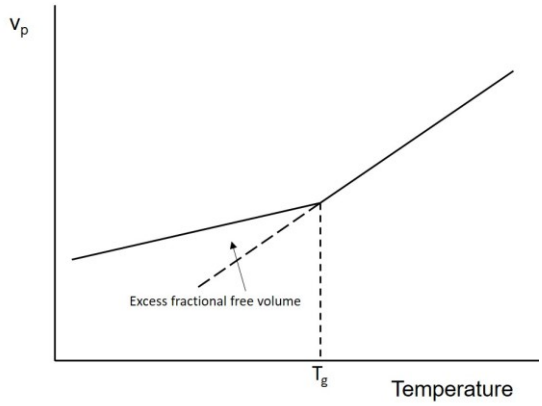

Figure 4.10. Simplified schematic representation of the excess fractional free volume (EFFV) of a polymer. This volume is considered as the space between polymer chains.

HBPAEKs bearing PEP end-groups have an EFFV of up to 9.5% after curing at 280-350 °C. This is relatively high compared to other glassy polymers such as the bisphenol A based polyetherimide Ultem 1000™ (7%), and the bisphenol A based polysulfone Udel P-3500™ (6.6%), but lower than Matrimid™ (12%) (data from unpublished work). Due to their high T_g and EFFV, the PEP containing HBPAEKs were further analysed for their CO_2 sorption behaviour and gas separation performance.

CO_2 sorption

The high T_g and high EFFV of HBPAEK-28K-10PEP and HBPAEK-25K-20PEP that were discussed in the previous paragraph, suggests that crosslinked HBPAEKs have potential to be used as gas separation membranes. High-pressure CO_2 sorption measurements were conducted to investigate the effect of CO_2 gas on these membranes. Figure 4.11 shows (a) the swelling, (b) relative refractive index, and

(c) adsorbed concentration of CO_2 as a function of the CO_2 pressure for HBPAEK-28K-10PEP that was cross-linked at 280-350 °C prior to the sorption measurements. Similar results were obtained for the HBPAEK-25K-20PEP and are presented in Appendix B.

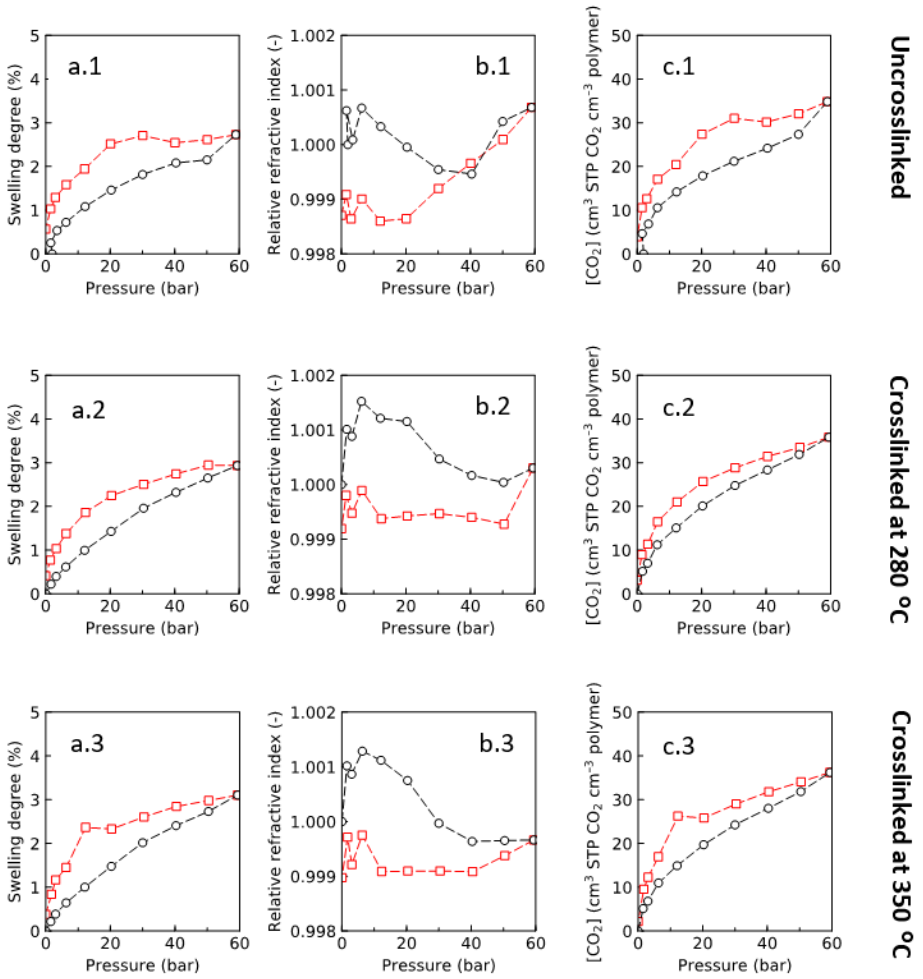

Figure 4.11. CO_2 sorption (**O**) and desorption (□) at 25 °C for HBPAEK-28K-10PEP, at pressures up to 60 bar. (a.1-3) Degree of swelling, (b.1-3) Relative refractive index, and (c.1-3) Concentration of CO_2 as function of pressure.

The obtained CO_2 induced swelling isotherms (Figure 4.11a.1-3) have a typical shape for a glassy polymer[25] with swelling degrees in the same order as linear sulfonated PEEK (SPEEK) (4% at 50 bar) but lower than Matrimid® (6.5% at 50 bar).[20] The relative refractive index of the HBPAEK films initially increases with increasing CO_2 pressures up to 60 bar, followed by a decrease in index with decreasing CO_2 pressure. This initial increase in refractive index can be attributed to filling of the EFFV by CO_2 molecules, while at higher pressures the dilation of the polymer matrix results in a decrease.[26,27] To what extent the index initially increases seems to be dependent on the EFFV. For example, HBPAEK-28K-10PEP that is uncured (Figure 4.11.b.1) has a lower EFFV, and therefore a lower initial increase in refractive index. The relative refractive index drops below 1 at vacuum after desorption, indicating that the polymer structure is changed due to dilation. The same behaviour is found for, for example, Matrimid®[27] or other poly(ether imide)s.[26] We note that the absolute changes in refractive index are extremely low, and in combination with a low sensitivity towards the refractive index, the data displays a trend instead of absolute numbers.

From the thickness and refractive index, the concentration of CO_2 in the polymer matrix was derived, as shown in Figure 4.11c. There is an initial steep increase in CO_2 concentration for all three samples due to filling of the EFFV, while at higher CO_2 pressures the sorption is limited by the dilation of the polymer network, and therefore the slope decreases.

HBPAEK-28K-10PEP, Figure 4.11.c1-3, shows a strong hysteresis between sorption and desorption for both the swelling and refractive index data. This originates from polymer chain reorganizations at the time scale of the measurements despite crosslinking of the polymer.

Plasticization

The glass transition temperature (T_g) of a polymer greatly affects the performance as a membrane. Above the T_g, the chains become more mobile, often resulting in a loss of selectivity. Polyimides have, among various other good properties, very high T_gs and are therefore among the best performing membranes to date. However, a process called plasticization is affecting the performance in a negative way and this happens not only in polyimides, but also in poly(etherimide)s. In the presence of CO_2, these polymers tend to become plasticized and the associated increase in chain mobility results in a reduction in selectivity. A method to mitigate this effect is to crosslink the polymer chains. By crosslinking, the chain mobility becomes significantly reduced and it was found to have a positive effect on membrane stability, physical ageing and plasticization. The downside of this method is that it is often accompanied with a decrease in permeability.

From the sorption isotherm the onset of plasticization could be determined as the point where the isotherm shows a steep linear increase with CO_2 pressure. In addition to this steep linear increase, no hysteresis between sorption and desorption is observed in the case of plasticization. The sorption isotherms for all 3 HBPAEKs (Figure 4.11 c1-3) show no increase in slope up to pressures of 50 bar CO_2, and thus we can conclude that no plasticization occurs at CO_2 pressures up to at least 50 bar. After this point the slope of the sorption isotherm seems to increase, however the signal noise and therefore errors at these extreme pressures are relatively large, making it impossible to conclude from this data the presence or absence of plasticization at pressures above 50 bar. This lack of plasticization is in great contrast to often used linear polymers for gas separation.[28]

4.3.5. Contact angle measurements

Figure 4.12 shows the contact angle results for the 3 HBPAEK films on silicon wafers measured with the sessile drop method using Mili-Q water. From these data it cannot be concluded that there is a difference in contact angle between the different HBPAEKs and the uncross-linked or cross-linked state. The average contact angle varies between 95° and 103°, confirming the hydrophobic character of the HBPAEKs. The values are similar to earlier reported contact angles for comparable aromatic hyperbranched polymers with fluorine groups.[29]

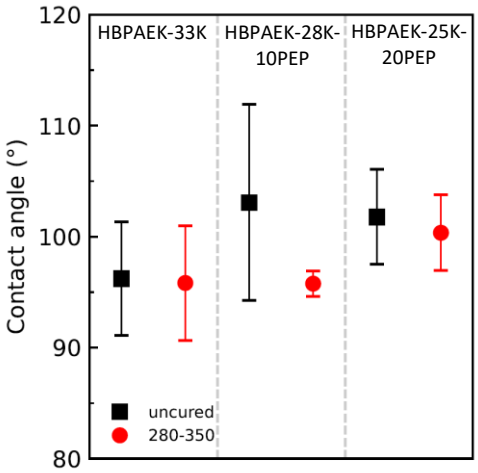

Figure 4.12. The contact angle of uncross-linked and cross-linked (temperature program 280-350 °C) HBPAEK films on silicon wafers. The error bars represent the 95% confidence interval determined over 5 measurements.

4.3.6. Water sorption

Gas separation membranes can suffer from the presence of water vapor in the feed stream. Membranes like Matrimid® can lose up to 60% of the CO_2 and CH_4 permeability due to occupation of the voids with water.[30] Figure 4.13 shows the relative thickness (a), and relative refractive index (b) for HBPAEKs containing 10%

PEP (□) and 20% PEP (**O**) cross-linked at 350 °C as a function of relative humidity, measured by SE. The PEP end-capped HBPAEKs show very little swelling in water vapour. There is a slight increase in relative refractive index, due to the replacement of voids (*n* = 1.00) with water (*n* = 1.33).

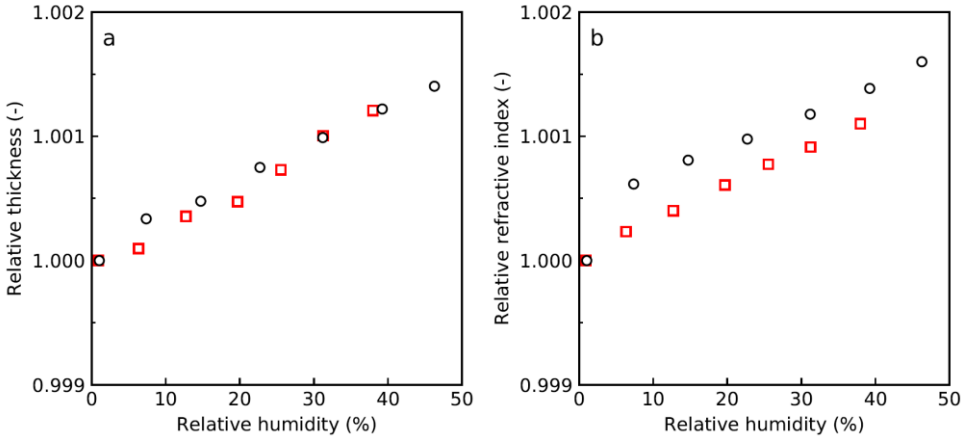

Figure 4.13. Relative thickness (a) and relative refractive index (b) for HBPAEK-28K-10PEP (□) and HBPAEK-25K-20PEP (**O**) cross-linked at 350 °C as function of relative humidity.

The experimental set-up was limited to 50% relative humidity (RH), but from the data we expect the relative thickness to not exceed 0.3%. For Matrimid®, a 2% increase in thickness is observed at 50% RH with a 1% increase in refractive index. For bisphenol A-based polysulfone (PSF) an increase in thickness of 0.1% was observed at a 50% RH with hardly any change in refractive index.[31]

4.4 Conclusion

We have demonstrated that our all-aromatic HBPAEKs with reactive phenylacetylene functionalities can be processed into 150 nm thin films on an alumina support using a standard solution-based spin-coating method. The obtained membranes are fully amorphous and upon thermal treatment, they can be crosslinked into robust defect free films. The T_g and EFFV can be tuned using a simple thermal cure program. Membranes cured at 280 °C for 1 h. and 350 °C for 1 hour show an increase in T_g from 150 to 250 °C and an increase in EFFV from 4 to 9.5%. CO_2 sorption and desorption experiments at 25 °C showed that the HBPAEK membranes swell to about 3% at 50 bar CO_2 with no signs of plasticization, which is a major improvement over current state-of-the-art membranes. The HBPAEKs are also insensitive to moisture. Membranes showed minimal swelling of 0.15% when exposed to air with a relative humidity of 50%. The gas separation performance of the crosslinked HBPAEKs will be discussed in detail in Chapter 5.

4.5 Appendices

4.5.1. Appendix A

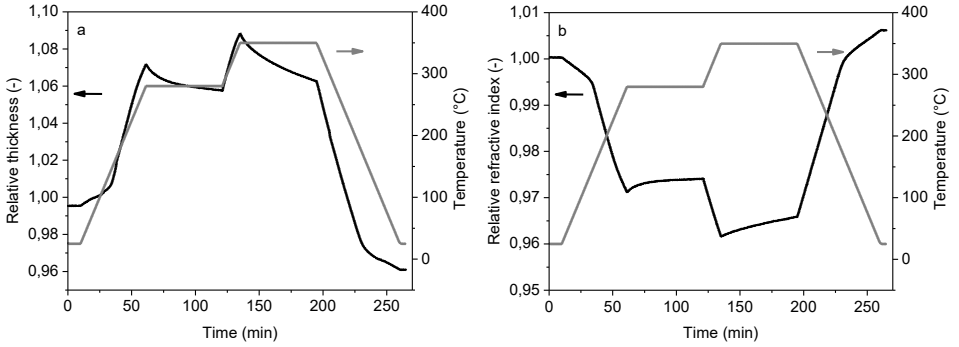

Figure A1. Thermal behaviour of HBPAEK-33K using the 280-350 °C temperature program. (a) Relative thickness as function of time, and (b) relative refractive index as function of time. The second y-axis represents the temperature for both graphs.

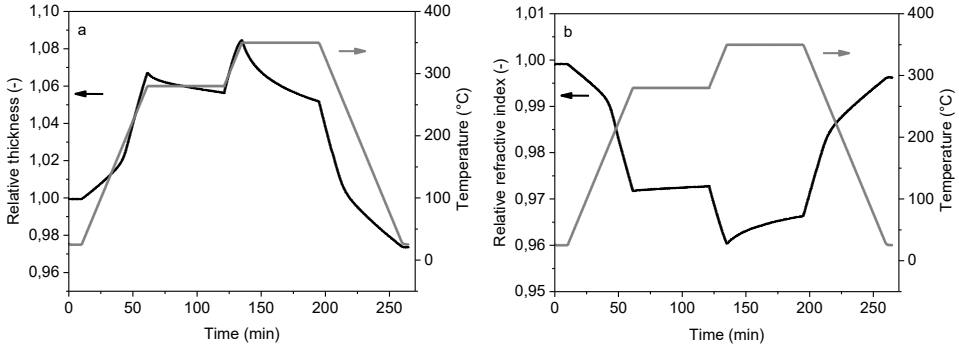

Figure A2. Thermal behaviour of HBPAEK-25K-20PEP using the 280-350 °C temperature program. (a) Relative thickness as function of time, and (b) relative refractive index as function of time. The second y-axis represents the temperature for both graphs.

4.5.2. Appendix B

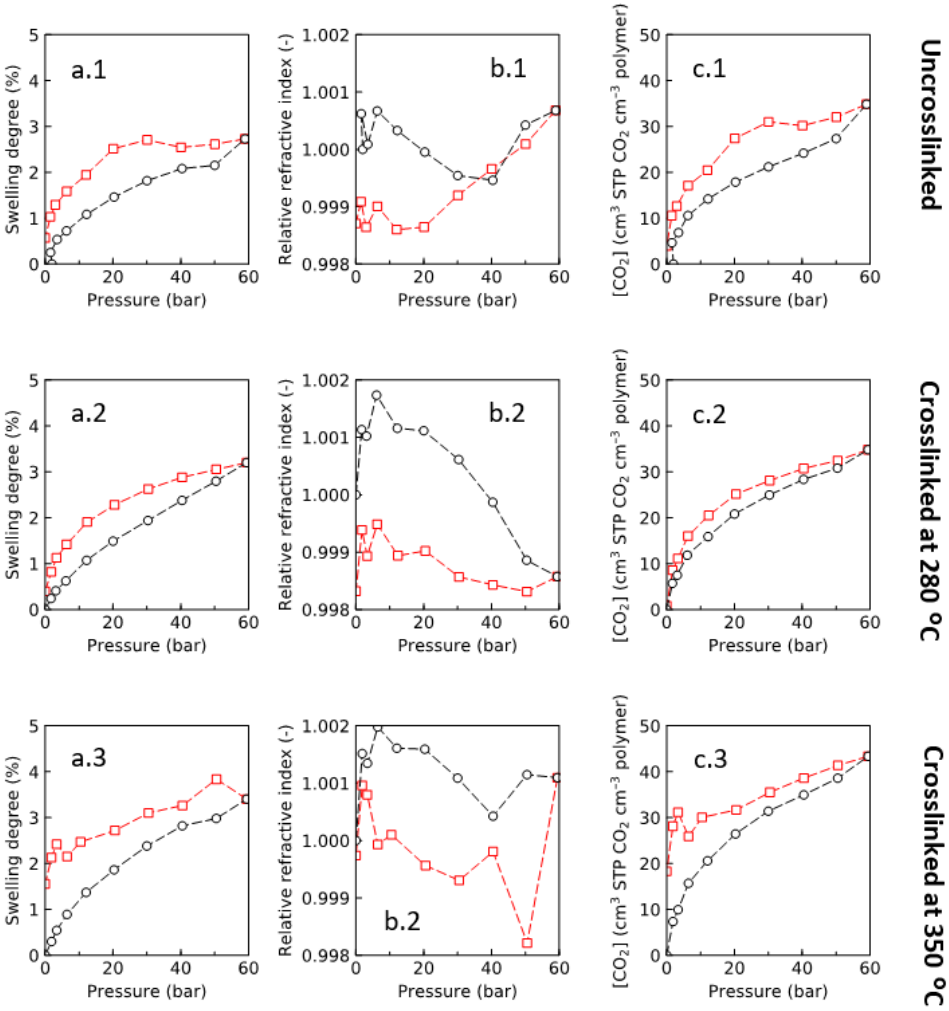

Figure B1. CO_2 sorption (**O**) and desorption (□) at 25 °C for HBPAEK-25K-20PEP, at pressures up to 60 bar. (a.1-3) Degree of swelling, (b.1-3) Relative refractive index, and (c.1-3) Concentration of CO_2 as function of pressure.

4.6 References

1. Baker, R. W. & Lokhandwala, K. Natural Gas Processing with Membranes : An Overview. *Ind. Eng. Chem. Res.* **47,** 2109–2121 (2008).
2. Scholz, M., Melin, T. & Wessling, M. Transforming biogas into biomethane using membrane technology. *Renew. Sustain. Energy Rev.* **17,** 199–212 (2013).
3. Sanders, D. F. *et al.* Energy-efficient polymeric gas separation membranes for a sustainable future : A review. *Polymer* **54,** 4729–4761 (2013).
4. Bernardo, P., Drioli, E. & Golemme, G. Membrane Gas Separation : A Review / State of the Art. *Ind. Eng. Chem. Res.* 4638–4663 (2009).
5. Tanaka, K., Okano, M., Toshino, H., Kita, H. & Okamoto, K.-I. Effect of methyl substituents on permeability and permselectivity of gases in polyimides prepared from methyl-substituted phenylenediamines. *J. Polym. Sci. Part B Polym. Phys.* **30,** 907–914 (1992).
6. Matsumoto, K. & Xu, P. Gas permeation of aromatic polyimides. II. Influence of chemical structure. *J. Memb. Sci.* **81,** 23–30 (1993).
7. Hirayama, Y. *et al.* Relation of gas permeability with structure of aromatic polyimides I. *J. Memb. Sci.* **111,** 169–182 (1996).
8. Yampolskii, Y. Polymeric Gas Separation Membranes. *Macromolecules* **45,** 3298–3311 (2012).
9. Raveendran, P. & Wallen, S. L. Exploring CO2-philicity: Effects of stepwise fluorination. *J. Phys. Chem. B* **107,** 1473–1477 (2003).
10. Zheng, Y., Li, S. & Gao, C. Hyperbranched polymers: advances from. *Chem. Soc. Rev.* **44,** 4091–4130 (2015).

11. Jikei, M. & Kakimoto, M. Hyperbranched polymers: a promising new class of materials. *Prog. Polym. Sci.* **26,** 1233–1285 (2001).

12. Morikawa, A. Comparison of Properties among Dendritic and Hyperbranched Poly(ether ether ketone)s and Linear Poly(ether ketone)s. *Molecules* **21,** (2016).

13. Lederer, A. & Burchard, W. *Hyperbranched Polymers: Macromolecules in between Deterministic Linear Chains and Dendrimer Structures*. (The Royal Society of Chemistry, 2015).

14. Mu, J., Zhang, C., Wu, W., Chen, J. & Jiang, Z. Synthesis, Characterization, and Functionalization of Hyperbranched Poly(ether ether ketone)s with Phenoxypheyl Side Group. *J. Macromol. Sci. Part A* **45,** 748–753 (2008).

15. Kappert, E. J. *et al.* Temperature calibration procedure for thin film substrates for thermo-ellipsometric analysis using melting point standards. *Thermochim. Acta* **601,** 29–32 (2015).

16. Ogieglo, W., Wormeester, H., Wessling, M. & Benes, N. E. Effective medium approximations for penetrant sorption in glassy polymers accounting for excess free volume. *Polymer* **55,** 1737–1744 (2014).

17. Herzinger, C. M., Johs, B., McGahan, W. A., Woollam, J. A. & Paulson, W. Ellipsometric determination of optical constants for silicon and thermally grown silicon dioxide via a multi-sample, multi-wavelength, multi-angle investigation. *J. Appl. Phys.* **83,** 3323–3336 (1998).

18. Obriot, J., Ge, J., Bose, T. K. & St-Arnaud, J.-M. Determination of the density from simultaneous measurements of the refractive index and the dielectric constant of gaseous CH4, SF6, and CO2. *Fluid Phase Equilib.* **86,** 314–350 (1993).

19. Horn, N. R. & Paul, D. R. Carbon Dioxide Sorption and Plasticization of Thin Glassy Polymer Films Tracked by Optical Methods. *Macromolecules* **45,** 2820–2834 (2012).

20. Simons, K. *et al.* CO2 sorption and transport behavior of ODPA-based polyetherimide polymer films. *Polymer* **51,** 3907–3917 (2010).

21. Buck, A. L. New Equations for Computing Vapor Pressure and Enhancement Factor. *J. Appl. Meteorol.* **20,** 1527–1532 (1981).

22. Hawker, C. J. & Chu, F. Hyperbranched Poly(ether ketones): Manipulation of Structure and Physical Properties. *Macromolecules* **29,** 4370–4380 (1996).

23. Kim, Y. H. & Webster, O. W. HYPERBRANCHED POLYPHENYLENES. *Macromolecules* **25,** 5561–5572 (1992).

24. Kim, Y. H. & Beckerbauer, R. Role of End Groups on the Glass Transition of Hyperbranched Polyphenylene and Triphenylbenzene Derivates. *Macromolecules* **27,** 1968–1971 (1994).

25. Visser, T., Koops, G. H. & Wessling, M. On the subtle balance between competitive sorption and plasticization effects in asymmetric hollow fiber gas separation membranes. *J. Memb. Sci.* **252,** 265–277 (2005).

26. Ogieglo, W., Madzarevic, Z. P., Raaijmakers, M. J. T., Dingemans, T. J. & Benes, N. E. High-Pressure Sorption of Carbon Dioxide and Methane in All-Aromatic Poly (etherimide) -Based Membranes. *J. Polym. Sci. Part B Polym. Phys.* **54,** 986–993 (2016).

27. Raaijmakers, M. J. T. *et al.* Sorption Behavior of Compressed CO2 and CH4 on Ultrathin Hybrid Poly(POSS-imide) Layers. *ACS Appl. Mater. Interfaces* **7,** 26977–26988 (2015).

28. Bos, a., Pünt, I. G. M., Wessling, M. & Strathmann, H. CO2-induced plasticization phenomena in glassy polymers. *J. Memb. Sci.* **155,** 67–78 (1999).

29. Mueller, A., Kowalewski, T. & Wooley, K. L. Synthesis, characterization, and derivatization of hyperbranched polyfluorinated polymers. *Macromolecules* **31,** 776–786 (1998).

30. Ansaloni, L., Minelli, M., Giacinti Baschetti, M. & Sarti, G. C. Effect of relative humidity and temperature on gas transport in Matrimid s : Experimental study and modeling. *J. Memb. Sci.* **471,** 392–401 (2014).

31. Rowe, B. W., Freeman, B. D. & Paul, D. R. Effect of sorbed water and temperature on the optical properties and density of thin glassy polymer films on a silicon substrate. *Macromolecules* **40,** 2806–2813 (2007).

Chapter 5

Gas Separation Performance of a Crosslinked HBPAEK Membrane

Abstract

We have explored crosslinked HBPAEK-28K-10PEP as a gas separation membrane for high-pressure gas separation applications. The membrane was compared with Matrimid® and showed better selectivity for H_2/CH_4 (85 vs. 64) and H_2/CO_2 (10 vs. 2), where the separation of H_2/CO_2 approached the Robeson upper limit. The activation energy for the used gasses, He, H_2, N_2, CH_4 and CO_2, ranged from 14-29 KJ/mol, indicating that these gasses all exhibit similar affinities to the crosslinked HBPAEK-28K-10PEP membrane. The constant slope of the activation energy suggests that the HBPAEK does not suffer from temperature induced changes in mobility. In addition, HBPAEK-28K-10PEP was tested at 200 °C for 14 days and was able to retain its selectivity for H_2 over N_2. Our results show that the use of crosslinked HBPAEKs is a viable approach towards high temperature gas separation membranes.

This chapter is based on the paper: “All-aromatic Crosslinked Hyperbranched Poly(aryletherketone)s for gas separation at elevated temperatures” by Vogel et al., to be submitted.

5.1 Introduction

Dense polymer membranes for gas separation operate based on the solution-diffusion principle where the size of the gas molecules is typically in the range of a few angstrom (Å). In a solution-diffusion mechanism the gases are dissolved in the polymer membrane after which they are separated by diffusion. The polymers have no pores but the transport of the gasses take place through the small spaces in between the polymer chains, also known as the excess fractional free volume. The solution-diffusion mechanism is schematically shown in Figure 5.1.

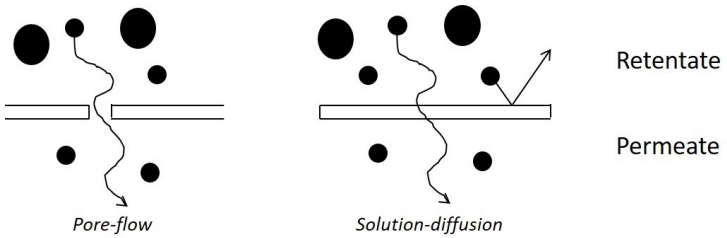

Figure 5.1. Schematic representation of the solution-diffusion mechanism.

The permeate is the gas that has passed the membrane and can be collected after. The so-called flux is the amount of gas transported per unit area per unit time. When the flux is corrected for pressure and thickness, we call it the permeability of the membrane. According to the solution-diffusion model, the permeability depends on both the solubility (S) and diffusivity (D) and gives the following equation for gas *i*:

$$P_i = S_i \times D_i \qquad (1)$$

A difference in either S or D gives a selectivity (α), which is defined as:

$$a_{i/j} = \frac{Pi}{Pj} = \left(\frac{Di}{Dj}\right) \times \left(\frac{Si}{Sj}\right) \qquad (2)$$

The ability of a membrane to separate binary gasses, i.e. *i* over *j*, can be described with $\alpha_{i/j}$ and is actually dependent on the feed composition and operating conditions and is thus not a material property. A higher value for α will result in better separation of *i* over *j*.

Diffusion in polymer membranes is slow and therefore these membranes are often very thin to maintain an acceptable flux. When striving for membranes that have both high selectivity and high permeability, one runs into a dilemma. A more permeable membrane will be less selective, while a more selective membrane will be less permeable. This classical trade-off is to be considered in the design of membranes. Another consideration is that many industrial processes take place at elevated temperatures (> 150 °C), which makes it desirable to separate gases at the processing temperatures used.

Typical polymer membranes show an increase in chain mobility at elevated temperature, compromising their performance. To overcome this temperature restriction, several high temperature polymers were developed, of which poly(benzoxazole)s (PBOs),[1] poly(benzoxazole-co-imides)s[2] and poly(benzoxazole-co-pyrrolone)[3] are examples. Unfortunately, their limited solubility hinders processing and the close molecular packing of the linear chains reduces the permeance. Also, they are still susceptible to plasticization by CO_2. Currently, one of the best performing gas separation membranes is Matrimid®, which we will use as a bench mark reference. It is one of the polyimides that are relatively easy to prepare from diamines and dianhydrides. Typical gas permeance values for H_2, CH_4 and alike for this polymer are in the nmol m^{-2} s^{-1} Pa^{-1} range.[4] The chemical structure of Matrimid® is shown in Figure 5.2.

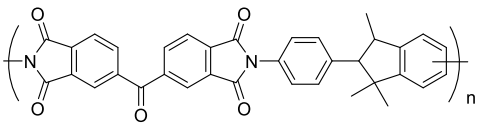

Figure 5.2. Chemical structure of the polyimide that is sold under the trade name Matrimid®.

The T_g of this polymer is 320 °C, while additional bulky side groups prevent efficient chain packing and thus reduce crystallinity and increase free volume. The disadvantage of Matrimid® is the susceptibility to plasticization by CO_2. The selectivity of Matrimid® is listed together with several other types of high-performance polymer membranes in Table 5.1.

Table 5.1. Comparison of the selectivity for various gaseous mixture for various types of high-performance polymer membranes.

Polymer Membrane	**Selectivity**			
	H_2/CH_4	**H_2/N_2**	**CO_2/CH_4**	**H_2/CO_2**
PI[a]	64	56	36	1.8
PBO[b]	130	52	47	-
PEEK-WC[c]	32	36	10	-
POSS-imide[d]	9	12	2	6.5

[a] polyimide (PI), values for Matrimid® are taken as an example.[5]

[b] polybenzoxazole (PBO).[1]

[c] polyetheretherketone with cardo (PEEK-WC).[6]

[d] polyPOSS−imide derived from PMDA.[7]

Another approach is the use of inorganic-organic membranes. Ammonium functionalized polyhedral oligomeric silsesquioxane (POSS) cages can be linked

together with dianhydrides forming a hyper-crosslinked polyamic acid network that was imidized in an additional thermal treatment step.[8] The selectivity of these membranes are listed in Table 5.1. Although ultra-thin homogeneous films could be prepared via interfacial polymerization, the prolonged thermal stability is still poor, as the amino groups on the POSS are linked with sp^3 carbons, which have limited thermal stability.

Modified PEEK with a so-called cardo group was also reported in the literature, as the cardo group increases the solubility, while maintaining the good thermal and mechanical properties that is typical of PEEK.[6] The permeance of N_2 and CH_4 was increased, indicating that a cardo group can be used to tune gas separation properties. PEEK-WC (with cardo) has a benzolactone group attached that introduces a spiro functionality into the polymer backbone. The chemical structure of PEEK-WC is shown in Figure 5.3. The drawback of this approach is that spiro building blocks are very expensive and therefore not desirable for industrial applications.

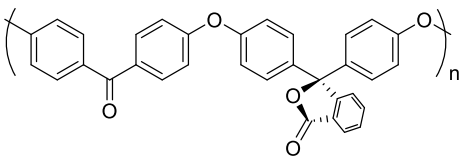

Figure 5.3. Polyether ether ketone (PEEK) with a cardo group (PEEK-WC).

From the described approaches, crosslinked hyperbranched poly(aryletherketone)s (HBPAEKs), may offer a novel route towards the design of amorphous gas separation membranes with a tuneable excess fractional free volume (EFFV). Poly(aryletherketone)s are chemically and thermally very stable and are potentially useful but hardly explored for gas separation purposes. This is

due to the semi-crystalline nature of the polymer and limited solubility in organic solvents, resulting in complex processing and reduced flux. In the previous chapter we have shown that reactive HBPAEKs have the desired solubility and that they can be processed into amorphous membranes.

Based on the preliminary membrane results reported in Chapter 4, we selected HBPAEK-28K-10PEP as a representative sample for further evaluation of the gas separation performance, as it showed minimal differences compared to HBPAEK-25K-20PEP. In this chapter we will measure the activation energies for commonly used gasses H_2, He, N_2, CO_2 and CH_4, determine the selectivity for commonly used gas mixtures H_2/CO_2, H_2/N_2, H_2/CH_4 and CO_2/CH_4 for both uncured and cured HBPAEK-28K-10PEP and measure the selectivity at an elevated temperature (200 °C) for 2 weeks. This is graphically illustrated in Figure 5.4.

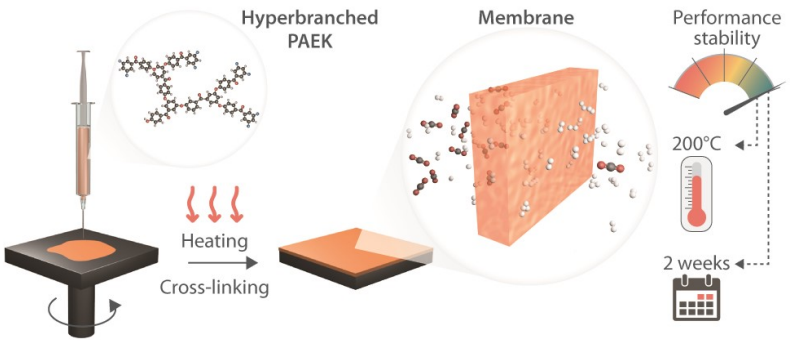

Figure 5.4. HBPAEK-28K-10PEP is spin-coated onto an alumina substrate, after which it is heated to form a crosslinked amorphous network. The resulting membrane is tested for its gas separation performance at 200 °C for 2 weeks.

A broad operating temperature range for membranes is desirable, as separating process gasses (e.g. N_2 from H_2) at the processing temperature (> 150 °C) is much

more energy efficient than traditional methods where gasses need to be cooled prior to separation.[9]

5.2 Experimental section

HBPAEK-28K-10PEP was used as a membrane and the synthetic details are described in Chapter 4. After spin-coating on the alumina substrate, the membrane was annealed at 200 °C for 30 minutes to remove any anisotropy before the membrane was cured according to the temperature profile as shown in Figure 5.5.

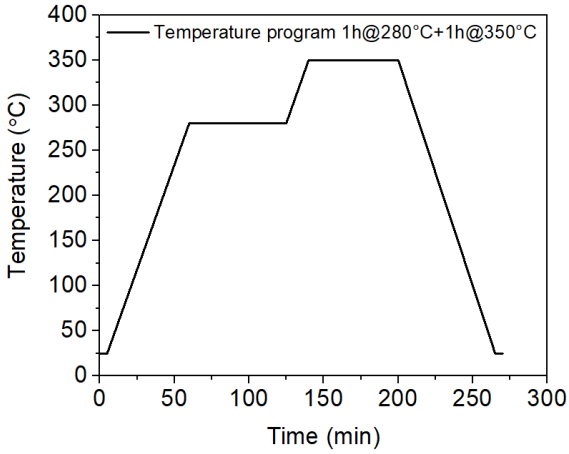

Figure 5.5. Spin-coated HBPAEK-28K-10PEP membranes were cured for 1h at 280 °C and 1h at 350 °C.

Membrane Single Gas Permeation Measurements

Single gas (He, H_2, CO_2, N_2, and CH_4) permeation measurements were performed using a custom build setup (Convergence, the Netherlands). All experiments were performed in dead-end mode at a transmembrane pressure of 2 bar. The membrane module was heated to temperatures between 50 and 200 °C. At least

two individual membranes were measured for each polymer and crosslink program.

Long-term stability test

The long-term stability of a cured HBPAEK-28K-10PEP membrane was investigated by alternating the hydrogen and nitrogen permeance at 200 °C for two weeks. The nitrogen permeance was measured for 5.5 hours, after which the feed gas was switched to hydrogen for 30 minutes. The reported permeance was defined as the average permeance during the last 5 minutes for every step.

5.3 Results and discussion

5.3.1. Single gas permeation through the alumina support

The gas permeation through the alumina support must be determined before the gas separation properties of the crosslinked HBPAEK films can be measured. Figure 5.6 shows the single gas permeation characteristics of the alumina support. The pore size of the γ-alumina allows for separation by Knudsen diffusion.[10] Knudsen diffusion describes molecules passing through very narrow pores with a diameter of <50 nm. This results in a condition where gas molecules more often collide with the pore walls than with each other, a process that is also called Knudsen flow. The size of the molecules determines the amount of interaction with the pore wall, resulting in a gradient in flow and thus opportunity for separation.

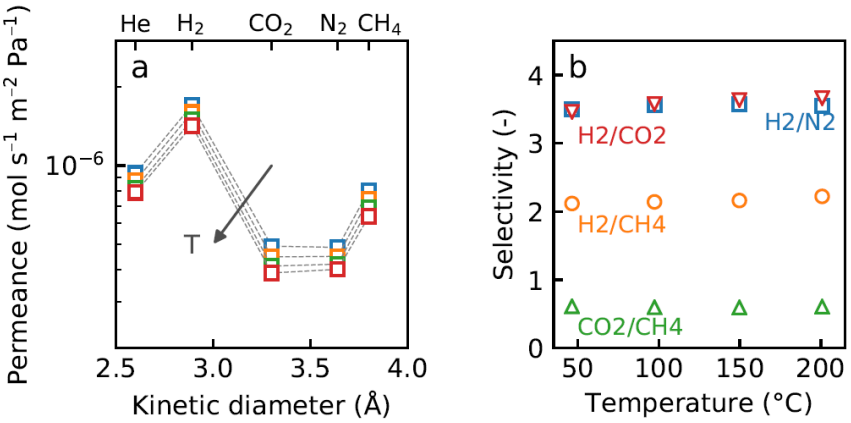

Figure 5.6. Single gas permeation results for the bare alumina membrane support. (a) The difference in kinetic diameter gives a difference in permeance. Data points shown represent 4 measurements for each gas and confirm reproducibility. (b) The selectivity for each gas mixture was measured at 4 different temperatures. The selectivity for the bare substrate is temperature independent.

The selectivity in the case of Knudsen diffusion can be calculated by:

$$\alpha_{a/b} = \sqrt{\frac{M_b}{M_a}} \qquad (3)$$

Where $\alpha_{a/b}$ is the selectivity (-) of the membrane and M_a and M_b are the molar mass of the gas molecules a and b (g/mol), respectively. All values are in good agreement with the theoretical Knudsen selectivity that are shown in Table 5.2, except the 3.6 value for H_2/CO_2, which is lower than the theoretical 4.7 value. This can be due to the condensability of CO_2.

Table 5.2. Theoretical Knudsen and measured selectivities for various gas pairs.

Gas pair	Knudsen selectivity	Measured selectivity at 50 °C
H_2/CO_2	4.7	3.6
H_2/N_2	3.7	3.6
H_2/CH_4	2.8	2.1
CO_2/CH_4	0.6	0.6

The adsorbed CO_2 molecules onto the pore wall can move by surface diffusion, resulting in an increased CO_2 permeability and therefore reduced selectivity.[11]

5.3.2. Preparing crosslinked HBPAEK-28K-10PEP membranes

The HBPAEK polymers were spin-coated onto a porous alumina support and thermally crosslinked before they were tested for their membrane performance. Figure 5.7 shows a scanning electron micrograph of the cross-section of a crosslinked HBPAEK-28K-10PEP film. Three layers can be distinguished: the bottom layer is >2 mm thick α-alumina layer (pore size ~100 nm, porosity ~30%), the middle layer with approximately 3 µm thick γ-alumina (pore size ~3 nm, porosity ~40%) and the top layer is a ~700 nm thick crosslinked HBPAEK film. The film thicknesses of all samples was assumed to be 700 nm, because all samples were prepared using identical spin-coating conditions. To remove anisotropy induced by spin-coating, all samples were heated to 200 °C for 30 minutes. Uncrosslinked membranes as well as crosslinked membranes that were cured for 1h at 280 °C and 1h at 350 °C were tested for their single gas permeation characteristics.

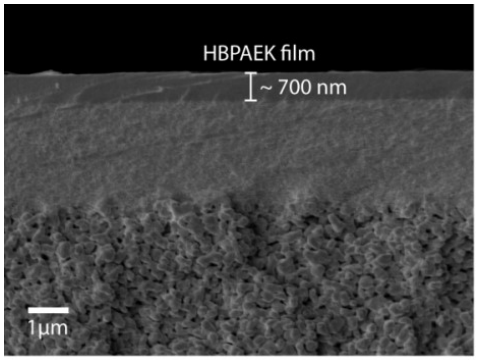

Figure 5.7. Cross-section scanning electron micrograph of a crosslinked HBPAEK-28K-10PEP film atop of a ceramic support. The ceramic support is made of an α-alumina support with a 3 µm thick γ-alumina layer. On top of this γ-alumina layer sits the 700 nm thick HBPAEK film.

5.3.3. Gas separation performance of crosslinked HBPAEK membranes

To test the gas separation performance of a crosslinked HBPAEK-28K-10PEP membrane, several standard gasses and gas mixture were used. He, H_2, CO_2, N_2 and CH_4 were used as single gasses and H_2/CH_4, H_2/N_2, CO_2/CH_4 and CO_2/CH_4 were used as gaseous mixtures (50/50, mol%). All are frequently used in membrane science and this makes a good comparison with literature values possible. The results are shown in Figure 5.8. The single gas permeance as function of gas kinetic diameter for the uncrosslinked HBPAEK is given in panel a, and for the HBPAEK crosslinked for 1h at 280 °C and 1h at 350 °C in panel b. Due to the lower T_g of the uncured HBPAEK, the maximum temperature was set to 150 °C instead of 200 °C. For both uncrosslinked and crosslinked HBPAEK-28K-10PEP we found that the single gas permeance decreases with increasing gas kinetic diameter. This is a typical trend observed for glassy polymers, indicating a sieving mechanism. With increasing temperature, the permeance increased due to the increased mobility of a gas at higher temperatures.

The Arrhenius plots of the ln(permeance) as a function of T^{-1} for both uncrosslinked and crosslinked HBPAEK-28K-10PEP are shown in Figure 5.8c and d. The activation energy of the gas transport could be derived from the slope of this plot for every measured gas.

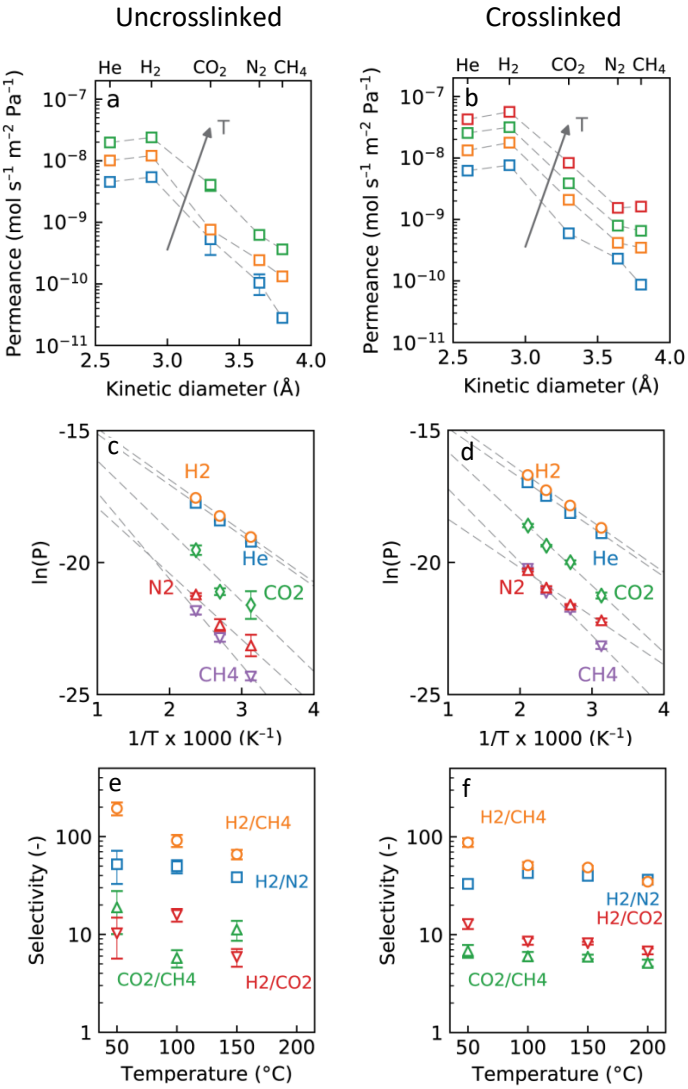

Figure 5.8. Gas permeation for uncrosslinked HBPAEK-28K-10PEP (a, c and e) and crosslinked HBPAEK-28K-10PEP (1h at 280 °C and 1h at 350 °C) (b, d and f). (a, b) Permeance as function of the gas kinetic diameter; (c, d) Arrhenius plot of single gas permeances; (e, f) Ideal selectivity of H_2/CH_4, H_2/N_2, H_2/CO_2, and CO_2/CH_4 as function of temperature. All error bars represent the standard error.

Table 5.3 shows the values of the activating energy for the HBPAEKs and gasses. The constant slopes of the activating energy suggest that the HBPAEK films do not suffer from temperature induced chain mobility.

Table 5.3. Activating energies (kJ mol^{-1}) for transport through the HBPAEK films for several gases.

	Activation energy, E_a (kJ mol^{-1})	
Gas	**HBPAEK-28K-10PEP uncrosslinked**	**HBPAEK-28K-10PEP crosslinked**
Helium	16 ± 0.4	16 ± 0.3
Hydrogen	16 ± 0.5	16 ± 0.5
Carbon dioxide	21 ± 8.3	21 ± 1.3
Nitrogen	17 ± 3.9	15 ± 1.5
Methane	27± 1.7	23 ± 1.7

In general, the activation energy is similar for all gases and membranes. Typically, fluorine-rich polymers, e.g., polyimides containing trifluoromethyl (CF_3) groups, show a low activation energy for CO_2 transport due to the high solubility of CO_2 in the membrane matrix at lower temperatures. At higher temperatures the CO_2 solubility decreases, while the diffusivity increases. The permeability is the product of solubility and diffusivity, and therefore this effect is cancelled out at elevated temperatures. Studies on 6FDA-based polyimides show that the CO_2 permeability was constant or even decreases with increasing temperature while for other gases the permeability increases with temperature.[12,13] Polyimides without these CF_3 groups also showed an increase in permeability with temperature for CO_2.[14] The activating energy for CO_2 transport does not differ

from the other gases for the HBPAEK films measured in this study. The remaining fluorine functionalities on the HBPAEKs show no increased affinity for CO_2 in the gas separation measurements, hinting that fluorine atoms only display an effect when employed as bulky groups (e.g. in $-CF_3$ groups). However, there is still a lot of debate on the nature of the CO_2-F interaction.[15,16]

The ideal selectivity ($\alpha_{a/b}$) of H_2/CH_4, H_2/N_2, H_2/CO_2, and CO_2/CH_4 gas pairs as function of temperature is shown in Figure 5.8e (uncrosslinked) and f (crosslinked). We can conclude from these data that the crosslinked HBPAEK-28K-10PEP membrane is still selective at temperatures up to 200 °C. Independent of temperature, the selectivity of H_2/CH_4 and H_2/N_2 is higher compared to that of H_2/CO_2 and CO_2/CH_4, which agrees with the molecular sieving mechanism. The selectivity of uncured HBPAEK over the cured HBPAEK is minimal, with the exception of CO_2/CH_4. The advantage, though, is the increased temperature window, as the T_g of the cured polymers is higher.

When we compare the performance of the HBPAEKs measured at 50 °C with the linear polyimide Matrimid®, measured at 35 °C there are some interesting differences, as shown in Table 5.4. The small temperature difference is expected not to be of significant influence on the comparison.

Table 5.4. Selectivity of crosslinked HBPAEK-28K-10PEP compared to Matrimid® for various gas compositions.

Gas Mixture	Crosslinked HBPAEK-28K-10PEP Selectivity (α) at 50 °C	Matrimid[a] Selectivity (α) at 35 °C
H_2/CH_4	85	64
H_2/N_2	33	56
CO_2/CH_4	7	36
H_2/CO_2	10	2

[a] Taken from literature.[5]

The selectivity of H_2/CH_4 (85) for our HBPAEK-28K-10PEP is higher than that of Matrimid® (64). The selectivity for H_2/N_2 (33) is slightly lower. The CO_2/CH_4 selectivity (7) of HBPAEK-28K-10PEP is also lower when compared to Matrimid® (36). Additionally, the selectivity of H_2/CO_2 (10 for the HBPAEK-28K-10PEP is much higher as compared to Matrimid® (2).[5]

Fang et al. reported the synthesis and membrane performance of hyperbranched polyimide membranes.[17] The chemical structure is shown in Figure 5.9.

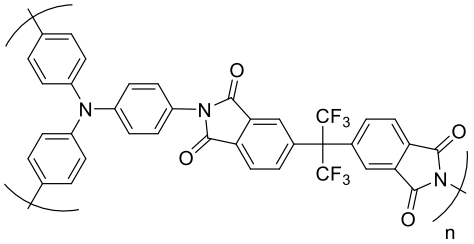

Figure 5.9. Chemical structure of a hyperbranched polyimide, based on triphenylamine and 6FDA.

The authors report that besides the end-groups, the crosslinking mechanism of a hyperbranched polymer has a great influence on the membrane performance. They used amine terminated polyimides that were crosslinked with a difunctional crosslinker (terephthaldehyde) or ethylene glycol diglycidyl ether. In their work, the permeability is presented in Barrer, a unit that that is often used in Robeson plots that will be discussed in the next paragraph. In general, their measured CO_2 permeabilitiy is comparable (1-4 Barrer) up to significantly higher (65 Barrer) as compared to the crosslinked HBPAEK (1-4 Barrer). The relatively low CO_2 permeability found for our HBPAEKs fits very well with the low swelling degrees measured by *in-situ* SE (Chapter 4).

In addition, the CO_2/CH_4 selectivity reported by Fang et al. is much higher (41-61) compared to that of the HBPAEK (7).[17] The work of Suzuki et al. showed the CO_2 permeability of a TAPOB-6FDA hyperbranched polyimide.[18] They report either comparable or up to 3 times better CO_2 permeability compared to HBPAEK-28K-10PEP. To compare the performance of the HBPAEKs membranes to other membranes available, their performance was plotted in Robeson plots.

5.3.4. Robeson plots

Robeson plots are used in membrane science to display the trade-off relationship between selectivity and permeability.[19] This empirical upper bound relationship is displayed in a plot where the permeability (=permeance*thickness) is reported on the x-axis (in Barrer) and the selectivity on the y-axis. We measured the permeances at 50 °C with a 700 nm thick membrane. From the Robeson plots in Figure 5.10 we can see that our HBPAEK performs far below the present upper limit for CO_2/CH_4 and H_2/N_2 gas pairs. However, the H_2/CH_4 gas pair is close to the 1991 upper bound, and the H_2/CO_2 gas pair is even at the 2008 upper bound for the crosslinked HBPAEK-28K-10PEP membrane.

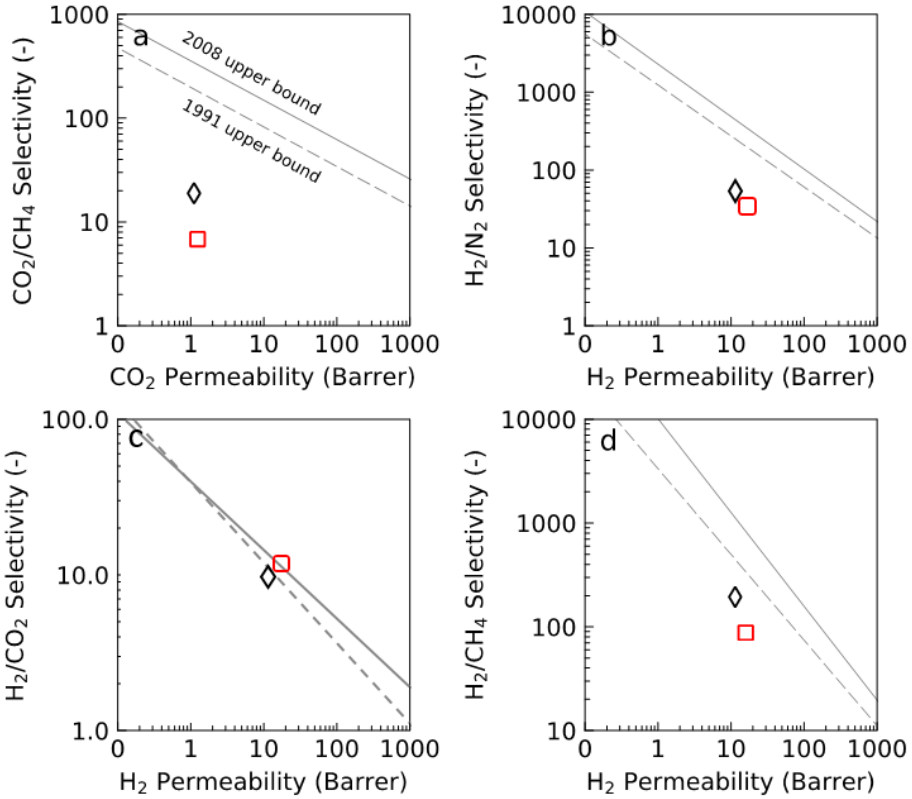

Figure 5.10. Robeson plots for (a) CO_2/CH_4, (b) H_2/N_2, (c) H_2/CO_2, and (d) H_2/CH_4 gas pairs with their permeabilities, obtained from the permeances measured at 50 °C. The thickness of the separating layer was assumed to be 700 nm for all membranes. The theoretical upper bound as in 1991 (dashed line) and 2008 (solid line) were plotted for reference purposes. The symbols represent: HBPAEK-28K-10PEP uncrosslinked (◊) and HBPAEK-28K-10PEP crosslinked (□).

5.3.5. Long-term performance at high temperature

Most state-of-the-art polymeric membranes show a decline in membrane performance at elevated temperatures caused by an increase in macromolecular dynamics.[20] The development of a membrane stable at elevated temperatures would be of great interest to industry. Because of the excellent thermal stability of the polymer backbone in combination with the amorphous nature of the hyperbranched polymer, the HBPAEK membrane remains selective at temperatures up to 200 °C (the experimental limit of the apparatus used). To investigate the gas separation performance of crosslinked HBPAEK-28K-10PEP under more demanding industrial operating conditions, we examined the performance using an H_2/N_2 gas mixture at 200 °C for 2 weeks. As can be concluded from Figure 5.11, a cured HBPAEK-28K-10PEP membrane did not show any sign of loss of performance in permeance or selectivity, indicating the great potential of these materials for gas separation at elevated temperatures.

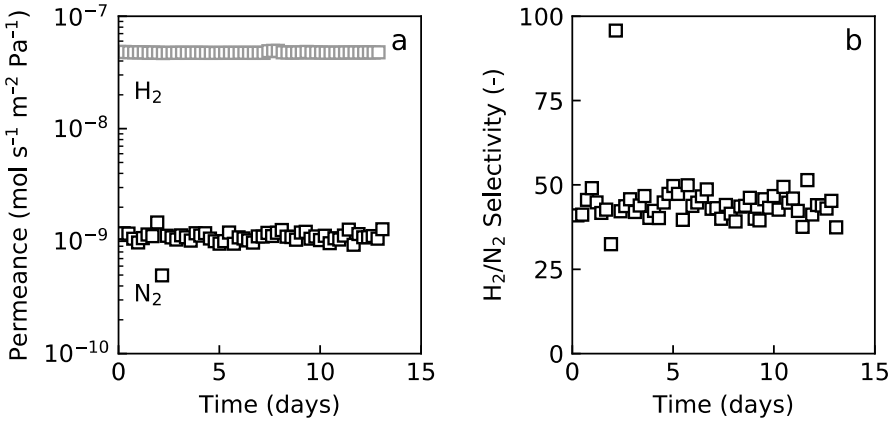

Figure 5.11. Long term thermal stability of cured HBPAEK-28K-10PEP, kept at 200 °C. (a) The permeance of H_2 and N_2 as a function of time, and (b) the H_2/N_2 selectivity as function of time. No decrease in selectivity is observed after 14 days.

5.4 Conclusion

HBPAEK-28K-10PEP was spin-coated onto an alumina substrate with a thickness of 700 nm and evaluated as gas separation membrane. The activation energy for the used gasses, i.e. He, H_2, N_2, CH_4 and CO_2, showed similar affinities towards the HBPAEK backbone with values ranging from 14 to 29 KJ/mol. The selectivity of the uncrosslinked HBPAEK-28K-10PEP membrane could be measured up to 150 °C, whereas crosslinked HBPEAK-28K-10PEP membranes could be measured up to 200 °C due to a higher T_g. Noteworthy is the trade-off between selectivity and permeability when using a H_2/CO_2 gas mixture as this gets close to the 2008 Robeson upper bound. When we compare the selectivity (α) of crosslinked HBPEAK-28K-10PEP with Matrimid® we find that HBPEAK-28K-10PEP outperforms Matrimid®(85 vs. 64). A crosslinked HBPAEK-28K-10PEP membrane shows excellent stability at elevated temperatures for a prolonged period of time, as the selectivity and permeance of H_2 over N_2 remains unchanged at 200 °C for up to 2 weeks. Our work confirms that the use of crosslinked amorphous HBPAEKs is a viable approach towards designing high temperature gas separation membranes.

5.5 References

1. Kushwaha, A. *et al.* Preparation and properties of polybenzoxazole-based gas separation membranes: A comparative study between thermal rearrangement (TR) of poly(hydroxyimide) and thermal cyclodehydration of poly(hydroxyamide). *Polymer* **78,** 81–93 (2015).
2. Jo, H. J. *et al.* Thermally Rearranged Poly(benzoxazole- *co* -imide) Membranes with Superior Mechanical Strength for Gas Separation Obtained by Tuning Chain Rigidity. *Macromolecules* **48,** 2194–2202 (2015).
3. Choi, J. I., Jung, H., Han, S. H., Bum Park, H. & Lee, Y. M. Thermally rearranged (TR) poly(benzoxazole-co-pyrrolone) membranes tuned for high gas permeability and selectivity. *J. Memb. Sci.* **349,** 358–368 (2010).
4. Falbo, F., Tasselli, F., Brunetti, A., Drioli, E. & Barbieri, G. Polyimide hollow fiber membranes for CO2 separation from wet gas mixtures. *Brazilian J. Chem. Eng.* **31,** 1023–1034 (2014).
5. Sanders, D. F. *et al.* Energy-efficient polymeric gas separation membranes for a sustainable future: A review. *Polymer* **54,** 4729–4761 (2013).
6. Jansen, J. C., Buonomenna, M. G., Figoli, A. & Drioli, E. Ultra-thin asymmetric gas separation membranes of modified PEEK prepared by the dry–wet phase inversion technique. *Desalination* **193,** 58–65 (2006).
7. Raaijmakers, M. Hyper-crosslinked, hybrid membranes via interfacial polymerization (PhD Thesis). (University of Twente, 2015).
8. Raaijmakers, M. J. T., Kappert, E. J., Nijmeijer, A. & Benes, N. E. Thermal Imidization Kinetics of Ultrathin Films of Hybrid Poly(POSS-imide)s. *Macromolecules* **48,** 3031–3039 (2015).
9. Li, X., Singh, R. P., Dudeck, K. W., Berchtold, K. A. & Benicewicz, B. C. Influence of polybenzimidazole main chain structure on H 2 /CO 2

separation at elevated temperatures. *J. Memb. Sci.* **461,** 59–68 (2014).

10. Uhlhorn, R. J. R., Keizer, K. & Burggraaf, A. J. Gas and surface diffusion in modified γ-alumina systems. *J. Memb. Sci.* **46,** 225–241 (1989).
11. Richardson, J. J., Bjornmalm, M., Caruso, F. & Baker, R. W. *Membrane Technology and Applications*. *Membrane Technology* **348,** (John Wiley & Sons, Ltd, 2012).
12. Duthie, X. *et al.* Operating temperature effects on the plasticization of polyimide gas separation membranes. *J. Memb. Sci.* **294,** 40–49 (2007).
13. Lin, W. H. & Chung, T. S. Gas permeability, diffusivity, solubility, and aging characteristics of 6FDA-durene polyimide membranes. *J. Memb. Sci.* **186,** 183–193 (2001).
14. Villaluenga, J. P. G., Seoane, B., Hradil, J. & Sysel, P. Gas permeation characteristics of heterogeneous ODPA-BIS P polyimide membranes at different temperatures. *J. Memb. Sci.* **305,** 160–168 (2007).
15. Raveendran, P. & Wallen, S. L. Exploring CO2-philicity: Effects of stepwise fluorination. *J. Phys. Chem. B* **107,** 1473–1477 (2003).
16. Singley, E. J., Liu, W. & Beckman, E. J. Phase behavior and emulsion formation of novel fluoroether amphiphiles in carbon dioxide. *Fluid Phase Equilib.* **128,** 199–219 (1997).
17. Fang, J., Kita, H. & Okamoto, K. Gas permeation properties of hyperbranched polyimide membranes. *J. Memb. Sci.* **182,** 245–256 (2001).
18. Suzuki, T., Yamada, Y. & Tsujita, Y. Gas transport properties of 6FDA-TAPOB hyperbranched polyimide membrane. *Polymer* **45,** 7167–7171 (2004).
19. Robeson, L. M. The upper bound revisited. *J. Memb. Sci.* **320,** 390–400 (2008).
20. Koros, W. J. & Woods, D. G. Elevated temperature application of polymer

hollow-fiber membranes. *J. Memb. Sci.* **181,** 157–166 (2001).

Summary

The work presented in this thesis will open a pathway towards the design of crosslinkable hyperbranched poly(aryetherketone)s (HBPAEKs). In addition to addressing the chemistry, crosslinking characteristics and (thermo)mechanical properties we will demonstrate that crosslinked HBPAEKs are excellent candidates for membrane-based gas separation applications.

An amorphous, all-aromatic hyperbranched polyaryletherketone (HBPAEK) formulation was selected because this offers a thermal and chemical stable model system that could easily be modified. The synthetic details and molecular weight analysis of a series HBPAEKs (22K, 69K and 123K) are reported in **Chapter 2**. AFM confirmed the globular nature of the HBPAEKs and the globular diameter was found to be in the range of 4–7 nm. Using melt rheology, we found minimum storage moduli of 100-300 Pa at ~240 ˚C, which confirmed the non-entangled behaviour of the hyperbranched polymer melts. Above this temperature the HBPAEKs start to crosslink via existing -OH/-F end-groups, indicating that these systems are still reactive. The T_g increased from 158 °C to 169 °C for the 123K HBPAEK with a maximum gel fraction of 98%. We confirmed that curing takes place via a post-condensation mechanism and we were able to control the final network properties by controlling time (t) and temperature (T) at cure. Crosslinking the HBPAEKs resulted in films that were too brittle too handle. The crosslink density is believed to be too low, meaning that a more efficient crosslinking method is needed.

In **Chapter 3** we propose a method to improve the mechanical properties of the HBPAEKs by increasing the crosslink density. In addition to post-condensation

induced crosslinking, the HBPAEKs can be crosslinked using phenylethynyl reactive end-group functionalities. Rapid and effective crosslinking was confirmed using melt rheology. Replacing at least 10% of the fluorine end-groups with phenylethynyl phenol (PEP) end-groups followed by temperature-induced crosslinking protocol resulted in flexible and transparent films that gave storage moduli of 3-4 GPa, tensile strengths of ~40 MPa and ~2% elongation at break. Upon crosslinking, the T_g of the films cSould be increased by as much as 100 °C, i.e. from 151 °C to 252 °C, indicating that PEP induced crosslinking is very effective in immobilizing the final polymer network.

In **Chapter 4** we demonstrated that thin (150 nm) crosslinked HBPAEK films can be used for high-pressure gas separation applications. Compared to the neat HBPAEK, the PEP crosslinked HBPAEK films exhibit high T_g's (up to 250 °C) and an effective free volume (EFFV) of 9%; two favourable characteristics that are beneficial for membranes used for gas separation applications. Upon exposure to CO_2, the membranes showed minimal swelling (~3%) at 50 bar CO_2 and no signs of plasticization, which is an important improvement over existing gas separation membranes. Our results showed that incorporating 10 mol% of PEP was enough to obtain stable gas separation membranes.

HBPAEKs with 10% PEP were processed into thin (700 nm) cured films and tested as membranes for separating gas mixtures and the results are reported in **Chapter 5**. Our membranes are able to separate CO_2/CH_4, H_2/N_2, H_2/CO_2 and H_2/CH_4 gas mixtures. Especially the H_2/CO_2 selectivity is impressive as it is close to the 2008 Robeson upper bound. With a long duration gas separation experiment, i.e. 2 weeks at 200 °C using a H_2/N_2 mixture, we were able to demonstrate the unusual long-term stability of our crosslinked HBPAEK membrane. The permeance and selectivity remained constant throughout the duration of the experiment,

unequivocally proving the fact that the aryletherketone backbone in combination with crosslinking results in membranes that do not suffer from CO_2 plasticization. Our preliminary results suggest that crosslinked HBPAEKs hold great promise as high temperature gas separation membranes for industrial applications.

Samenvatting

Het werk gerapporteerd in deze thesis is bedoeld om een methode te introduceren die leidt naar vernette hyperbranched polyaryletherketonen (HBPAEKs). Naast de chemie zullen we ook het vernetten en de daaraan gerelateerde (thermo)mechanische eigenschappen beschrijven. Tevens laten we laten zien dat vernette HBPAEKs zeer geschikte kandidaten zijn voor membraan-gebaseerde gasscheidingstoepassingen.

Vanwege de goede thermische en chemische stabiliteit hebben we gekozen voor een amorf en geheel aromatische HBPAEK modelsysteem. Het bijkomende voordeel van dit modelsysteem is dat de eindeigenschappen makkelijk te sturen zijn. In **Hoofstuk 2** rapporteren we de synthetische details en de moleculaire gewichtsanalyse van een serie HBPAEKs (22K, 69K en 123K). Met AFM kon de sferische structuur van de HBPAEKs bevestigd worden en werd de diameter bepaald op 4–7 nm. Middels smelt reologie experimenten vonden we opslag moduli van rond de 100–300 Pa bij ~240 ˚C, wat bewijst dat deze specifieke polymeren niet met elkaar verstrengeld zijn in de smelt. Boven deze temperatuur beginnen de HBPAEKs te vernetten via bestaande -OH/-F eindgroepen. Dit bevestigd dat deze polymeren nog steeds reactief zijn. De T_g steeg van 158 °C tot 169 °C voor het 123K polymeer, met een gel fractie van 98%. We hebben bevestigd dat het vernetten plaatsvindt via een post-condensatie mechanisme, en dat we in staat zijn om de eigenschappen van het netwerk te sturen, door de tijd (t) en de temperatuur (T) aan te passen. Het vernetten van deze hyperbranched polymeren resulteerde in brosse films die niet op mechanische eigenschappen konden worden getest. Een te lage vernettingsdichtheid is hier waarschijnlijk de reden van.

In **Hoofdstuk 3** stellen we een methode voor om de mechanische eigenschappen van de HBPAEKs te verbeteren door de vernettingsdichtheid te verhogen. Naast het vernetten middels post-condensatie, kunnen de HBPAEKs vernet worden door het introduceren van phenylethynyl reactieve eindgroepen. Snelle en effectieve vernetting kon worden bevestigd middels smelt reologie experimenten. Flexibele en transparante films konden worden verkregen wanneer 10% van de fluor-eindgroepen werd vervangen door phenylethynyl (PEP). De films hebben een storage modulus van 3-4 GPa, een treksterkte van ~40 MPa en 2% rek bij breuk. Het vernetten resulteerde in een stijging van de T_g van 100 °C, namelijk van 151 °C tot 252 °C, wat aangeeft dat het vernetten met PEP een efficiënte methode is om het polymeernetwerk te immobiliseren.

In **Hoofdstuk 4** laten we zien dat dunne (150 nm) vernette films gebruikt kunnen worden voor hogedruk gassenscheidingstoepassingen. Vergeleken met de ongemodificeerde HBPAEKs konden de PEP getermineerde HBPAEKs gebruikt worden om membranen te produceren met een hoge T_g (tot 250 °C) en een hoog vrij volume van 9%. Beide eigenschappen zijn gunstig voor membranen die gebruikt worden voor gassenscheidingstoepassingen. De membranen zwellen nauwelijks, te weten 3%, bij blootstelling aan 50 bar CO_2 en er was geen sprake van CO_2 geïnduceerde plasticering, wat een belangrijke verbetering is ten opzichte van bestaande gassenscheidingsmembranen. Onze resultaten laten zien dat het gebruik van 10 mol% PEP voldoende is om stabiele gassenscheidingsmembranen te produceren.

De HBPAEKs met 10% PEP zijn verwerkt tot dunne (700 nm) vernette films en deze zijn getest als membranen voor het scheiden van gasmengsels. Deze resultaten bespreken we in **Hoofdstuk 5**. Onze membranen zijn in staat om gasmengsels bestaande uit CO_2/CH_4, H_2/N_2, H_2/CO_2 en H_2/CH_4 te scheiden. Vooral de

selectiviteit van H_2/CO_2 is indrukwekkend en ligt dicht tegen de Robeson limiet uit 2008 aan. Middels een gasscheidingstest van 2 weken werd een H_2/N_2 gasmengsel gescheiden bij een continue gebruikstemperatuur van 200 °C. Het HBPAEK membraan met 10% PEP liet een ongebruikelijke stabiliteit zien. De permeatie en selectiviteit bleven constant gedurende het hele experiment, wat onomstotelijk bewijst dat het vernette HBPAEK membraan geen last heeft van het plasticerende effect van CO_2. Deze eerste resultaten laten zien dat deze polymeren grote potentie hebben om als hoge temperatuur gassenscheidingsmembranen toegepast te worden.

Acknowledgements

First of all I would like to thank Theo Dingemans for given me the opportunity to do a PhD in the Novel Aerospace Materials group. We have done quite some projects together over the last years and I'm grateful for the constant support and believe in my abilities. I enjoyed our time working together and you made it possible for me to see parts of the world I always dreamt about seeing. You gave me all the freedom in the world to pursue this degree and I am grateful for that.

I also want to thank Sybrand van der Zwaag for the support over the years and the warm reception in the group. NovAM felt like home to me and there were very few days that I went to work without a smile on my face. So many events, so many friends, so many achievements, so much fun. All possible due to the NovAM atmosphere. This atmosphere is created and supported by many people that I also want to thank. To name a few: Atsushi, Santiago, Johan, Nicolas, Vincenzo, Paul, Michael, Marlies, Hussein, and a lot of former NovAM members: Wouter P., Silvia, Michiel, Casper, Maruti, Mina, Zeljka, Arianna, Hari, Jimmy, Nan, Hongli, Quinbao, Daniella and, waitforit, Martino. I can't believe you guys survived my bad jokes, memes and other photoshop madness. Martino, sorry I borrowed your webcam indefinitely (quite useful though). Also thanks to my friends in the US, the half year I spent there was simply great.

Thanks to Russell Varley, he was on and off around and it was a pleasure to work with him. I think we've done some cool work together. I also would like to mention Sergei Sheiko and Andrew Keith and thank them for the fruitful collaboration in the US and useful discussions.

I also want to thank Evelien. Working together with you was nice and productive and I was happy to plan Skype meetings on times where you could skip other meetings that you didn't want to go to. Your supervisor Nieck Benes was also very supportive and I'm happy that a significant part of this thesis was in collaboration with you guys.

A special thanks to Arek Kotlewski, of which people still find samples and chemicals everywhere. You were a supporting pillar for the lab and I have yet to meet another researcher with such a diverse skill set. You also inspired me to improve my photoshopping (especially on Maruti), which I enjoyed a lot over the years. You gave me solid scientific training in theory and practice and were involved in a significant part of my education and I will be forever thankful for that.

Also thanks to Alex, your smile makes me happy and relaxed. Best girlfriend ever. Thanks for the space you gave me to finish this thesis. Grateful to Wouter P. for setting us up.

A very special thanks to my parents. You guys have always supported me. Most people know that I like to complain a lot, but you never got tired of it (remarkable) and you were always ready to give advice and love. You guys are so important to me. Also thanks to the rest of the family, my sister Madelon, my brother Robbert, and their spouses Mandy and Reinier and kids Teun, Brent, Mels, and Linn.

Curriculum Vitae

I was born in Naaldwijk in June 1989 but grew up in a city called Vlaardingen. After completing my high school there I did my Bachelors in organic chemistry in Leiden, where I spent a significant part doing projects with Theo Dingemans in the Novel Aerospace Materials group at the TU Delft. After a minor project on aramids with Teijin, I spent my Bachelor thesis on the synthesis of new sulphur containing epoxides that I have synthesized for Boeing. For this project I went to Australia for 2 months to finish the mechanical testing on my own synthesized products. To continue on organic chemistry I did my Masters in Amsterdam. I worked on chiral isocyanide blocks within the group of Romano Orru and got my diploma in 2014. To pursue my interest in high performance materials and polymers I accepted a PhD position with Theo Dingemans at the TU Delft.

During my PhD I worked on high performance all-aromatic hyperbranched polymers to see if branching is a way to deal with the disadvantages of linear high performance polymers and to explore if there are additional benefits. The results of this work are described in this thesis. As part of this thesis I have spent 6 months at the University of North Carolina in Chapel Hill, US.

After my PhD I joined Croda in Gouda, The Netherlands, as applications scientist to work on bio-inspired and bio-based innovative polymer systems in a broad range of applications.

List of publications and oral presentations

Publications

[1] Vogel, W. et al. In preparation.

"Curing Behaviour and Thermomechanical Properties of All-aromatic Hyperbranched Poly(aryletherketone)s"

[2] Vogel, W. et al. In preparation.

"All-aromatic Crosslinked Hyperbranched Poly(aryletherketone)s: Gas separation, selectivity and permeance"

[3] Maaskant, E. Vogel, W. et al. In preparation.

"The synthesis and pH-stability of poly(aryl ether) films prepared from the interfacial polymerization of cyanuric chloride with trialcohols"

[4] Varley, R. Vogel, W. et al. Accepted.

"Effect of Aromatic Substitution on the Kinetics and Properties of Epoxy cured Tri-Phenylether Amines"

[5] Maaskant, E. Vogel, W. et al. *Journal of Membrane Science*, **567**, 321-328 (2018).

"The use of a star-shaped trifunctional acyl chloride for the preparation of polyamide thin film composite membranes"

[6] Vogel, W. *et al. High Perform. Polym.* **26,** 420–435 (2014).

"Synthesis and characterisation of new sulphur-containing epoxy networks"

[7] Janssen, G. V, Vicente-García, E., Vogel W. *et al. European J. Org. Chem.* **2014,** 3762–3766 (2014).

"Stereoselective Synthesis of β-Sulfinylamino Isocyanides and 2-Imidazolines"

Oral presentations

[1] Dutch Polymer Days, workshop/oral presentation & posters (2014, 2015, 2016 and 2017)

"Thermally curable All-aromatic High Performance Polymers"

[2] European Polymer Federation (EPF) Dresden, oral presentation & poster (2015)

"Hyperbranched Curable All-aromatic High-Performance Polymers"

[3] Advanced Polymers for Macromolecular Engineering (APME) Ghent, poster (2017)

"Thermally Curable All-aromatic High-performance Hyperbranched Poly(aryl ether ketone)s"

[4] International workshop on dendrimers and hyperbranched polymers, Freiburg, oral presentation (2015)

"Hyperbranched Thermally Curable All-aromatic High Performance Polymers"

[5] DPI meetings, oral presentations & posters (2014, 2015, 2016 and 2017)